ABSTRACT

CARDIAC REGENERATIVE MEDICINE:
INSIGHTS FROM HEALTHY AND DISEASED ENGINEERED TISSUES

by
Pamela Grace Hitscherich

Cardiovascular disease remains the leading cause of mortality in the United States. Current tissue engineering approaches have fallen short of promoting fully functional cardiovascular cells and the post-myocardial infarction microenvironment is still not well understood. These gaps in knowledge are addressed in this dissertation through the development of *in vitro* engineered cardiac tissues using electroactive materials to enhance the differentiation of pluripotent stem cell derived cardiomyocytes and through the development of *in vitro* myocardial inflammation models dedicated to understanding cardiomyocytes and macrophages interactions.

Specifically, piezoelectric poly (vinylidene fluoride-trifluoroethylene) (PVDF-TrFE) supports the attachment and survival of mouse embryonic stem cell derived cardiomyocytes (mES-CM) and endothelial cells (mES-EC). Characterization of mES-CM confirms expression of classical cardiac specific marker such as cTnT and Cx43, as well as efficient calcium handling properties when cultured on PVDF-TrFE including response to ryanodine receptor and β-adrenergic stimulation. MES-EC also retain their ability to uptake low density lipoprotein when cultured on PVDF-TrFE scaffolds and express classical endothelial cell specific markers such as eNOS and PECAM-1.

Additionally, a novel graphene composite scaffold (PCL+G) exhibiting even distribution of graphene particles within the matrix allowing miniscule amounts of graphene to increase conductivity is developed and characterized. MES-CM seeded on

conductive PCL+G scaffolds attach well and begin migrating into the scaffold matrix. They exhibit well-registered sarcomeres, express cardiac specific markers such as cTnT, MHC and Cx43 and spontaneous beat for up to two weeks. MES-CM on PCL+G scaffolds can be electrically paced and respond to ryanodine receptor and β-adrenergic stimulation. The combination of highly aligned fiber orientation and the presence of graphene promoted significantly improve calcium cycling efficiency by a fractional release of over 40%.

Finally, *in vitro* myocardial inflammation models are developed to examine both direct and indirect co-culture of mES-CM with polarized macrophage subpopulations present in the post-myocardial infarction (MI) microenvironment. Direct co-culture with macrophage subsets cause significant changes in mES-CM calcium handling function, especially in store operated calcium entry (SOCE). Additionally, a macrophage secreted matricellular protein osteopontin (OPN) is also found to affect mES-CM SOCE response at concentrations similar to plasma levels in patients post-MI. A pathway connecting OPN to SOCE response through ERK1/2 activation is analyzed through indirect co-culture with macrophage conditioned media and found to be affected by OPN inhibition, suggesting this pathway is involved with calcium homeostasis in the post-MI microenvironment, specifically in the pro-healing, anti-inflammatory phase.

Taken together, the presented results expand the current state of research in cardiac regenerative medicine by demonstrating the potential of two electroactive biomaterials for the formation of functional cardiac tissues and by illuminating a novel target involved in changes in cardiomyocytes calcium homeostasis during post-MI healing through an in vitro engineered diseased model.

CARDIAC REGENERATIVE MEDICINE:
INSIGHTS FROM HEALTHY AND DISEASED ENGINEERED TISSUES

by
Pamela Grace Hitscherich

A Dissertation
Submitted to the Faculty of
New Jersey Institute of Technology
And Rutgers University Biomedical and Health Sciences – Newark
In Partial Fulfillment of the Requirements for the Degree of
Doctor of Philosophy in Biomedical Engineering

Department of Biomedical Engineering

December 2018

.

APPROVAL PAGE

CARDIAC REGENERATIVE MEDICINE:
INSIGHTS FORM HEALTHY AND DISEASED ENGINEERED TISSUES

Pamela Grace Hitscherich

Dr. Eun Jung Lee, Dissertation Advisor	Date
Associate Professor of Biomedical Engineering, NJIT	

Dr. Dominic P. Del Re, Committee Member	Date
Assistant Professor of Cell Biology and Molecular Medicine, Rutgers NJMS	

Dr. Vivek A. Kumar, Committee Member	Date
Assistant Professor of Biomedical Engineering, NJIT	

Dr. Bryan J. Pfister, Committee Member	Date
Professor and Department Chair of Biomedical Engineering, NJIT	

Dr. Lai-hua Xie, Committee Member	Date
Associate Professor of Cell Biology and Molecular Medicine, Rutgers NJMS	

BIOGRAPHICAL SKETCH

Author: Pamela Grace Hitscherich

Degree: Doctor of Philosophy

Date: December 2018

Undergraduate and Graduate Education:

- Doctor of Philosophy in Biomedical Engineering,
  New Jersey Institute of Technology, Newark, NJ, 2018

- Bachelor of Science in Biomedical Engineering,
  The College of New Jersey, Ewing, NJ, 2013

Major: Biomedical Engineering

Presentations and Publications:

Hitscherich, P. *et al.* Macrophages Affect Cardiomyocyte Calcium-Handling Function
  Via Matricellular Protein Secretion. (In preparation, 2018).

Hitscherich, P. *et al.* Electroactive Graphene Composite Scaffolds for Cardiac Tissue
  Engineering. *J. Biomed. Mater. Res. A* **106,** 2923-2933, (2018).

Hitscherich, P. *et al*. Injectable Self-Assembling Peptide Hydrogels for Tissue Writing
  and Embryonic Stem Cell Culture. *J. Biomed. Nanotech.* **14**, 802-807, (2018).

Hitscherich, P. & Lee, E.J. *Cardiac Tissue Engineering*. Vol. 2 (Hoboken, NJ): Wiley
  (2017).

Hitscherich, P. *et al*. The Effect of PVDF-TrFE Scaffolds on Stem Cell Derived
  Cardiovascular Cells. *Biotechnol. Bioeng*. **113**, 1577-85, (2016).

Alfonso, A.L., Hitscherich, P., Ma, X. & Lee, E.J. Decellularized Pancreatic Tissue. *J.
  Health Dispar. Res. Prac.* **9**, 60, (2016)

Hitscherich, P., Xie, L.H., and Lee, E.J., Macrophages Affect Cardiomyocyte Calcium
  Handling Function via Matricellular Protein Expression, Biomedical Engineering
  Society 2018 Annual Meeting, Atlanta, GA: October 2018

Hitscherich, P. and Lee, E.J. *In vitro* Myocardial Inflammation Model to Examine Macrophage and Cardiomyocyte Interaction, Biomedical Engineering Society 2017 Annual Meeting, Phoenix, AZ: October 2017

Hitscherich, P. and Lee, E.J., The Role of Macrophages on Cardiomyocyte Function, 2017 National Heart, Lung and Blood Institute Symposium on Cardiovascular Regenerative Medicine, Bethesda, MD: September 2017

Hitscherich, P., Aphale, A., Gordan, R., Xie, L.H., Patra, P. & Lee, E.J., Functional Maturation of Mouse Embryonic Stem Cell-derived Cardiomyocytes on Graphene Composite Scaffolds, Tissue Engineering and Regenerative Medicine International Society Americas 2016 Conference, San Diego, CA: December 2016

Hitscherich, P., Aphale, A., Gordan, R., Xie, L.H., Patra, P. & Lee, E.J. Engineered Cardiac Tissue Using Graphene Composite Nanostructured Scaffolds, Biomedical Engineering Society 2015 Annual Meeting, Tampa, FL: October 2015

Hitscherich, P., Wu, S., Gordan, R., Xie, L.H., Arinzeh, T. & Lee, E.J., The Biocompatibility of Piezoelectric PVDF-TrFE Scaffolds with Stem Cell derived Cardiovascular Cells, Tissue Engineering and Regenerative Medicine International Society 2015 World Congress, Boston, MA: September 2015

Hitscherich, P., Aphale, A., Gordan, R., Xie, L.H., Patra, P. & Lee, E.J. Biocompatibility of PCL-Graphene Electrospun Scaffold with Mouse Embryonic Stem Cell-derived Cardiomyocytes, Tissue Engineering and Regenerative Medicine International Society Americas 2014 Conference, Washington, DC: December 2014

I dedicate this dissertation to my family:
To my **Dad** for inspiring a love of science and for showing me what it takes to succeed
To my **Mom** for your unwavering love, support and optimism
To **Elyse** and **Alanna** for your steadfast belief in me and the well timed comic relief
To my **Grandparents** for your prayers and ceaseless encouragement
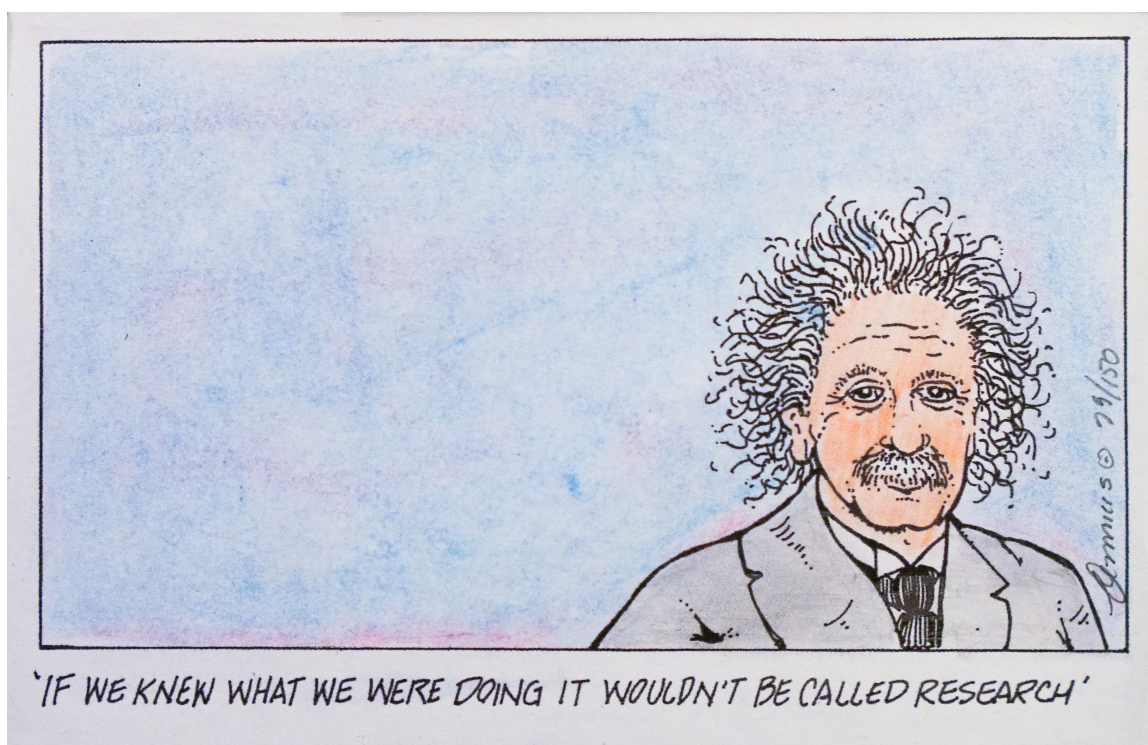To **Joey** for your love, devotion and eternal dedication to our happiness and success

'IF WE KNEW WHAT WE WERE DOING IT WOULDN'T BE CALLED RESEARCH'

Illustration by John DeAmicis ©

ACKNOWLEDGMENTS

I want to start by thanking my advisor Dr. Eun Jung Lee. Thank you for your guidance and never ending search for perfection. It has helped to improve both my writing and research beyond what I could have imagined. It has been so wonderful to get to know you and your family over the last five years and I am grateful for my time working with you.

Dr. Lai-hua Xie, thank you for taking a chance on me and allowing me to learn and perform some of the most vital experiments for my dissertation in your lab. Thank you for also never saying no to a last minute scheduling change and for allowing me to take as much time as I needed to master the techniques, even at 5 in the morning.

Dr. Bryan Pfister, thank you for always believing in me and thinking of me when amazing opportunities came up, like the speech at the Life Science and Engineering Building groundbreaking. Despite your hectic schedule not only running a lab, but also the BME department, you have always made time to meet with and encourage me and I cannot say how much I have appreciated that.

Dr. Vivek Kumar, thank you for always bringing levity to the sometimes boring and monotonous days at the lab. Thank you for taking an interest in my success when you started at NJIT, even if it started from a mutual need for sharing lab space and supplies. I am lucky to have had you as a never-ending source of research and career advice.

Dr. Dominic Del Re, thank you for your generosity of time, knowledge and antibodies. Thank you for helping me to transition into the topic of inflammation/macrophages and for your patience, as I definitely would have been lost without your guidance.

Thank you to NJIT Provost's office and BME department, the National Science Foundation and the National Institutes of Health for your financial support.

Dr. Alev Erdi, we started our time at NJIT together and I could not have asked for a better experience as a teaching assistant. Even after our first 2 years teaching together you never waivered in your support or enthusiasm for my success. Running into you always brightened my day and I was so lucky to have someone like you cheering me on.

Dr. William Hunter, thank you for being so patient and kind to me as I learned Matlab along with your students when I was supposed to be the TA! Thank you for being such an amazing and inspiring teacher and mentor. It was a pleasure to work with you and be your student.

Dr. Samuel Lieber, although we only met last year, it has been such a pleasure to work with and learn from you. Thank you for your generosity of time as well as your invaluable advice on my research and future career.

Thank you also to all of the peers I have had the pleasure to work with. Neha Jain, thank you for answering all of my questions from day 1. You taught me everything I needed to know to succeed at cell culture and managing a lab.

Rick Gordan, thank you for spending countless hours, and every Friday for over a year, teaching me everything I know about electrophysiology and any other topics that happened to come up. I am so lucky to have met you and call you a friend.

Jessica Ma, I cannot even begin to thank you enough for your friendship and generosity from your start in the Lee lab until now. You have become one of my dearest friends and I am so lucky to have you and Jerry, in my life.

Candi Rocha and Selenny Fabre, thank you for knowing the answers to every question. Thank you for responding to the countless frantic emails/phone calls/drop ins from me over the last 5 years. It has been so lovely to get to know you both and such a pleasure to work with you.

Now I would like to thank my family. To my cousin Kristen, thank you for being such a great role model for me. Thank you for always being willing to share your experience and answer all of my questions. Your advice has been so helpful and encouraging.

To my grandparents, Gloria and Kenneth, thank you for being a constant source of love, support and entertainment. You have always been two of my most dedicated cheerleaders and your faith in me has never waivered. Thank you for your prayers during this whole experience, because as we always say "From Glo's mouth to God's ears". I love you and am so lucky to have you both.

To my sisters, Elyse and Alanna, thank you for always being there to hear me complain. Thank you for always helping me to relax and de-stress. Your daily texts always cheered me up no matter what was going on in the lab. You have been there to support me through it all and I am lucky for it. To my future brother, Paul, thanks for always being willing to listen to me talk about my research. Your genuine interest and willingness to listen have been so heartening to me.

To my parents, Karen and Michael, you instilled in me the need to work hard and never give up. You have supported me in all of my dreams, including this, although I think it turned out to be a lot more than any of us had bargained for. Mom, you never missed an opportunity to help me in whatever way you could, from helping me pick out

outfits for presentations to flying across the country with me to a conference to just talking to me on the phone after a long day. Dad, you inspired me to study science and have been my role model and mentor through it all. I would not be who I am today without you two and I love you both so much.

Finally, Joey, thank you for being everything I ever could have hoped for. Your unwavering support has meant everything to me. Your encouragement, your willingness to come to the lab at all hours of the night, on weekends or holidays, your enthusiasm for listening to me talk endlessly about cardiomyocytes and complain about the long and stressful days have been my saving grace. The past 5 years have been long, and you have sacrificed a lot for my success and I am eternally grateful. Honestly, I think you deserve a degree yourself! I love you and am so lucky to have had you by my side.

TABLE OF CONTENTS

Chapter   **Page**

LIST OF TABLES

LIST OF FIGURES

CHAPTER 1

INTRODUCTION

1.1 The Heart and Cardiovascular Disease

Cardiac muscle, or the myocardium, is a complex tissue with a highly organized extracellular matrix. Collagen fibers throughout the thickness of the tissue are highly aligned which allows for organization of cardiac cells for efficient, coordinated and functional pumping of the heart [1]. Numerous cell types are present in the heart including cardiomyocytes, the functional and contractile cells of the heart, fibroblasts, macrophages, endothelial cells and smooth muscle cells. Cardiac fibroblasts have long been considered to be the most abundant cell type in the myocardium, although recent findings suggest that fibroblasts make up only about 15% of nonmyocytes in the heart [2]. Fibroblasts form a 3D network between cells and tissue layers and are involved in electrical signaling. The vascular network, composed of endothelial cells, is estimated to be within 2-3 μm of any cardiomyocytes in the heart [3,4], with endothelial cells being the most abundant nonmyocyte cell type in the myocardium [2]. Complex paracrine interactions between endothelial cells and cardiomyocytes are important in both the healthy and diseased tissue [3,4]. Very recently, it has also been demonstrated that resident cardiac macrophages contribute to healthy and steady state cardiac function as they facilitate electrical signal propagation in the AV node through intricate interactions with cardiomyocytes via connexin43 gap junctions [5].

Cardiovascular disease, including heart attack or myocardial infarction (MI), is the leading cause of disability and death in the Western world. Every 40 seconds

someone in the United States will suffer a heart attack, amounting to almost 800,000 per year [6]. Twenty percent of heart attacks are silent, or unknown to the patient while over 25% of heart attacks are recurrences [6]. The risk factors associated with MI include high age, smoking and sex, as men are more likely to suffer heart attack, and comorbidities such as high blood pressure, high cholesterol and diabetes [7].

MI is caused by a blockage of the vasculature in the heart leading to ischemia, which results in a large-scale loss of cardiac muscle tissue. Hence, cardiac regenerative medicine has focused on both cell-based [8] and engineered tissue strategies [9] to replace or repair damaged or dead tissue. The most recent clinical trial examining autologous stem cell therapy for treatment post-MI in the United States is PreSERVE-AMI, a randomized, double-blind and placebo controlled Phase II clinical trial [10,11]. PreSERVE-AMI examined the safety and efficacy of intracoronary injection of autologous bone marrow-derived stem cells. These specific endothelial progenitor cells, characterized by CD34 expression (CD34+), migrate from the bone marrow to the site of injury through the circulation and promote neovascularization and tissue regeneration. The initial Phase I trial including 31 patients had found dose dependent improvement in myocardial perfusion[12] but improvements in ejection fraction, scar size or perfusion were not demonstrated in PreSERVE-AMI study including 161 patients [11]. Although CD34+ cells were found to be safe, offering encouragement for continued examination of CD34+ cell-based therapy, they do not offer any re-muscularization of the infarcted tissue.

To complement this strategy, it is imperative to understand the post-MI microenvironment in which cell-based therapies will be deployed. The first stage of healing post-MI is inflammation [13]. It is critical to better understand how macrophages

influence the inflammatory response post-MI, as the prolonging of inflammation is associated with detrimental remodeling and function [14]. Initial damage to the myocardium is followed by extensive tissue remodeling, which leads to structural changes and functional alterations causing a decrease in cardiac pump performance. In order to develop successful therapies for post-MI regeneration, numerous components of the tissue *in vivo* need to be carefully considered [15].

1.2 Cardiac Tissue Engineering

1.2.1 Therapeutic Cell Sources

The number of cardiomyocytes in a human left ventricle is estimated at up to four billion [16-18]. MI is thought to cause the death of nearly one billion [16,17]. The heart is inherently unable to replace the loss of these cells, as adult cardiomyocytes have very limited ability to proliferate [19-22]. Hence, it is imperative to find a reliable cell source for the replacement of lost cardiomyocytes. An ideal cell source for cardiac regenerative medicine would have high proliferative capacity, to replace the large-scale loss of cells, and should have the ability to differentiate into functional cells that can integrate into the myocardial tissue.

Different cell populations have been explored for their potential for cardiac regeneration [23]. One cell type of interest is adult stem cells, including mesenchymal stem cells (MSC) and resident cardiac stem cells (CSC). CSC are a recently discovered population of cells, small in number and highly heterogeneous, present in the adult myocardium that can be extracted and expended *in vitro* [9,24-26]. A clinical trial exploring CSC demonstrated encouraging results [27-29]. However much is still unknown about CSC

and their place in the adult heart and further exploration is necessary.

MSC can be isolated from multiple sources including the bone marrow and adipose tissue [30] [31]. MSC have been demonstrated to differentiate into osteogenic, adipogenic, chondrogenic and cardiac cell types under the correct set of stimuli [32,33] [30,34]. MSC were considered immune privileged, or able to be allogeneically transplanted without immune rejection [35], however more recently, data demonstrates that allogeneic MCS can cause an immune response [36]. MSC are known to secrete factors that promote angiogenesis and stem cell recruitment, prevent apoptosis and contribute to matrix remodeling [37,38] [39]. MSC transplantation has demonstrated improved heart function in animal models of acute myocardial injury [40-42]. Localization of MSC to the site of cardiac injury and improved cardiac function were demonstrated in patients with heart failure [43-49]. However, MSC populations are highly heterogeneous, depending on their tissue of origin, so it is difficult to fully understand their potential [50]. It is also unclear whether MSC can differentiate into functional cardiomyocytes or conversely, induce dedifferentiation and proliferation of endogenous cardiomyocytes [51,52]. Because of this, it has been proposed that improvements in heart function after MSC transplantation are related to secretion of paracrine factors that augment the inflammatory response [53-55]. Therefore, the safety of long-term MSC use and its mechanistic effects for cardiac repair remain to be elucidated.

Pluripotent stem cells, including embryonic (ESC) and induced pluripotent stem (iPSC) cells, have also been explored for regenerative medicine applications. They offer unlimited proliferative ability and have been successfully differentiated toward the cardiac lineage to generate stem cell derived cardiomyocytes [56]. Pluripotent stem cell

differentiation follows a well-defined developmental lineage through mesoderm induction as shown in Figure 1.1. Mesodermal cells differentiate into cardiac progenitor cells exhibiting specific gene markers such as GATA4 and Nkx2.5. Cardiac progenitors then further differentiate into immature cardiomyocytes expressing genes associated with the contractile apparatus such as myosin heavy chain β and cardiac troponin T [57,58]. The goal of differentiation is for the cells to ultimately mature into adult cardiomyocytes exhibiting similar mature cardiomyocyte structure, phenotype and function as seen in the isolated, adult myocyte in Figure 1.1.

Induced pluripotent stem cells (iPSC) add an additional step to the differentiation, as they require first the reprogramming of an adult cell type back to a pluripotent stem cell like cells. The generation of iPSC was seen as a turning point in stem cell research, as it generates a pluripotent stem cell type without the ethical concerns associated with ESC and the potential for autologous sourcing [59]. However, the initial method of reprogramming using viral vectors posed some risks [60-62]. Because of this, other methods have been developed including the using of Cre-loxP sites and treatment with small molecules such as reversine and mir-302 [63-67].

5
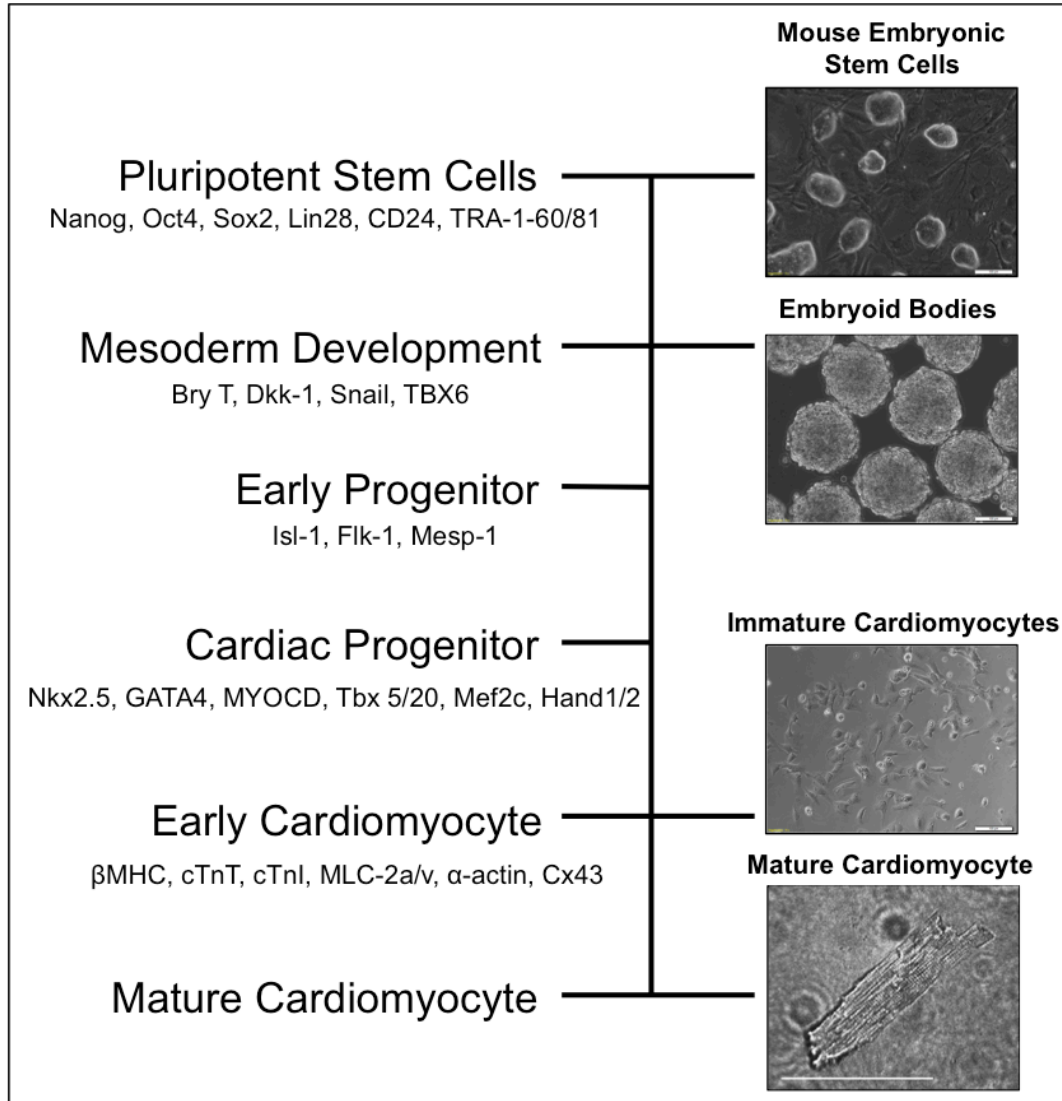
Figure 1.1 Stages of cardiomyogenesis from pluripotent stem cells to mature cardiomyocytes demonstrates changes in cell size, organization, morphology, gene and protein expression (Scale bar = 100 μm).

Source: Hitscherich, P. & Lee, E.J. in Tissue Engineering for Artificial Organs Vol. 2 (ed Anwarul Hasan) (2017).

Differentiation protocols for ESC and iPSC have included the formation of embryoid bodies via hanging drops for mouse derived cells as well as microwell centrifugation or micropatterning for human derived cells [68-71]. Monolayer culture with treatment of activin A and BMP4, treatment with ECM proteins or even co-culture with other cell types, such as END-2 or OP9 cells have been shown to generate differentiated cardiomyocytes from ESC and iPSC [72-75]. Animal models have demonstrated great success in ESC and iPSC-derived cardiomyocytes survival and integration into host tissues, including in nonhuman primates, where ESC-derived cardiomyocytes were shown to not only integrate, but also electrically couple with the host tissue [72,76-84]. However, pluripotent stem cell derived populations remain immature post differentiation displaying heterogeneous phenotype and asynchronous contraction [85].

Immaturity limits the clinical potential of pluripotent stem cell derived cardiomyocytes, as functional maturity is required for excitation-contraction coupling and proper host integration to reduce the risk of secondary side effects such as arrhythmia or even teratoma formation [56]. Because of this, current clinical trials examining cell injection or transplantation for the replacement of lost cardiomyocytes post-MI have only been performed with adult autologous cell sources, most in an undifferentiated state, and have offered only moderate, if any, improvements due to large scale cell death as well as migration away from the injury site [86]. Hence, a more mature pluripotent stem cell derived cardiomyocyte population is essential.

7

1.2.2 Biomaterials

Structural cues are important for tissue organization and function. In the myocardium, the highly organized and anisotropic extracellular matrix [87] is essential for the functional efficiency of the heart and should be considered in cardiac tissue engineering approaches [88]. Specifically, electrical signal propagation is enhanced along the direction of cellular alignment due to the formation of gap junctions. During diseased states when the native myocardial architecture and organization is disturbed, there is increased risk for arrhythmia [88].

One class of biomaterial of interest in cardiac tissue engineering is hydrogels. Hydrogels are highly tunable in their chemical, mechanical and physical properties and can form 3 dimensional culture environment of various shapes and sizes [89]. They can be composed of natural proteins such as collagen or fibrin. Collagen type I is a highly biocompatible, biodegradable material that is present in high degree in most tissues of the body, including the heart [90-93]. Fibrin or collagen combined with Matrigel can be embedded with cardiac cells to form functional cardiac tissues [90,94-98]. These tissues can then be implanted and have caused functional improvements in rat MI models [99-101]. Synthetic materials, such as poly(ethylene glycol) (PEG) have also been explored and found to foster differentiation of pluripotent stem cell derived cardiomyocytes [102,103]. Injectable hydrogels are a newer class of materials that have immense potential for tissue engineering applications as they reduce the risk associated with large, invasive procedures [104,105]. Poly(N-isopropylacrylamide) (PNIPAAM) can form an injectable hydrogel that has been shown to support myocardial contractility by decreasing left ventricular wall stress and promoting angiogenesis and cell migration [106]. Cell embedded

injectable hydrogels have also been explored. Very recently, Hitscherich et al. examined the potential for self-assembling peptide hydrogels for use with ESC [107]. Peptide hydrogels can be tailored to include specific sequences based upon the application of interest and exhibit thixotropic behavior by liquefying under shear stress but retaining shape at rest [107]. Although they have been characterized for dental [108], immune [109] and hind-limb ischemia [110,111] applications, their potential for cardiac tissue engineering application remains to be seen.

Preformed scaffolds are another method for cardiac tissue engineering [88,112,113]. Anisotropic and aligned scaffolds can be generated using fibrous polymers, which can provide structural and mechanical guidance to seeded cells to form cardiac tissue *in vitro*. Common polymers used for tissue engineering applications are inherently insulative and may impede the propagation of electrical signals between cells, increasing the risk of arrhythmia [114]. For electroactive tissues such as the myocardium, electroactive materials might better recapitulate the native myocardial environment.

Since native cardiomyocytes *in vivo* are subjected to constant electrical signals, a number of research groups have developed external electrical stimulation protocols to promote the function and differentiation of cardiomyocytes. Studies have shown enhanced cell-cell coupling and tissue organization as well as improved electrophysiological and calcium-handling properties in stem cell derived cardiomyocytes exposed to electrical stimulation [115,116]. Piezoelectric materials such as poly (vinylidene fluoride-trifluoroethylene) (PVDF-TrFE) generate electrical voltage in response to even minute mechanical deformation allowing for electrical stimulation independent of external sources [117-120]. These surface charge changes have been shown to affect protein

adsorption as well as cellular adhesion and activity [121-123]. The potential for PVDF-TrFE in cardiovascular applications has yet to be determined. Additionally, conductive scaffolds have been shown to enhance cell-cell communication, organization and transmission of electrical potentials that result in increased cardiac marker expression, conduction velocity and beating frequency [114,124,125]. Studies have also demonstrated improved differentiation and enhanced function of pluripotent stem cell derived cardiomyocytes on other 3D conductive scaffolds [114,126,127]. 2D films and composite materials of graphene, a highly conductive carbon derivative, have been shown to be highly biocompatible with adult and pluripotent stem cells as well as primary cardiomyocytes [128-134]. This is in contrast to concerns of cytotoxicity with some of the current conductive hybrid scaffolds limiting their clinical relevance [114,135-137]. However, the functional maturity of these cells and translation of graphene into 3D tissues has yet to be explored.

1.3 Cardiac Inflammation

The post-MI microenvironment is very complex. Lack of oxygen and nutrients causes downstream hypoxia and massive amounts of cell death, igniting both an innate and adaptive immune response. Inflammation plays a crucial role in the pathogenesis of MI injury and considered to be instrumental in determining whether healing will be constructive or maladaptive [14,138,139].

Following MI, macrophages are among the key cells activated during the initial phases of the host response and mediate inflammation [14,140]. Pro-inflammatory or classically activated M1 phenotype macrophages are initially responsible for removing

necrotic cardiomyocytes and fibroblasts along with apoptotic neutrophils that have responded before them [141]. As healing continues, polarization shifts toward the anti-inflammatory or alternatively activated M2 phenotype [142]. It remains unknown what mechanism underlies the polarization shift, but the resolution of inflammation is critical to healing. In fact, a prolonged inflammatory response is associated with dysfunctional matrix deposition, scar formation and heightened cardiomyocytes apoptosis [14].

Despite their critical role in the healing process post-MI, specific interaction between macrophages and surviving resident cardiomyocytes is not known. Additionally, how the inflammatory microenvironment post-MI could affect potential cellular based therapies is also unknown. In recent studies, survival and apoptosis of murine embryonic and adult cardiomyocytes was explored in co-culture with isolated murine macrophages. Cells were examined under normoxic and hypoxic conditions for up to 24 hours to explore the role of CB2 receptor in inflammation after MI [143]. In addition, Trial et al. examined the effect of macrophages activated by fibronectin fragments on the survival of primary rat cardiomyocytes and demonstrated that stimulated macrophages protect cardiomyocytes from apoptosis [144]. The most recent study by Ai *et al.* utilized microfluidic channels to co-culture macrophages with H9c2 myoblasts for up to 3 days [145]. Macrophages polarized by lipopolysaccharides (LPS) into a pro-inflammatory phenotype promoted myocyte apoptosis through mitochondrial damage. These studies are limited however, as none of them examined any phenotypic or functional measures to evaluate the effect of macrophage co-culture. Since *in vivo* exploration is too complex to tease out direct cellular interactions, a controlled *in vitro* model examining macrophage

phenotype specific effects on cardiomyocyte function would aid in the understanding of the post-MI microenvironment.

1.4 Significance and Aims

This dissertation aims to develop fully functional engineered cardiac tissues as well as to better understand the environmental niche for efficient therapy for cardiac regeneration. This is achieved through developing *in vitro* models of healthy cardiac tissue and diseased condition following these specific aims:

- Aim 1: To explore the potential of electroactive scaffolds for the generation of *in vitro* cardiac tissue

- Aim 2: To develop an *in vitro* myocardial inflammation model for a better understanding of the post-MI microenvironment

In **Chapter 2** the potential of a piezoelectric biomaterial to form *in vitro* cardiovascular tissues is investigated [146]. Cardiomyocytes are electroactive cells [147] and electrical stimulation has been considered to promote differentiation and functional maturity of cardiomyocytes *in vitro.* Since piezoelectric materials generate electrical charge in response to mechanical deformation, this feature is especially attractive for cardiac cells that contract. The cytocompatibility and function of mouse embryonic stem cell-derived cardiomyocytes and endothelial cells are investigated.

In **Chapter 3** the benefits and limitation of a conductive, graphene containing biomaterials for the generation of *in vitro* cardiac tissues is explored [148]. Highly conductive materials are especially attractive for cardiac applications, as cardiomyocytes exist in an electrically and mechanically dynamic microenvironment in the heart. In fact, the electro-conductive networks within the myocardium control the contractile behavior

of cardiac cells. Other conductive materials such as carbon nanotubes have shown promise in the promotion of pluripotent stem cell-derived cardiomyocyte maturation. However, their application is limited due to problems with biocompatibility. Hence, the creation of a highly biocompatible scaffold material with conductive networks for the creation of functional cardiac tissues is examined.

What is currently lacking and poorly understood are the implications of the highly complex inflammatory response that occurs after myocardial infarction. No existing models investigate the effects of myocardial inflammation on the function of cardiomyocytes. How specific interaction between cardiomyocytes and activated inflammatory cells, such as macrophages, affect myocardial function is also unknown.

In **Chapter 4**, two myocardial inflammation models are created to examine the interactions between cardiomyocytes and different polarized macrophage subpopulations. This chapter describes specifically how macrophages affect mouse embryonic stem cell-derived cardiomyocyte calcium-handling function. It is important to understand how polarized macrophages affect cardiomyocyte function in order to determine potential therapeutic targets for the improvement of cell-based therapies and post-MI cardiac function.

Chapter 5 includes a summary of the studies with discussion on limitations and future directions for the generation of functional *in vitro* cardiac tissues and myocardial inflammation models.

Together, the work in this dissertation contributes to the current knowledge in cardiac regenerative medicine by demonstrating the potential of two electroactive biomaterials for the formation of functional cardiac tissues and by illuminating a novel

target involved in cardiomyocytes calcium (Ca^{2+}) homeostasis during post-MI healing through an *in vitro* engineered disease model.

CHAPTER 2

PIEZOELECTRIC SCAFFOLD FOR CARDIAC TISSUE ENGINEERING

2.1 Introduction

Cardiovascular disease (CVD) remains one of the leading causes of death and disability in the western world [149]. Since the myocardium has a limited ability to regenerate after injury, cardiac tissue engineering has emerged as a promising approach to repair or replace damaged tissue in the heart. Several groups have explored various types of biomaterials including hydrogels [95,150], fibrous scaffolds [151,152] and cell-mediated biomaterials [153,154] to construct three-dimensional (3D) cardiac tissues. In addition, different cell sources have been explored for cardiac tissue engineering including pluripotent stem cells, with infinite proliferative capacity and the ability to differentiate into cardiac cells. Studies have demonstrated differentiation of human embryonic and induced pluripotent stem cells into cardiomyocytes [56,74,155] and the differentiation methods have been extensively reviewed elsewhere [71]. However, one of the remaining challenges with pluripotent stem cell derived cardiomyocytes is their immature phenotype post differentiation [85].

Native cardiomyocytes undergo continuous mechanical stretching and electrical signaling *in vivo*. As cardiomyocytes are electroactive cells [147], electrical stimulation has been considered to promote differentiation and functional maturity of cardiomyocytes *in vitro*. Radisic *et al.* demonstrated enhanced excitation-contraction coupling and ultrastructural organization in electrically stimulated neonatal ventricular myocytes [116]. Another study demonstrated that electrical stimulation promoted mature

electrophysiological and calcium-handling properties for both human embryonic and induced pluripotent stem cell derived cardiomyocytes [115]. Enhanced ultrastructural organization and alignment as well as decreased expression of fetal cardiac genes, such as α-myosin heavy chain and atrial natriuretic peptide have been demonstrated.

In addition to external electrical stimulation, electrical stimulation through the use of piezoelectric material may be beneficial in inducing functional improvements of cardiomyocytes. Recently, poly (vinylidene) fluoride (PVDF) and its copolymer poly (vinylidene fluoride-trifluoroethylene) (PVDF-TrFE), both exhibiting piezoelectric characteristics, have been explored as potential scaffold materials for tissue engineering applications. Piezoelectric scaffolds possess the intrinsic property of producing an electrical voltage in response to mechanical deformation without the need for external power sources or electrodes [117-120]. While the feasibility of PVDF-TrFE scaffolds for bone and neural cell studies have recently been demonstrated, the effect of PVDF-TrFE scaffolds on cardiovascular cells has not yet been explored. Thus, this study describes the viability, phenotype, and function of both mouse embryonic stem (mES) cell derived cardiomyocytes (mES-CM) and endothelial cells (mES-EC) on PVDF-TrFE scaffolds to determine the feasibility of PVDF-TrFE scaffolds for cardiovascular tissue engineering applications.

2.2 Methods

2.2.1 Mouse Embryonic Stem (mES) Cell Culture and Differentiation

A stable cardiac troponinT-eGFP mES cell line (generous gift from Dr. Yibing Qyang at Yale University) was used. MES cells were cultured on a mouse embryonic fibroblast (Global Stem, MD) feeder layer for 2 days in a DMEM medium supplemented with 15% knockout serum replacement, 1% NEAA, sodium-pyruvate, penicillin/streptomycin (Gibco, NY), 2-mercaptoethanol (Sigma Aldrich, MO) and leukemia inhibiting factor (LIF, 5ng/mL). To differentiate mES cells into cardiomyocytes, mES cells were transferred to and cultured in a feeder-free condition with IMDM medium supplemented with 15% knockout serum replacement, 1% penicillin/streptomycin (GIBCO, NY),

Figure 2.1 Schematic of mES-CM differentiation via hanging drop method.

Thioglycerol (Sigma Aldrich, MO) and LIF (5ng/mL) for 2 days. Embryoid bodies (EBs) were then formed by a hanging drop method, as described previously [68]. After 2 days, EBs were collected in a differentiation medium containing IMDM medium supplemented with 15% fetal bovine serum, L-glutamine (GIBCO, NY), ascorbic acid and thioglycerol (Sigma Aldrich, MO) and cultured for 8-9 additional days. Spontaneously contracting and GFP positive cells were yielded starting as early as differentiation day 6-7. MES-CM were purified on day 10-11 of differentiation using a discontinuous Percoll (GE Healthcare) separation technique [57,156,157]. Purity of mES-CM was assessed by fluorescent imaging by counting the number of GFP positive cells to the total number of cells post-purification. A schematic of mES-CM differentiation can be seen in Figure 2.1.

2.2.2 Endothelial Cell Culture

Endothelial cells (EC) were derived from mES cells as previously described [158]. MES-ECs were cultured in MCDB complete endothelial growth medium containing 10% FBS, 1% penicillin-streptomycin and Endogro (VEC Technologies, NY) in 0.1% gelatin (Sigma Aldrich, MO) coated flasks. Fresh culture medium was exchanged every 2 days. MES-ECs were passaged when they reached 80% confluency using 0.25% trypsin-EDTA (Gibco, NY). MES-ECs of passage 6 to 11 were used in this study.

2.2.3 Fabrication and Characterization of PVDF-TrFE Scaffolds

Electrospun PVDF-TrFE scaffolds having aligned fibers were fabricated and characterized as previously described [119,159]. Briefly, PVDF-TrFE (65/35) (Solvay Solexis, Inc.) was dissolved in methyl ethyl ketone and electrospun using a fast rotating

drum to collect aligned fibers. Scaffolds were annealed via heating at 135°C for 96 hours followed by cooling in ice water. The annealed and aligned PVDF-TrFE scaffolds exhibited an elastic modulus of 359.77±143.26 MPa and an ultimate tensile strength of 21.42±9.62 MPa along the fiber axis [119]. The average fiber diameter of 575±139 nm and the average fiber alignments of 89%±10% were obtained by analyzing scanning electron micrographs using ImageJ, as previously described [159]. For fiber alignment, a line was drawn perpendicular to the major axis of fibers and angular difference among the fibers was calculated. The average alignment was calculated by using the following equation:

$$\text{Alignment} = \frac{(90° - \text{angular difference})}{90°} \qquad (2.1)$$

2.2.4 Cell Seeding onto Scaffolds

Scaffolds of 0.5 cm x 0.5 cm (Figure 2.2A) with thickness ranging from 0.1 to 0.25 mm thickness were UV sterilized followed by preconditioning in 20% FBS containing culture medium overnight. Scaffolds were then left to dry for 30 minutes prior to cell seeding. MES-CM or mES-EC were seeded onto pre-treated scaffolds at a density of 8×10^6 cells/cm^2 and were left to attach for 2.5 hours before additional culture medium was added. MES-CM seeded scaffolds were cultured in the differentiation medium as described above, and mES-EC were cultured in MCDB complete medium for 6 days prior to characterization. Both cell types on 2D culture dishes served as controls.
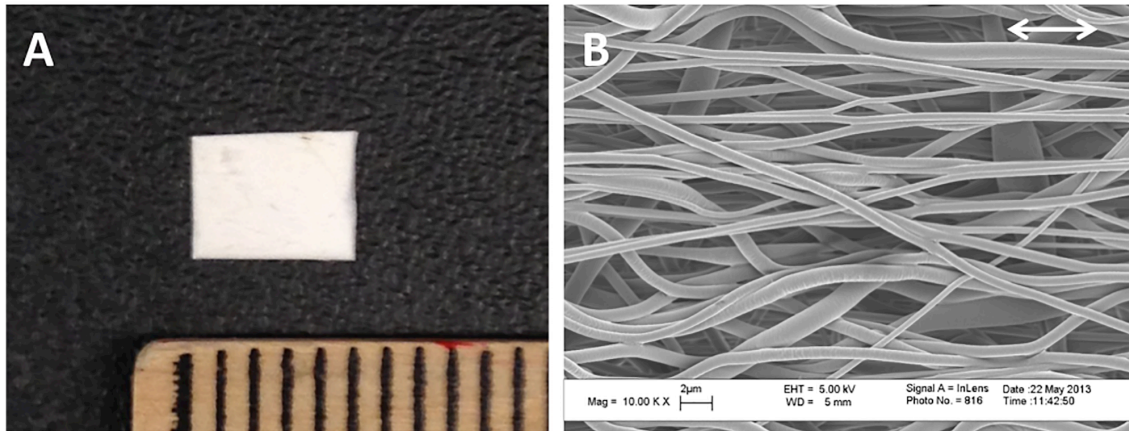
Figure 2.2 (A) Macroscopic image of PVDF-TrFE scaffold used for cell seeding, Scale bar = 1 mm/tick mark. (B) Scanning electron microscope image of a PVDF-TrFE scaffold with aligned fibers. Arrows indicate principle fiber axis.
*Source: Hitscherich, P. et al. The Effect of PVDF-TrFE Scaffolds on Stem Cell Derived Cardiovascular Cells. Biotechnol. Bioeng. **113**, 1577-85, (2016).*

2.2.5 Cell Viability

A LIVE/DEAD Viability/Cytotoxicity kit (Life Technologies, NY) was used to determine viability of cells on scaffolds after 3 and 6 days of culture. Briefly, scaffolds were rinsed with warm PBS and then stained with 0.2 M ethidium homodimer and 0.005 M calcein for 30 minutes at 37 °C. Immunofluorescent images were obtained using a confocal fluorescence microscope (IX81 DSU, Olympus, Somerset, NJ) and the ratio of live/dead cells to the total number of cells was analyzed using ImageJ software.

2.2.6 Immunofluorescence Imaging

The use of a stable cardiac troponinT-eGFP mES cell line allowed examination of cardiac troponin T expression by mES-CM during culture. GFP expression of mES-CM was

visualized using a confocal fluorescence microscope (IX81 DSU, Olympus, Somerset, NJ).

2.2.7 F-actin Imaging

For the visualization of sarcomeres, samples including mES-CM seeded scaffolds and 2D control cells were fixed overnight using 4% formaldehyde (Sigma Aldrich, MO) after 6 days of culture. Samples were stained for F-actin using Rhodamine-conjugated phalloidin (1:20, Life Technologies, NY) for 2 hours at room temperature and were counter-stained with DAPI to visualize nuclei.

2.2.8 Low Density Lipoprotein Assay

To determine the phenotype of mES-EC on the scaffolds, low-density lipoprotein (LDL, Alfa Aesar, MA) uptake was performed. Scaffolds were incubated with a 1:10 dilution of LDL to culture medium for 4 hours at 37 °C and 5% CO_2 and then washed twice with culture medium before imaging with a confocal fluorescence microscope (IX81 DSU, Olympus, Somerset, NJ).

2.2.9 Western Blot Analysis

After 6 days of culture, cell lysates of scaffolds and controls were prepared using a lysis buffer containing RIPA buffer, 1% Triton X100 (Boston BioProducts, MA) and 1% protease inhibitor (Sigma Aldrich, MO). Samples were then diluted 1:1 in Laemmli SDS buffer (Bio-rad, CA) with 5% 2-mercaptoethanol (Sigma Aldrich, MO). Primary antibodies used for mES-CM samples were mouse anti-cardiac troponin T (cTnT, 1:1000,

Abcam, MA), rabbit anti-connexin43 (Cx43, 1:3000, Abcam, MA) and mouse anti-heavy chain cardiac myosin (MHC, 1:1000, Abcam, MA). Primary antibodies used for mES-EC samples were rabbit anti-endothelial nitric oxide synthase (eNOS, 1:200, Santa Cruz Biotechnology, TX), rabbit anti-ephrin type B receptor 4 (EphB4, 1:500, Santa Cruz Biotechnology, TX), mouse anti-thrombomodulin (TM, 1:500, Abcam, MA), rabbit anti-Notch1 (1:500, Santa Cruz Biotechnology, TX) and rabbit anti-platelet endothelial cell adhesion molecule (PECAM1, 1:200, Santa Cruz Biotechnology, TX). Mouse anti-β-actin (1:2000, Sigma Aldrich, MO) was used as a loading control. Secondary antibodies used were goat anti-rabbit (1:2000, Santa Cruz Biotechnology, TX) and goat anti-mouse (1:2000, Santa Cruz Biotechnology, TX). Fresh fetal rat heart homogenates, mES cell lysates and 2D plated mES-CM lysates served as controls for mES-CM samples. Rat aortic endothelial cell (RAEC) lysate, mES cell lysate and 2D cultured mES-EC lysates served as controls for mES-EC samples. For quantitative analysis, protein bands were normalized to the loading control, β-actin, and analyzed using densitometry (ImageJ).

2.2.10 Evaluation of Calcium-Handling

After 6 days of culture, 2D mES-CM and scaffold samples were digested to a single cell suspension via collagenase (0.1 g/mL, Roche, NJ) and accutase (GIBCO, NY) treatment for single cell calcium-handling analysis. Digested cells were reseeded onto collagen-coated (50 μg/mL collagen, BD Biosciences, CA) glass bottom dishes overnight. Intracellular Ca^{2+} transients were examined as previously described [160,161]. Briefly, samples were incubated at room temperature with Rhod-2AM (4 μM) for 30 minutes, followed by a 20 minutes washout (for AM cleavage) in normal Tyrode's solution.

Samples were then placed in a heated chamber (35˚C) with a fluorescent inverted microscope (Nikon Eclipse TE200) with an Andor Ixon Charge-Coupled device (CCD) camera (Andor Technology, at 50 frames/s, 512 x 180 pixels). The intensity of fluorescence from spontaneously contracting cells was recorded and normalized to the basal diastolic fluorescence levels. Cells were electrically stimulated to examine their response to electrical pacing at 0.5, 1 and 2 Hz frequencies (4.5 ms duration, 150 V, Grass S48 Stimulator, Grass Medical Instruments, West Warwick, RI). In addition, cells were treated with 10 mM caffeine, a ryanodine receptor agonist, to investigate sarcoplasmic reticulum Ca^{2+} content and fractional Ca^{2+} release. Cell response to β-adrenergic stimulation was also examined with the treatment of 1μM isoproterenol.

2.2.11 Statistical Analysis

Results are presented as mean ± SEM. Statistical analysis of cell viability and beating frequency was performed with an independent-samples t-test. Statistical analysis of protein expression of mES-CM and mES-EC as well as functional properties of mES-CM in 2D and on PVDF-TrFE scaffolds were analyzed via independent-samples t-test, or the nonparametric alternative, Mann-Whitney U Test. Statistical significance was accepted for $p<0.05$.

2.3 Results

2.3.1 Characterization of mES-CM in 2D

Through a previously described method [68], mES-CM were successfully derived from mES cells. Spontaneously contracting cells were yielded as early as 6 days into the differentiation process. Since a stable mES cTnT-eGFP cell line was used, differentiated cardiomyocytes expressing cTnT gene exhibited extensive GFP expression (Figure 2.3A). Higher expression of GFP was observed with more days in culture. The average beating frequency of purified mES-CM was 1.14 ± 0.12 Hz on day 6 of culture. Figure 2.3B demonstrates that mES-CM exhibit well-registered sarcomeres as shown by F-actin staining. Moreover, they express classical cardiac specific markers such as MHC, cTnT, and gap junction protein Cx43 as demonstrated by western blot analysis (Figure 2.3C). As expected, there was a significant increase in the expression of both cTnT and MHC in mES-CM compared to mES ($p < 0.05$). Cx43 expression was not significantly different, as mES cells are known to express Cx43 in their undifferentiated state as well [162].
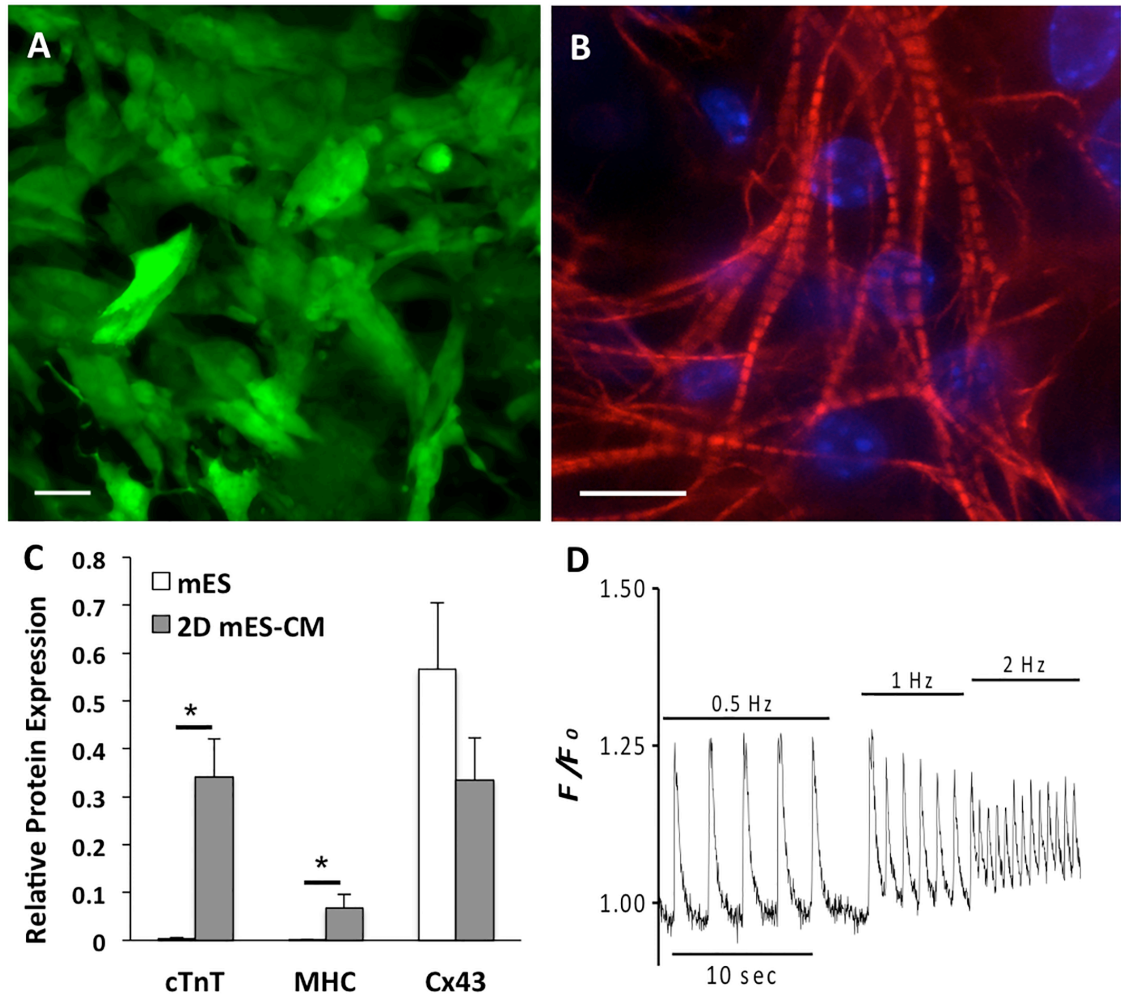
Figure 2.3 (A) Expression of cTnT-eGFP by mES-CM in 2D culture, Scale bar=20 μm. (B) Well-registered sarcomeres were demonstrated in mES-CM in 2D culture. F-actin in red and DAPI stained nuclei in blue, Scale bar=10 μm. (C) Quantitative analysis of protein expression of Cx43, MHC and cTnT by mES and mES-CM cultured in 2D. MES-CM expressed significantly higher amounts of cTnT and MHC ($p < 0.05$), however similar Cx43 expression was shown, n=4, mean± SEM. (D) MES-CM response to exogenous electrical pacing at 0.5, 1 and 2 Hz, respectively.

*Source: Hitscherich, P. et al. The Effect of PVDF-TrFE Scaffolds on Stem Cell Derived Cardiovascular Cells. Biotechnol. Bioeng. **113**, 1577-85, (2016).*

To examine contractile and electrophysiological performance of mES-CM, intracellular Ca^{2+} transients were measured from single cells. The digestion of 2D cultured mES-CM was necessary to provide consistent treatment as the cells cultured on the scaffolds. Digested cells adhered well and initiated spontaneous contraction within 24 hours. MES-CM also responded to external electrical pacing at varying frequencies such as 0.5, 1 and 2 Hz frequencies (Figure 2.3D).

2.3.2 Characterization of mES-CM on PVDF-TrFE Scaffolds

Purified mES-CM were seeded onto PVDF-TrFE scaffolds at a density of 8 x 10^6 cells per cm^2 to achieve complete and consistent coverage of cells on the scaffolds. Cells required a minimum of 2 hours to attach to preconditioned scaffolds. Within 24-48 hours post seeding, cells were not only fully adhered, but also initiated spontaneous contraction. Live/dead assay revealed that most of the cells remain viable on the scaffolds exhibiting 99.90 % viability on day 3 (Figure 2.4A) and 99.70 % viability on day 6 with no significant changes. MES-CM became highly aligned in the direction of the fiber alignment and GFP expression was evident throughout the culture period, as shown in Figure 2.4B. Strong expression of GFP indicates high expression of cTnT by mES-CM. Cells exhibited spontaneous contractions after 3-4 days of culture resulting in synchronous contraction of entire scaffolds, which can be detected under the microscope. Beating frequency of mES-CM on scaffolds was approximately 1.49 ± 0.19 Hz, which was similar to that of 2D cultured mES-CM after 6 days of culture. Confocal fluorescent microscopy of mES-CM seeded scaffolds revealed a homogeneous distribution of highly aligned mES-CM with well-developed myofilaments having registered sarcomeres
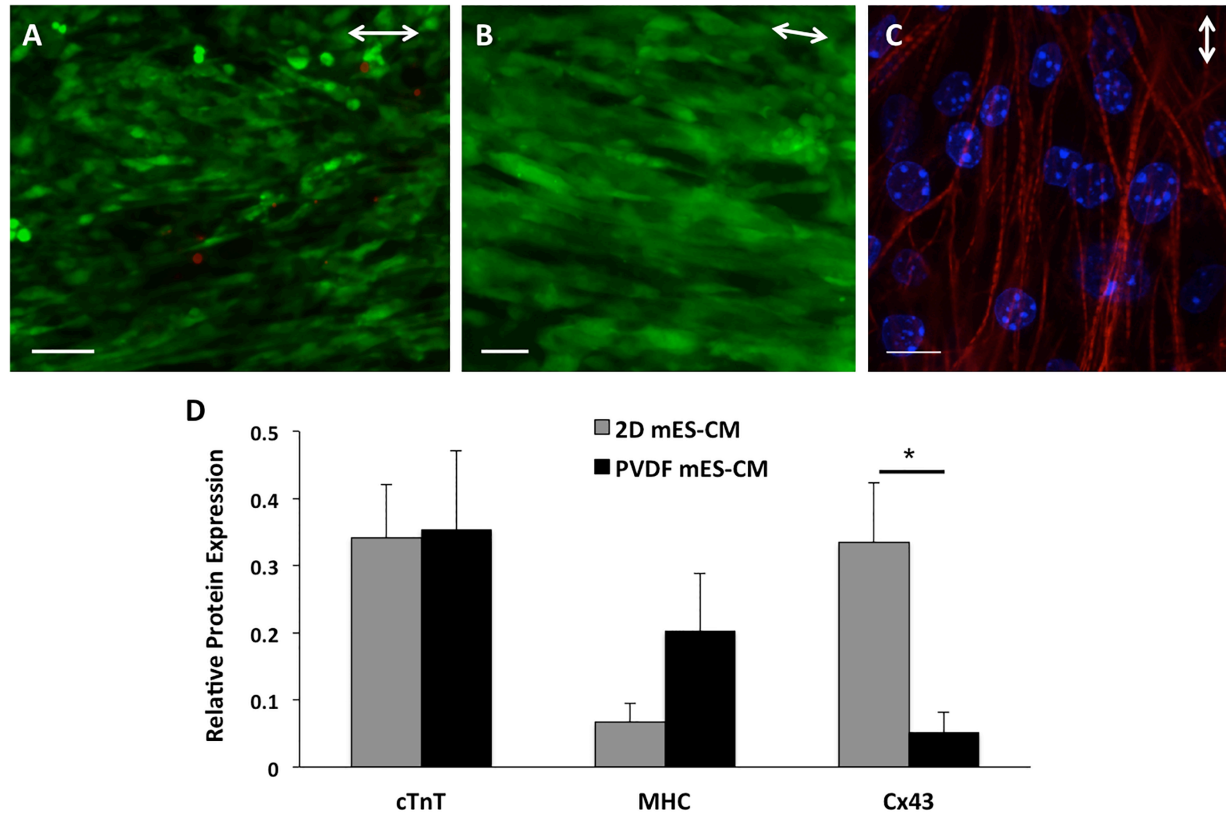
Figure 2.4 Characterization of mES-CM on annealed and aligned PVDF-TrFE scaffolds. (A) Over 99.9% cell viability was evident on day 3 of culture. Live cells stained green with calcein and dead cells stained red with ethidium homodimer, Scale bar=50 μm. (B) Strong cTnT-eGFP expression is shown on day 6, Scale bar=20 μm. (C) Immunofluorescent analysis revealed highly aligned actin filaments with well-registered sarcomeres. F-actin in red and DAPI stained nuclei in blue, Scale bar=10 μm. (D) Quantitative analysis of protein expression of Cx43, MHC and cTnT in mES-CM cultured on PVDF-TrFE scaffolds (n=4,) compared to mES-CM cultured in 2D (n=10), mean ± SEM. No significant difference was found among groups. Arrows indicate principle fiber axis.

Source: Hitscherich, P. et al. The Effect of PVDF-TrFE Scaffolds on Stem Cell Derived Cardiovascular Cells. Biotechnol. Bioeng. 113, 1577-85, (2016).

(Figure 2.4C). MES-CM on scaffolds also expressed cardiac specific markers such as cTnT, MHC and Cx43. No statistical difference was found in the MHC and cTnT expression, but expression by mES-CM cultured on PVDF-TrFE scaffolds appeared higher than in 2D, while Cx43 expression was significantly higher in mES-CM cultured in 2D (Figure 2.4D, p<0.05).

To compare the contractile and electrophysiological performance of mES-CM seeded on PVDF-TrFE scaffolds with mES-CM cultured in 2D, intracellular Ca^{2+} transients were measured on digested single cells. Digested cells adhered well to collagen-coated dishes and spontaneously contracted within 24 hours. The amplitude and morphology/duration of the Ca^{2+} transients, fractional Ca^{2+} release, and response to β-adrenergic stimulation using 1 μM isoproterenol were compared with 2D mES-CM. MES-CM cultured on scaffolds responded to pacing at 0.5, 1 and 2 Hz frequencies, similar to mES-CM cultured in 2D. The average Ca^{2+} transient amplitude, which indicates the amount of Ca^{2+} release and uptake within the cytoplasm, trended higher than mES-CM cultured in 2D (0.20 ± 0.01 vs. 0.29 ± 0.05). The average time to 50% of that peak amplitude (T_{50}) for mES-CM cultured on PVDF-TrFE scaffolds was significantly longer (p<0.05) than that of mES-CM cultured in 2D (143.17 ± 21.67 ms vs. 220.30 ± 39.19 ms). To assess the functional capacity of the sarcoplasmic reticulum (SR), 10 mM caffeine was added to the cells. Treatment with caffeine resulted in complete Ca^{2+} release from the SR, indicating functional SR calcium-handling properties and ryanodine receptor (RyRs) function, as shown in Figure 2.5A and 4B. The average amplitude and T_{50} of caffeine-induced Ca^{2+} release was 0.84 ± 0.07 and 1819.03 ± 427.85 ms, respectively for mES-CM cultured in 2D.
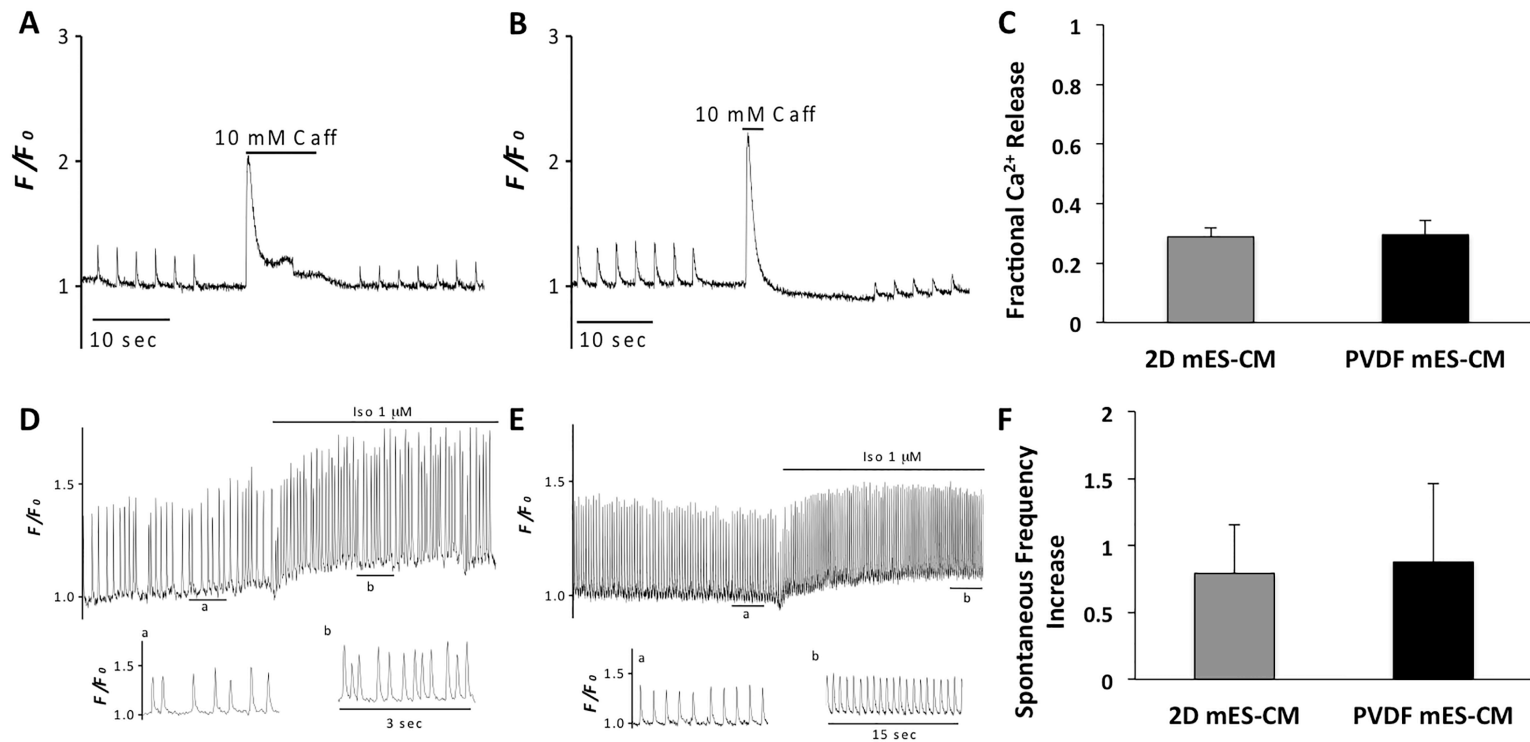
Figure 2.5 (A, B) Representative traces demonstrating Ca^{2+} transients and caffeine-induced SR Ca^{2+} release of mES-CM cultured in 2D and on PVDF-TrFE scaffolds, respectively. The Ca^{2+} transients were induced by electrical field stimulation at 0.5 Hz. (C) Comparison of fractional release of mES-CM cultured in 2D (n=20) vs. on PVDF-TrFE scaffolds (n=10). No significant difference was found between culture conditions. (D, E) Representative traces demonstrating the effect of β-adrenergic stimulation via treatment with isoproterenol on spontaneous Ca^{2+} transients. (F) Comparison of spontaneous frequency increase associated with β-adrenergic stimulation of mES-CM cultured in 2D (n=5) vs. on PVDF-TrFE scaffolds (n=4), mean± SEM.

*Source: Hitscherich, P. et al. The Effect of PVDF-TrFE Scaffolds on Stem Cell Derived Cardiovascular Cells. Biotechnol. Bioeng. **113**, 1577-85, (2016).*

Similar results were seen for mES-CM cultured on PVDF-TrFE scaffolds, having an amplitude of 1.02 ± 0.15 and T_{50} of 1141.99 ± 261.83 ms. The average fractional release, which demonstrates the amount of Ca^{2+} released per transient versus total Ca^{2+} content trended higher in mES-CM cultured on scaffolds than mES-CM in 2D ($26.34 \pm 2.27\%$ vs. $29.47 \pm 4.89\%$), as seen in Figure 2.5C. Moreover, the addition of 1 μM of isoproterenol, a β-adrenergic agonist, led to increased amplitude and frequency of Ca^{2+} transients by both mES-CM in 2D culture (Figure 2.5D) and on scaffolds (Figure 2.5E). The frequency was increased by approximately 42% and 88% for mES-CM cultured in 2D and on scaffolds, respectively (Figure 2.5F), indicating that mES-CM respond to β-adrenergic stimulation.

2.3.3 Characterization of mES-EC on PVDF-TrFE Scaffolds

To assess the biocompatibility of PVDF-TrFE scaffolds with vascular cells, mES-EC were seeded at the same density as mES-CM. Cells adhered well to preconditioned scaffolds within the first 2 hours of seeding and remained highly viable for 6 days as shown with viability assay (Figure 2.6A). No significant decrease in the number of viable cells were observed on day 6 compared to day 3 as samples from both days exhibited over 99.9 % viability. MES-EC cultured on scaffolds demonstrated an uptake of LDL, an indicator of mature mES-EC phenotype (Figure 2.6B). In addition, western blotting densitometry analysis showed high expression of endothelial cell markers including PECAM1, eNOS, and Notch1, similar to that of mES-EC cultured in 2D, further confirming the maintenance of EC phenotype on the PVDF-TrFE scaffolds (Figure 2.6C).
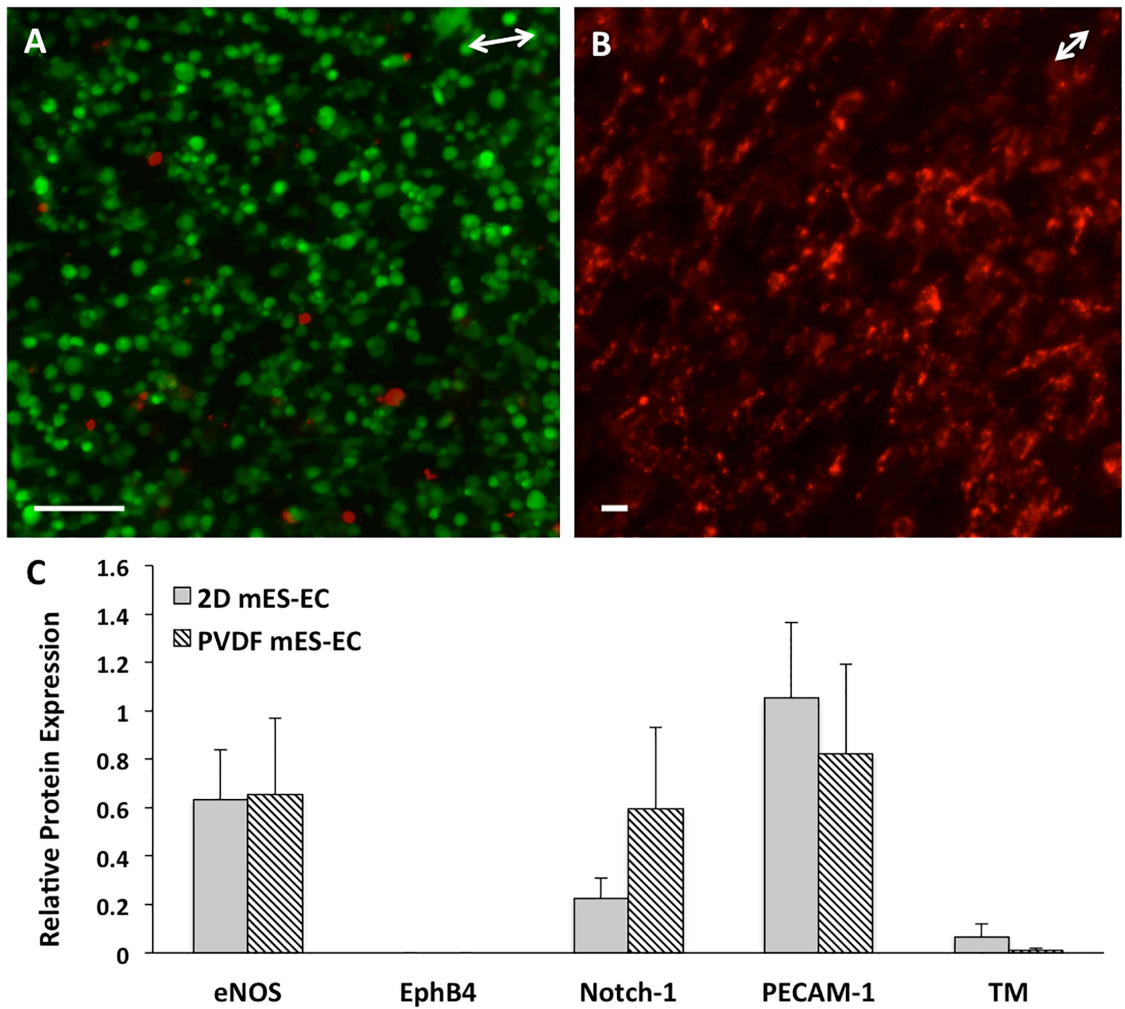
Figure 2.6 (A) Live/dead staining of mES-EC on PVDF-TrFE showing over 99.9% viability after day 3. Live cells stained green with calcein and dead stained red with ethidium homodimer, Scale bar=50 μm (B) LDL uptake by mES-EC cultured on PVDF-TrFE scaffolds shown in red after 6 days in culture, Scale bar=50 μm (C) Quantitative analysis of protein expression of eNOS, EphB4, Notch-1, PECAM-1 and TM in mES-EC cultured in 2D or on PVDF-TrFE scaffolds. No significant difference was found between groups, n=3 for EphB4, all other groups n=4. Arrows indicate principle fiber axis.

*Source: Hitscherich, P. et al. The Effect of PVDF-TrFE Scaffolds on Stem Cell Derived Cardiovascular Cells. Biotechnol. Bioeng. **113**, 1577-85, (2016).*

2.4 Discussion

This study describes the structural and functional properties of cardiovascular cells derived from mouse embryonic stem cells on PVDF-TrFE scaffolds. Electroactive, piezoelectric scaffolds have the intrinsic property of producing an electrical voltage in response to a mechanical deformation without the need for external power sources or electrodes [117]. Since cardiomyocytes exist in an electrically and mechanically dynamic and complex microenvironment in the heart and the contractile behavior of cardiac cells is controlled by the electro-conductive networks within the cardiac tissue [163], the unique features of electroactive materials are especially attractive for cardiovascular tissue engineering applications. In addition, the piezoelectric properties of the scaffold that results in changes in surface charge have the potential to affect protein adsorption, cellular adhesion and cellular activity [121-123], which may affect differentiation of stem cell derived cardiovascular cells.

In this study, a mouse embryonic stem cell line was characterized in a peptide hydrogel to demonstrate its potential to differentiate into all 3 germ layers. Specifically, cardiomyocytes and vascular endothelial cells derived from mouse embryonic stem cells were cultured on PVDF-TrFE scaffold for the first time. MES-CM were successfully derived using a differentiation protocol which does not require any supplemental growth factors added to the culture, but yet yields a high differentiation efficacy [68]. Moreover, our cardiac troponinT-eGFP mES cells allow us to sort GFP+ cardiomyocytes expressing cardiac troponin T and thereby give us an advantage of obtaining a high-purity cardiomyocyte population. MES-EC were also successfully derived as described in our previous study [158].

Our results show that PVDF-TrFE scaffolds support the attachment and survival of both cardiovascular cell types. Both mES-CM and mES-EC adhered well to the scaffolds with negligible numbers of apoptotic cells during 6 days of culture, without requiring additional surface coating. MES-CM spread and aligned along with the fibers resulting in a highly aligned cardiac tissue. PVDF-TrFE scaffold also support the contractile behavior of mES-CM as cells initiate spontaneous contraction as early as 24 hours post-seeding and becomes more evident with longer cultures. MES-CM on PVDF-TrFE exhibited well-registered sarcomeres demonstrating the presences of a functional contractile unit. The average beating frequency of mES-CM in 2D culture and on PVDF-TrFE scaffolds is similar to that of previous studies using mES-CM [164,165] as well as human iPSC-derived cardiomyocytes [166]. Moreover, cells on the scaffolds showed increased expression of both cTnT and MHC compared to that of 2D cultured mES-CM, although they were not statistically different. The expression of sarcomeric proteins such as cTnT and MHC provides basic assessment of contractile function of mES-CM. MES-CM also express the gap junction protein Cx43 on PVDV-TrFE scaffolds, indicating communication between adjacent cells for proper propagation of electrical signals within the tissue [167]. Since it has previously been reported that long term *in vitro* culture is required to obtain fully matured stem cell-derived cardiomyocytes [168], it is plausible that longer term culture may be required to see the changes in the expression of proteins in our samples.

To further characterize the function, calcium-handling properties of mES-CM were examined. Functional handling of Ca^{2+} is one of the most widely characterized parameters in stem cell-derived cardiomyocytes, which is necessary for cardiomyocytes

excitation contraction coupling and integration into host tissue [169,170]. A common method of obtaining calcium-handling properties is through a single cell analysis, which requires digestion of intact tissues into single cell preparation. To maintain the consistency between samples, both mES-CM in 2D culture and mES-CM on scaffolds were digested and re-seeded onto glass bottom dishes for analysis. MES-CM in both 2D and on scaffolds exhibited similar Ca^{2+} transient morphology and amplitude. However, transient duration, as expressed by T_{50}, was significantly longer for mES-CM cultured on scaffolds compared to mES-CM cultured in 2D. It is possible that culture on PVDF-TrFE scaffolds increases phospholamban production by mES-CM, which would inhibit SERCA and slow the reuptake of free Ca^{2+} ions as shown in canine skeletal muscle with constant low frequency stimulation [171]. In addition, caffeine-induced Ca^{2+} release by mES-CM suggests that these cells have functional SR release through the RyRs, which is essential for normal Ca^{2+}-induced Ca^{2+} release and excitation contraction coupling [169,172]. The trend of increasing fractional Ca^{2+} release, demonstrated by mES-CM cultured on scaffolds compared to mES-CM cultured in 2D suggests that a longer culture period on PVDF-TrFE scaffolds may promote fractional Ca^{2+} release that is similar to native cardiomyocytes. It is shown that the physiological fractional Ca^{2+} release of adult left ventricular rat cardiomyocytes is between 60-70% [173]. The increase in spontaneous contraction frequency in both mES-CM cultured in 2D and on PVDF-TrFE, with the treatment of isoproterenol, also suggests that these cells exhibit positive chronotropic responses to β-adrenergic stimulation, which is a hallmark of adult cardiomyocytes [58,98].

Similar to mES-CM, mES-EC remained highly viable and expressed classical endothelial makers such as eNOS, PECAM1 and TM on scaffolds. This demonstrates that

the PVDF-TrFE scaffolds support and maintain the phenotype of endothelial cells, which is known to be often altered in *in vitro* cultures [174]. Interestingly, mES-EC on scaffolds trended higher expression of Notch1, a common arterial marker, compared to 2D culture, suggesting that culture on PVDF-TrFE may also support arterial specialization [175]. Since Notch1 and Notch signaling are important for functional vascular development and vascular integrity, this increase in expression may potentially aid in the development of neovascularization. Further studies however are needed to examine the effects of Notch1 on endothelial cell differentiations as well as the signaling mechanisms involved with angiogenesis [176]. Moreover, mES-EC cultured on scaffolds retaining their ability to uptake LDL, a known characteristic of mature endothelial cells, further confirms the compatibility of PVDF-TrFE scaffold for vascular endothelial cell culture.

Given the increasing interest in electroactive materials for tissue engineering, piezoelectric PVDF-TrFE scaffolds provide a promising option for developing more advanced cardiovascular tissue constructs. However, they may require exogenous stimulation in order to achieve their full potential. Further studies of interest would be implantation into a mouse MI model to determine whether PVDF-TrFE fosters tissue integration. Scaffold would also be under constant mechanical stimulation due to the beating of the host heart, which could aid in further differentiation of mES-CM through the piezoelectric activity of the scaffold. PVDF is also a non-biodegradable material [177], which may be desirable for load bearing applications, but may limit its potential in soft tissue related applications as it increases the chances of an immune response and hence, different electroactive materials should also be explored.

CHAPTER 3

A CONDUCTIVE SCAFFOLD FOR CARDIAC TISSUE ENGINEERING

3.1 Introduction

Various biocompatible polymers, including poly-glycerol sebacate [178,179], collagen [95], and poly-caprolactone (PCL) [180] have widely been explored as candidate materials for engineered cardiac tissues. However, their inherent insulative properties may impede electrical signal propagation for electro-active cell types [114].

Conductive nanomaterials such as carbon nanotubes (CNTs) and graphene with unique electrical [136,181], mechanical, and thermal properties [182] have recently emerged as promising candidates for various biomedical applications including functional engineered tissue growth [183,184]. The highly conductive feature of graphene and CNTs is especially attractive for cardiomyocyte culture since cardiomyocytes exist in an electrically and mechanically dynamic microenvironment in the heart where the contractile behavior of cardiac cells is controlled by the electro-conductive networks within the myocardium [163].

Recent studies have demonstrated the potential of scaffolds composed of conductive polymers as well as conductive composite scaffolds and hydrogels with embedded conductive particles [114,124,125]. Specifically, CNTs have been shown to increase spontaneous beating rate and conduction velocity of neonatal cardiac cells promoting their electrophysiological properties [114,126,127,185-187]. However, the application of pristine CNTs for tissue engineering has been limited due to its cytotoxicity. *In vitro* studies have demonstrated that CNTs promote cell apoptosis through multiple mechanisms including mitochondrial [188,189] and lysosomal damage [190]. CNTs have also been implicated in the

formation of reactive oxygen species indicative of oxidative stress, which can damage proteins and alter gene expression [191]. Decreased proliferation and necrosis of various cell types has also been demonstrated after exposure to CNTs [192]. A previous *in vivo* study performed by Yamaguchi *et al.* demonstrated sustained pro-inflammatory response to CNTs resulting in changes in liver size, shape and fibrous deposits on other internal organs [193]. CNT exposure has been linked to blood clots and heart disease in humans as well [194]. It is suggested that the biocompatibility of pristine CNTs may be enhanced through functionalization, although this would alter their unique electrical properties [195,196].

Another conductive material, graphene, has also been explored for cell and tissue application. 2D forms of graphene, such as in coated slides or films, have been explored for cardiomyogenic differentiation of a few cell types including human pluripotent stem cells [128,197] and mesenchymal stem cells [130]. It is also shown that graphene particles mixed within embryoid bodies enhanced spontaneous cardiomyocyte differentiation [198]. Sayyer *et al.* created a 3D composite scaffold (rGO-PCL) using reduced graphene oxide and poly(caprolactone) via precipitation techniques, demonstrating viability and proliferation of L929 fibroblasts and C2C12 myoblasts after 2 days of culture [131]. Similarly, Murray *et al.* demonstrated attachment and proliferation of L929 fibroblasts on rGO-PCL composite scaffolds formed via microwave assisted polymerization [199]. These fabrication techniques, however, do not allow for specific organization of fiber orientation.

Here, nanofibrous scaffolds fabricated using poly(caprolactone) and graphene by electrospinning technique have been characterized for their feasibility and potential for cardiac tissue engineering application [148]. Scaffolds with as little as 0.01% graphene

demonstrated increased volume conductivity and an even distribution of graphene particles. Graphene particles provided local conductive sites within the PCL matrix, which enabled application of external electrical stimulation throughout the scaffold using a custom point stimulation device. To determine the biocompatibility and feasibility of graphene containing scaffolds, mouse embryonic stem cell-derived cardiomyocytes were used. The viability, phenotype, and function of embryonic stem cell derived cardiomyocytes cultured on 3D graphene-containing scaffolds were examined. Unlike CNTs that exhibit cytotoxicity, graphene-containing scaffolds provided a biocompatible niche for stem cell-derived cardiomyocytes. Moreover, enhanced functional calcium-handling properties of cardiomyocytes on graphene-containing scaffolds was demonstrated, which suggests the potential of these electroactive scaffolds as next generation engineered cardiac tissue for cardiac repair.

3.2 Methods

3.2.1 Scaffold Fabrication

Poly(caprolactone) (PCL) pellets (Sigma Aldrich, St. Louis, MO) were dissolved in acetone solvent and stirred at 60°C until a clear solution was achieved. For composite scaffolds, graphene (G) particles (Cheap Tubes Inc., Cambridgeport, VT) were then dispersed within the PCL solution via sonication for 1hr at room temperature. 15% PCL scaffolds with 0.01% graphene (PCL+G) were prepared via electrospinning to achieve randomly oriented fibers as well as highly aligned fiber orientation (17 kV, 15 cm, 1.5 mL/hr) as previously described [200].

3.2.2 Scaffold Characterization

3.2.2.1 Scanning Electron Microscopy. The morphological characterization of nanofibers and visualization of graphene nanoparticles was performed using scanning electron microscopy (SEM). The scaffold samples were gold sputter coated for 50 s at 45 mA (Desk V, Denton Vacuum, Moorestown, NJ) before SEM imaging (Quanta 250 FEG, FEI, Hillsboro, OR).

3.2.2.2 Electrochemical Impedance Spectroscopy. Electrochemical impedance spectroscopy was used to determine the distribution of graphene particle within the PCL scaffold matrix containing varying concentrations of graphene (0.01 – 0.5 %). A 10 mV AC field at a frequency of 100 Hz with a working distance at a constant 5 cm was applied to the scaffolds (eDaq, Colorado Springs, CO).

3.2.2.3 Conductivity Measurements. For volume conductivity, the electrical volume resistivity of PCL and PCL+G (0.005 – 0.05%) scaffolds was measured using an electrometer (Keithley 6517B, Beaverton, OR) [201]. An alternating polarity resistivity test was used to reduce noise due to background currents. Conductivity was calculated as an inverse of resistivity.

Local conductivity of PCL+G scaffolds of varying graphene concentrations (0.01 and 0.5%) was measured using a custom-built point electrical stimulator. Scaffolds were loaded into a custom-built electrical stimulation chamber (Figure 2a). A localized electrical stimulation (5 V, 1Hz, BW: 10 ms) was applied to the scaffold via a stimulating electrode (tungsten, A-M Systems, Carlsborg, WA). Signal propagation was recorded via

another tungsten electrode (A-M Systems, Carlsborg, WA), which is controlled by a micromanipulator (World Precision Instruments, Sarasota, FL). Specifically, points along the length of the scaffold in 1 mm increments were probed, first along the center line of the scaffold (Level 1) then 1 mm above (Level 2) and 1 mm below (Level 3) the center line. The voltage difference across the reference resistor, in series with the scaffold was recorded using an oscilloscope (Agilent Technologies, Santa Clara, CA).

3.2.3 Mouse Embryonic Stem (mES) Cell Culture and Differentiation

A stable cardiac troponinT-eGFP mES cell line (generous gift from Dr. Yibing Qyang at Yale University) was used. MES cells were cultured on a mouse embryonic fibroblast (Global Stem, MD) feeder layer for 2 days in a DMEM medium supplemented with 15% knockout serum replacement, 1% NEAA, sodium-pyruvate, penicillin/streptomycin (Gibco, NY), 2-mercaptoethanol (Sigma Aldrich, MO) and leukemia inhibiting factor (LIF, 5ng/mL). To differentiate mES cells into cardiomyocytes, mES cells were transferred to and cultured in a feeder-free condition with IMDM medium supplemented with 15% knockout serum replacement, 1% penicillin/streptomycin (GIBCO, NY), 1-Thioglycerol (Sigma Aldrich, MO) and LIF (5ng/mL) for 2 days. Embryoid bodies (EBs) were then formed by a hanging drop method, as described previously [68]. After 2 days, EBs were collected in a differentiation medium containing IMDM medium supplemented with 15% fetal bovine serum, L-glutamine (GIBCO, NY), ascorbic acid and thioglycerol (Sigma Aldrich, MO) and cultured for 8-9 additional days. Spontaneously contracting and GFP positive cells were yielded starting as early as differentiation day 6-7. MES-CM

were purified on day 10-11 of differentiation using a discontinuous Percoll (GE Healthcare) separation technique [57,156,157].

3.2.4 Cell Seeding onto Scaffolds

Scaffolds (0.5 cm x 0.5 cm) were UV sterilized followed by overnight preconditioning in 20% FBS containing differentiation medium. Scaffolds were dried for 30 minutes prior to cell seeding. MES-CM were seeded onto pre-treated scaffolds at a density of $8x10^6$ cells/cm^2 for 2.5 hours before additional culture medium was added. PCL scaffolds without graphene were used as a 3D control while cells cultured on culture dishes served as a 2D control. MES-CM seeded scaffolds were cultured for 6 or 14 days in the differentiation medium for further characterization.

3.2.5 Cell Viability

A LIVE/DEAD Viability/Cytotoxicity kit (Life Technologies, NY) was used to determine viability of cells on scaffolds after 7 days of culture as previously described [146]. Briefly, scaffolds were rinsed with warm PBS and then stained with 0.2 M ethidium homodimer and 0.005 M calcein for 30 minutes at 37 °C. Immunofluorescent images were obtained using a confocal fluorescence microscope (IX81 DSU, Olympus, Somerset, NJ) and the ratio of live/dead cells to the total number of cells was analyzed using ImageJ software.

3.2.6 Immunofluorescence Imaging

The use of a stable cardiac troponinT-eGFP mES cell line allowed examination of cardiac troponin T expression by mES-CM during culture. GFP expression of mES-CM was visualized using a confocal fluorescence microscope (IX81 DSU, Olympus, Somerset, NJ).

3.2.7 F-actin Imaging

For the visualization of sarcomeres, samples including mES-CM seeded scaffolds and 2D control cells were fixed overnight using 4% formaldehyde (Sigma Aldrich, MO) after 6 days of culture. Samples were stained for F-actin using Rhodamine-conjugated phalloidin (1:20, Life Technologies, NY) for 2 hours at room temperature and were counter-stained with DAPI to visualize nuclei.

3.2.8 Western Blot Analysis

After 6 or 14 days of culture, cell lysates from scaffolds and controls were prepared for western blot as previously described [146]. Primary antibodies used for mES-CM samples were mouse anti-cardiac troponin T (cTnT, 1:1000, Abcam, Cambridge, MA, ab8295), rabbit anti-connexin43 (Cx43, 1:3000, Abcam, Cambridge, MA, ab11370) and mouse anti-heavy chain cardiac myosin (MHC, 1:1000, Abcam, Cambridge, MA, ab15). Mouse anti-β-actin (1:2000, Sigma Aldrich, St. Louis, MO, A1978) was used as a loading control. Secondary antibodies used were goat anti-rabbit (1:2000, Santa Cruz Biotechnology, Dallas, TX, SC-2004) and goat anti-mouse (1:2000, Santa Cruz Biotechnology, Dallas, TX, SC-2005).

3.2.9 SEM of mES-CM Seeded PCL+G Scaffolds

MES-CM seeded PCL+G tissues were fixed in 2% glutaraldehyde (Fisher Scientific, Hanover Park, IL) for 24 hours, rinsed 3 times in phosphate buffered saline and dehydrated in varying concentrations of ethanol (Sigma Aldrich, St. Louis, MO). Samples were then critical point dried in a Samdri-790 (Tousimis, Rockville, MD) followed by sputter coating with gold palladium (Quorum 15-T, Quorum Technologies, Laughton, England). SEM images were taken using a Leo 1530 vp SEM (Leo Electron Microscopy Ltd, Cambridge, England).

3.2.10 Evaluation of Calcium-Handling Properties

After 6 days of culture, 2D mES-CM and mES-CM cultured on PCL and PCL+G scaffolds were digested to a single cell suspension via collagenase (0.1 g/mL, Roche, Nutley, NJ) and accutase (Gibco, Grand Island, NY) treatment, as previously described [146]. Digested cells were reseeded onto collagen-coated (50 μg/mL collagen, BD Biosciences, San Jose, CA) glass bottom dishes overnight. To examine intracellular Ca^{2+} transients, samples were incubated with Rhod-2AM (4 μM, Invitrogen, Carlsbad, CA) for 30 minutes at room temperature, followed by a 20-minute washout (for AM cleavage) in normal Tyrode's solution. Samples were then placed in a heated chamber (35˚C) mounted on a fluorescent inverted microscope (Nikon Eclipse TE200, Mellville, NY) with an Andor Ixon Charge-Coupled device (CCD) camera (50 frames/s, 512 x 180 pixels, Andor Technology, Concord, MA) as previously described [160,161]. The intensity of fluorescence from spontaneously contracting cells was recorded and normalized to the basal diastolic fluorescence levels. Cells were electrically stimulated to examine their

response to electrical pacing at 0.5, 1 and 2 Hz frequencies (4.5 ms duration, 150 V, Grass S48 Stimulator, Grass Medical Instruments, West Warwick, RI). In addition, cells were treated with 10 mM caffeine to investigate sarcoplasmic reticulum Ca^{2+} content and fractional Ca^{2+} release. Cell response to β-adrenergic stimulation was also examined with the treatment of 1μM isoproterenol.

3.2.11 Statistical Analysis

Results are presented as mean ± SEM or individual data points. Statistical analysis was performed in SPSS (Version 24, IBM) using a two-tailed independent samples t-test, one-way ANOVA or their nonparametric counterpart, followed by Bonferroni post hoc tests, where appropriate. Statistical significance was accepted for $p^* < 0.05$ for omnibus tests and adjusted for post-hoc tests. A sample size of at least n=5 was used for all cell studies to allow for statistical examination of the data.
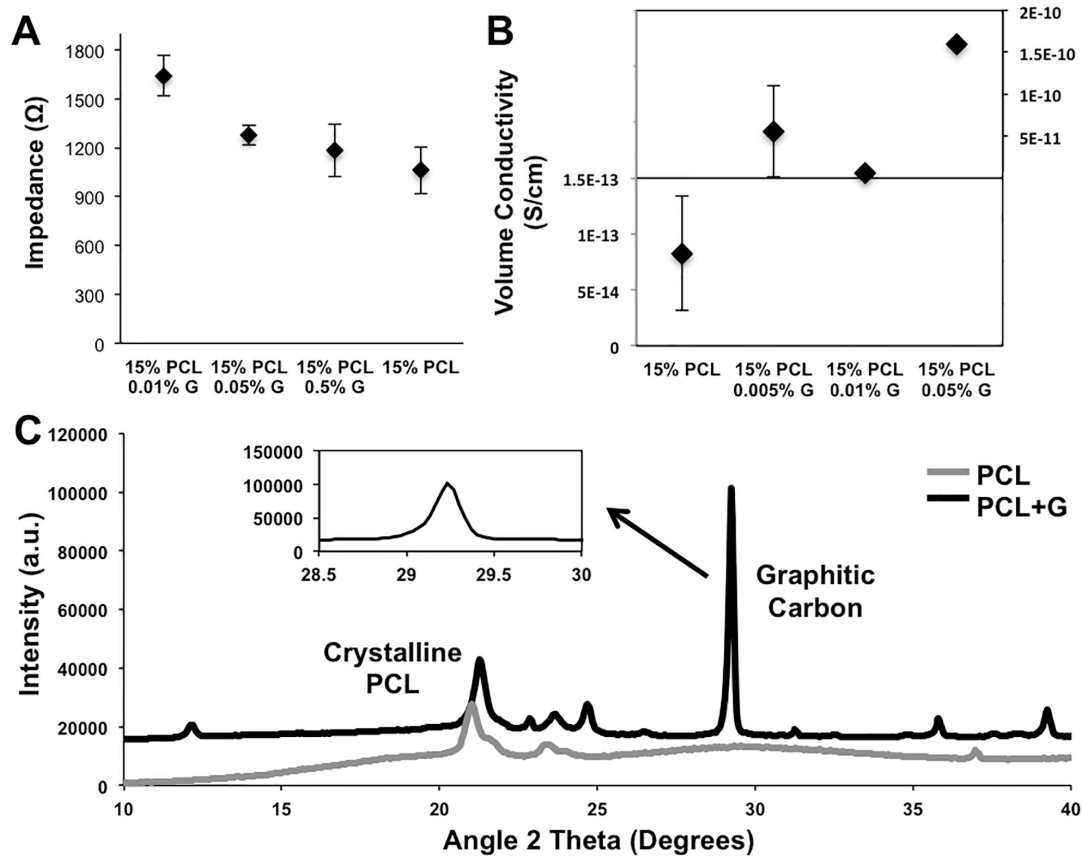
Figure 3.1 (A) Impedance analysis of 15% PCL and 15% PCL+G scaffolds with varying concentrations of graphene demonstrated a decrease in impedance with an increase in graphene concentration. (B) Volume conductivity of random PCL scaffolds with varying concentrations of graphene from 0 – 0.05% demonstrated higher conductivity with higher graphene concentrations. (C) XRD analysis revealed the presence of graphene within PCL+G scaffolds by an additional large, sharp peak along with the two characteristic crystalline PCL peaks at 21.37° and 23.73. Inset showed the peak at 29.23° demonstrating the presence of graphitic carbon.

3.3 Results

3.3.1 Fabrication and Characterization of Graphene Nanocomposite (PCL+G) Scaffolds

3D electroactive nanofibrous scaffolds were successfully fabricated by electrospinning graphene dispersed PCL solutions as previously described [200]. Scaffolds were prepared either with randomly oriented fibers or highly aligned fibers with (0.005 − 0.5%) and without graphene. To determine the distribution of graphene nanoparticles within the PCL matrix, electrochemical impedance spectroscopy was performed. Results revealed that as the graphene concentrations increased, the impedance of the scaffold decreased, indicating an even distribution of graphene particles within the scaffolds (Figure 3.1A). Resistivity measurements confirmed that the conductivity, which is the inverse of resistivity, increased with increased graphene concentrations as shown in Figure 3.1B. Moreover, XRD analysis displayed an additional sharp peak at 29.23° in PCL+G compared to that of PCL scaffold representing graphitic carbon further confirming the presence of graphene within the scaffold (Figure 3.1C).
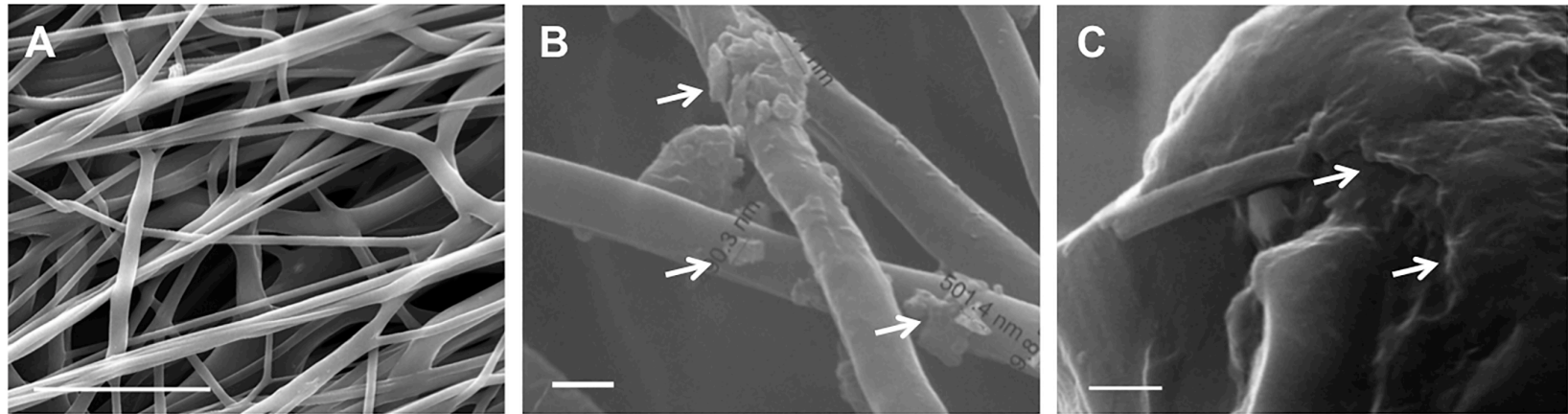
Figure 3.2 (A) Representative SEM image of aligned 15% PCL+G (0.01%) scaffold. Scale bar =10 μm. High magnification SEM images of 15% PCL+G scaffold (0.01% graphene) displayed (B) graphene particles within the matrix indicated by arrows, scale bar = 4 μm and (C) the edge of graphene particles on a fiber indicated by arrows, scale bar = 1 μm.
*Source: Hitscherich, P. et al. Electroactive Graphene Composite Scaffolds for Cardiac Tissue Engineering. J. Biomed. Mater. Res. A **106** 2923-2933, (2018).*

To further characterize the scaffolds, SEM images were used. A representative SEM image of aligned PCL+G scaffolds is shown in Figure 3.2A. The average scaffold thickness was measured at 64.88 ± 18.20 μm and 83.67 ± 25.31 μm for PCL and PCL+G scaffolds, respectively. The average inter-fiber spacing of PCL scaffolds (2483.60 ± 250.72 nm) was similar to that of PCL+G scaffolds (3365.50 ± 666.51 nm). The average fiber diameter of random PCL and PCL+G scaffolds were 431.96 ± 85.39 nm and 694.13 ± 82.46 nm, respectively. The average inter-fiber spacing of aligned PCL and PCL+G scaffolds were 5408.95 ± 1004.41 nm and 2905.30 ± 784.58 nm, respectively. The average fiber diameter for aligned PCL (932.40 ± 104.95 nm) was similar to that of aligned PCL+G scaffolds (994.79 ± 66.10 nm). Using SEM with higher magnification, graphene particles within the PCL matrix were visualized with the average thickness of graphene particles measuring 70 ± 2.64 nm (Figure 3.2B and C).

3.3.2 Application of Local Electrical Stimulation

To determine whether external electrical stimulation can be applied to PCL+G scaffolds, an electrical stimulation device was custom-built to provide localized, point stimulation (Figure 3.3A). Unlike field stimulation, which uses the conductance of liquids to stimulate an entire tissue or cell sheet simultaneously, point electrical stimulation allowed for controlled and localized stimulation at a site of the material in contact with the stimulating electrode. The electrical signal is then propagated throughout the rest of the scaffold based upon their properties. As the stimulating electrode made contact at one edge of the scaffolds, a recording electrode was moved to different locations on the
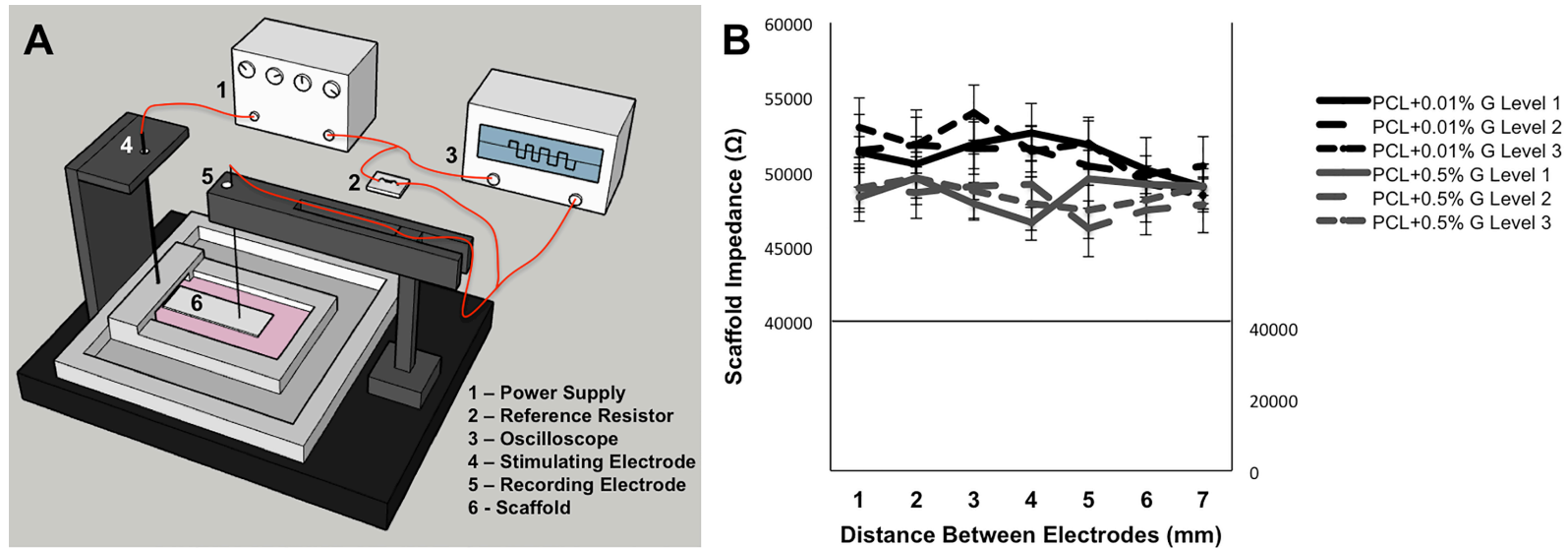
Figure 3.3 (A) Schematic of a custom-built electrical stimulation setup. (B) Scaffold impedance decreased with an increased graphene concentration. Small changes in impedance were demonstrated highlighting local changes in graphene distribution throughout the scaffold matrix. Level 1: along the centerline of the scaffold, Level 2: 1 mm above the centerline and Level 3: 1 mm below the centerline of the scaffold.

*Source: Hitscherich, P. et al. Electroactive Graphene Composite Scaffolds for Cardiac Tissue Engineering. J. Biomed. Mater. Res. A **106** 2923-2933, (2018).*

scaffold and a voltage drop could be measured across the reference resistor. The voltage drops were then converted to a scaffold impedance value assuming constant input current and voltage to the circuit. Results demonstrated decreased impedance with higher concentrations of graphene (Figure 3.3B), consistent with the results from electrochemical impedance spectroscopy. Local variations in scaffolds impedance due to graphene particles were also demonstrated confirming that the presence of local conductive sites formed by graphene particles disseminate the signal throughout the scaffold.

3.3.3 Characterization of mES-CM on Random PCL and PCL+G Scaffolds

A purified population of cardiomyocytes derived from mouse embryonic stem cells was seeded onto both PCL and PCL+G scaffolds with random fiber orientation. Cells adhered well and spread out within the first 24 hours. SEM images further demonstrated the adhesion and interaction of mES-CM with graphene-decorated fibers as shown in Figure 3.4A and 3.4B.

Spontaneous beating of the cells was detected as early as 48 hours after seeding and continued throughout the culture resulting in synchronous contraction of the scaffold, which can be detected macroscopically after 4-5 days of culture. Cells exhibited similar spontaneous beating frequency and maintained their phenotype on both PCL and PCL+G scaffolds as evidenced by expression of cardiac-specific cardiac troponin T (cTnT) visualized through cardiac troponinT-eGFP tagged cells (Figures 3.5A and 3.5B, respectively). The expression of cTnT continued to increase with longer time in culture as monitored up to 14 days. MES-CM also exhibited well-registered sarcomeres,
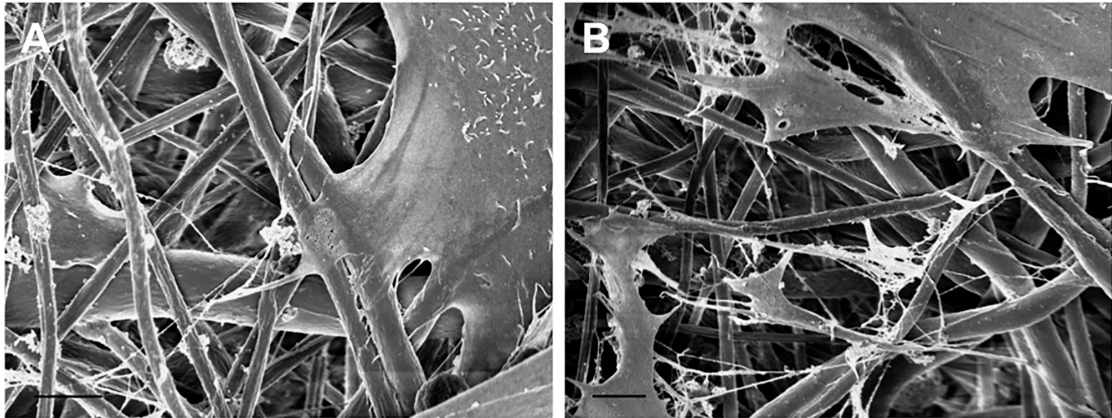
Figure 3.4 Representative SEM images of mES-CM cultured on random PCL+G scaffolds (A) demonstrated infiltration of the cells into the scaffold and wrapping of cell projections around scaffold fibers, and (B) forming close interactions with scaffold fibers after 14 days of culture. Scale bars = 3 μm.
*Source: Hitscherich, P. et al. Electroactive Graphene Composite Scaffolds for Cardiac Tissue Engineering. J. Biomed. Mater. Res. A **106** 2923-2933, (2018).*

demonstrated by F-actin staining on day 6 (Figure 3.5C and 3.5D) and day 14 (Figure 3.5E and 3.5F). Western blotting analysis confirmed the expression of cardiac specific markers including cTnT, myosin heavy chain (MHC) and connexin43 (Cx43) by cells on both scaffolds after 6 and 14 days of culture (Figure 3.6A). However, mES-CM on PCL+G scaffolds exhibited up-regulation of cTnT expression compared to mES-CM on PCL scaffolds after 2 weeks of culture. In addition, only mES-CM cultured on PCL+G scaffolds had a significantly lower frequency on day 14 compared to day 6 ($p^* < 0.05$, Figure 3.6B).

To compare the functional behavior of mES-CM cultured on these scaffolds, calcium-handling properties of the cells were examined using a single cell setup. For single cell analysis, mES-CM were digested after 6 days and re-plated onto a glass bottom cell culture dish. MES-CM cultured in 2D, on PCL scaffolds and on PCL+G
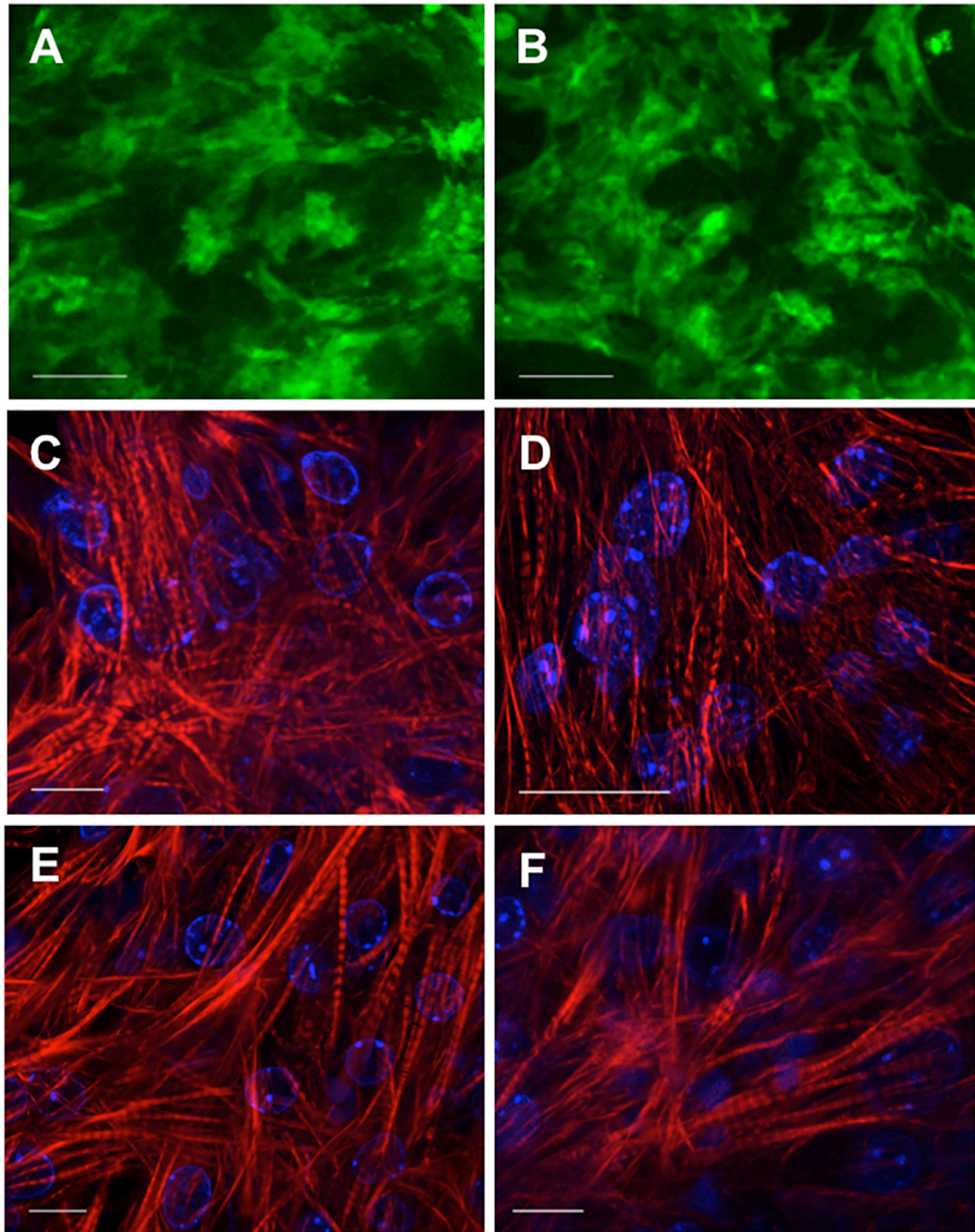
Figure 3.5 High expression of cTnT-eGFP by mES-CM cultured on random (A) PCL or (B) PCL+G was seen on day 6 of culture (green, scale bars = 100 μm). F-actin staining with rhodamin-conjugated phalloidin (red) demonstrated well-registered sarcomeres by mES-CM cultured on random (C, E) PCL and (D, F) PCL+G scaffolds, respectively on day 6 and day 14. Scale bars = 10 μm.

*Source: Hitscherich, P. et al. Electroactive Graphene Composite Scaffolds for Cardiac Tissue Engineering. J. Biomed. Mater. Res. A **106** 2923-2933, (2018).*

scaffolds were processed using the same protocol for direct comparison among the groups. Digested cells not only spontaneously contracted, but also responded to electrical pacing at varying frequencies of 0.5 - 2 Hz, as previously reported (Figure 3.7A and 3.7B, respectively) [146].
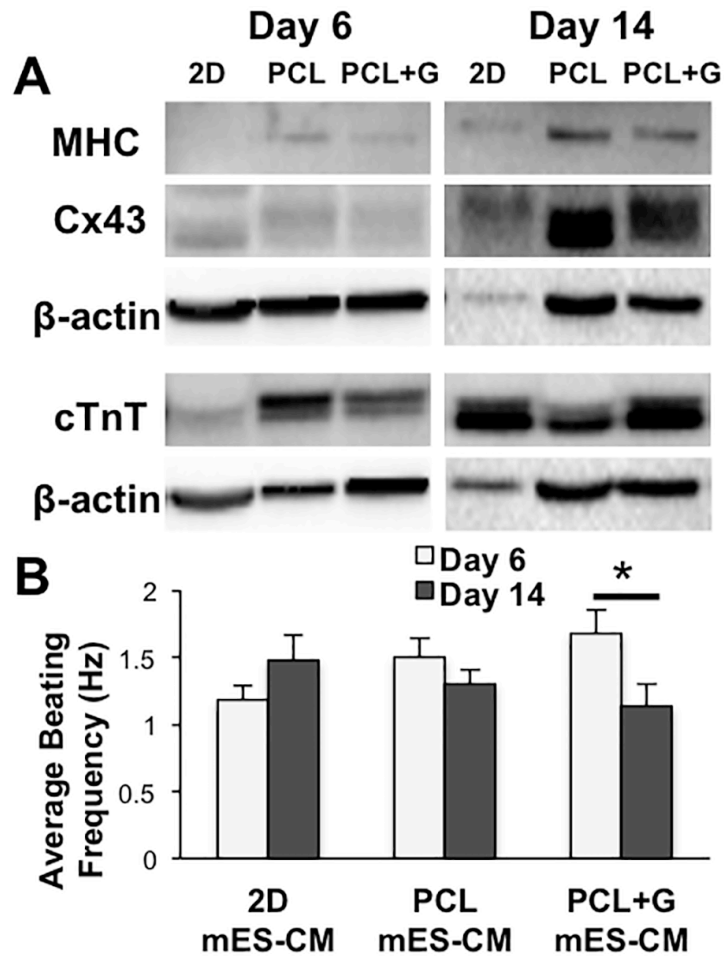
Figure 3.6 (A) Western analysis revealed similar expression of MHC, cTnT, and Cx43 among all the groups on day 6 of culture. However, up-regulation of cTnT expression in mES-CM on random PCL+G scaffolds on day 14 was demonstrated. (B) Average beating frequency for mES-CM cultured on random PCL+G scaffolds trended higher than those in 2D and on PCL scaffolds on day 6. However, the average beating frequency was significantly lower on day 14 in mES-CM cultured on PCL+G scaffolds when compared to day 6 ($p* = 0.045$).
*Source: Hitscherich, P. et al. Electroactive Graphene Composite Scaffolds for Cardiac Tissue Engineering. J. Biomed. Mater. Res. A **106** 2923-2933, (2018).*

MES-CM from all the groups demonstrated a positive response to β-adrenergic stimulation upon treatment with 1 µM isoproterenol as shown in Figure 3.7C. Cells also responded to treatment with caffeine (Figure 4d), which lowers the luminal Ca^{2+} threshold for opening of the ryanodine receptor. This allowed for the quantification of the total Ca^{2+} content in the sarcoplasmic reticulum, which can be measured from the largest
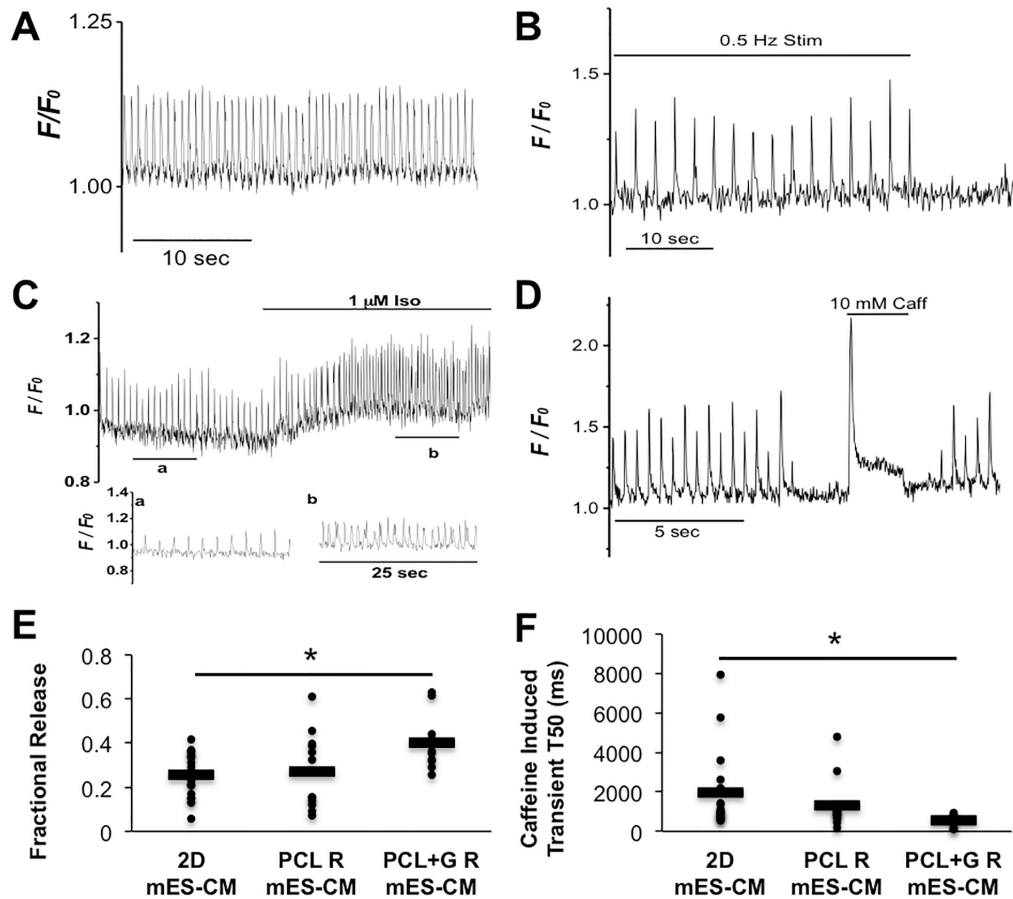
Figure 3.7 Representative traces of (A) spontaneous beating and (B) electrically paced beating at 0.5 Hz on PCL+G scaffolds. Representative traces of mES-CM in response to (C) 1 µM isoproterenol and (D) 10 mM caffeine. (E) MES-CM cultured on PCL+G scaffolds exhibited significantly higher fractional release (p* = 0.005) compared to 2D control. (F) MES-CM cultured on PCL+G scaffolds also exhibited a significantly shorter (p* = 0.001) caffeine induced transient T_{50} compared to 2D control. Mean denoted by −, R: random fiber orientation.
*Source: Hitscherich, P. et al. Electroactive Graphene Composite Scaffolds for Cardiac Tissue Engineering. J. Biomed. Mater. Res. A **106** 2923-2933, (2018).*

peak. The initial peaks represent the amount of Ca^{2+} released per paced beat (Figure 3.7D). Cells cultured on PCL+G scaffolds demonstrated significantly higher paced Ca^{2+} transient amplitude compared to that of a 2D control. The ratio of Ca^{2+} released per beat to the total sarcoplasmic reticulum stores, known as fractional release, was also significantly higher in cells cultured on PCL+G scaffolds compared to that of a 2D control ($p^* < 0.01$, Figure 3.7E). In addition, cells on PCL+G scaffolds exhibited sharper and narrower caffeine induced transient peaks compared to 2D controls, as demonstrated by significantly shorter caffeine induced T_{50} ($p^* < 0.005$), a representative measurement of transient length (Figure 3.7F).

3.3.4 Characterization of mES-CM on Aligned PCL and PCL+G Scaffolds

Similar to randomly oriented scaffolds, mES-CM adhered well and spread out within the first 24 hours on aligned PCL and PCL+G scaffolds. Viability of mES-CM after 7 days of culture was analyzed using a Live/Dead staining kit as demonstrated in Figure 3.8A. Cells remained mostly viable, shown in green, with a minimal number of dead cells in red color. MES-CM seeded onto aligned PCL and PCL+G scaffolds exhibited strong eGFP-cTnT expression as shown in Figures 3.8B and 3.8C, respectively. As anticipated, mES-CM aligned along the major fiber axis and exhibited well-registered sarcomeres (Figure 3.8D and 3.8E).

Moreover, western blotting assay revealed that mES-CM cultured on PCL+G exhibited higher expression of MHC and cTnT compared to PCL scaffolds after 6 days of culture (Figure 3.9A). Cx43 expression was also greatly up-regulated on aligned graphene containing scaffolds compared to PCL scaffolds and the difference became
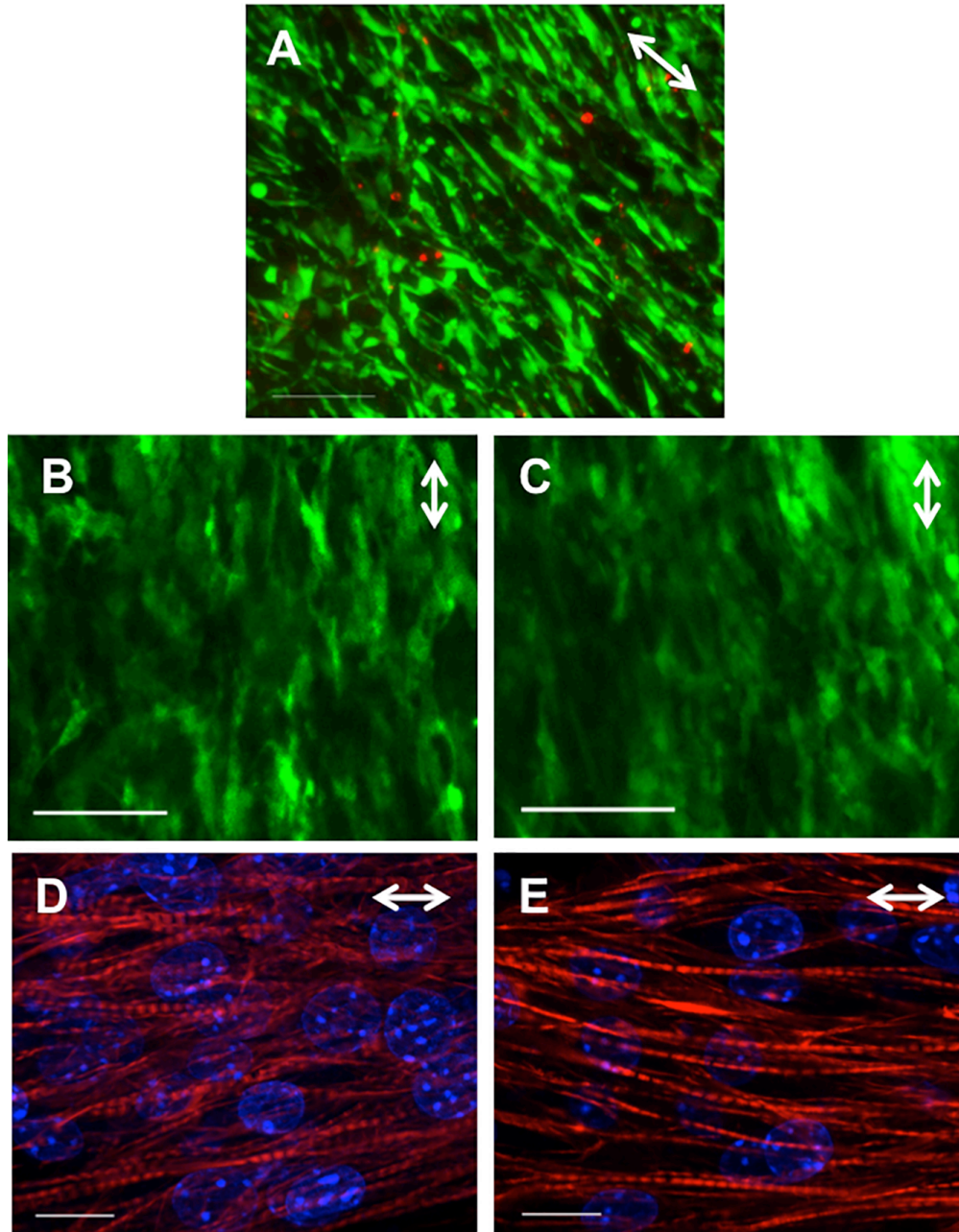
Figure 3.8 (A) Live/Dead analysis demonstrated high cell viability on day 7 (live: green, dead: red). High expression of cTnT-eGFP by mES-CM cultured on aligned (B) PCL or (C) PCL+G scaffolds was seen on day 6 of culture. (green, scale bars = 100 μm). F-actin staining with Rhodamine-conjugated phalloidin (red) demonstrated well-registered sarcomeres that were well aligned along the major fiber axis of the scaffolds in aligned (D) PCL and (E) PCL+G scaffolds. Scale bars = 10 μm.
*Source: Hitscherich, P. et al. Electroactive Graphene Composite Scaffolds for Cardiac Tissue Engineering. J. Biomed. Mater. Res. A **106** 2923-2933, (2018).*

more evident after longer culture of 14 days. MES-CM on both PCL and PCL+G scaffolds spontaneously contracted nearly twice as fast as the 2D control group demonstrating a significant increase in spontaneous beating frequency on aligned 3D scaffolds vs. 2D culture (p<0.001, Figure 3.9B).

Functional calcium-handling properties were assessed as described previously. Cells cultured on aligned scaffolds, as those on randomly oriented fibers, retained their ability
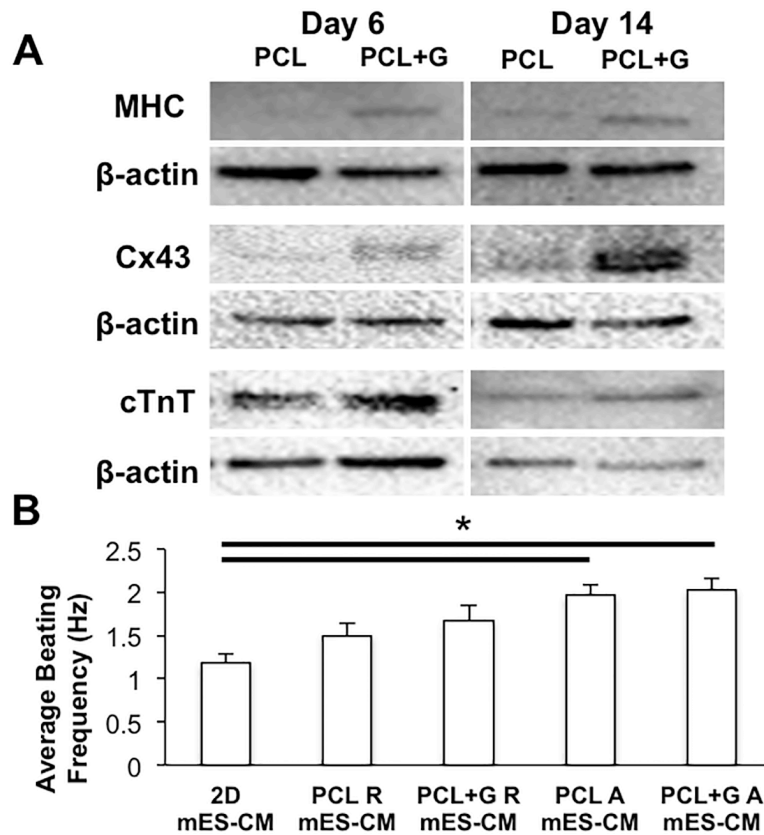
Figure 3.9 (A) Increased expression of MHC, Cx43 and cTnT was demonstrated in mES-CM cultured on PCL+G scaffolds compared to PCL at both 6 and 14 days. (B) Significantly higher average beating frequency was shown by mES-CM cultured on PCL and PCL+G scaffolds compared to 2D at day 6 of culture (p * <0.001, R: random fiber orientation, A: aligned fiber orientation).
*Source: Hitscherich, P. et al. Electroactive Graphene Composite Scaffolds for Cardiac Tissue Engineering. J. Biomed. Mater. Res. A **106** 2923-2933, (2018).*

to be electrically paced and stimulated by an inotropic agent and caffeine. Total sarcoplasmic reticulum Ca^{2+} stores were similar among all groups. However, mES-CM cultured on aligned PCL and PCL+G scaffolds exhibited significantly higher fractional release compared to that of 2D controls (p<0.02, Figure 3.10A). Similar to randomly oriented scaffolds, the presence of graphene promoted a sharper and narrower caffeine induced transient peak compared to 2D controls, as demonstrated by a significantly shorter caffeine induced T_{50}. Specifically, the time required for Ca^{2+} to efflux out of the cytoplasm after release from the SR, known as caffeine induced transient decay, was also significantly shorter in mES-CM on PCL+G scaffolds compared to 2D controls (p<0.01, Figure 3.10B).
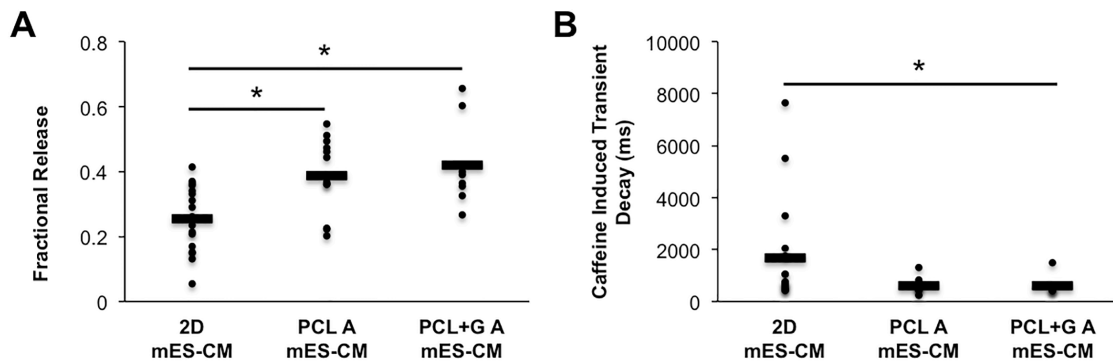
Figure 3.10 (A) Fractional release of mES-CM cultured on aligned PCL and PCL+G scaffolds was significantly higher compared to 2D control (p* = 0.003). (B) Caffeine induced transient decay was significantly shorter in mES-CM cultured on aligned PCL+G scaffolds compared to 2D controls (p* = 0.007).
Mean denoted by −.
*Source: Hitscherich, P. et al. Electroactive Graphene Composite Scaffolds for Cardiac Tissue Engineering. J. Biomed. Mater. Res. A **106** 2923-2933, (2018).*

3.4 Discussion

Conductive nanomaterials, including graphene and CNTs have emerged as highly promising candidate biomaterials [183,184] owing to their unique electrical and mechanical properties. Since cardiomyocytes exist in a highly complex and dynamic microenvironment *in vivo*, the unique features of graphene are especially attractive for cardiomyocyte culture. Previous studies have examined the biocompatibility and differentiation specificity of human pluripotent stem cells [128,197], and mesenchymal stem cells [130] on 2D graphene films. However, the effects of a 3D graphene scaffolds on cardiac cells are not yet known. In this study, 3D graphene-containing electroactive nanocomposite scaffolds providing local conductive sites was examined for the first time with stem cell derived cardiomyocytes for cardiac tissue engineering applications.

Despite the difficulties in properly processing 3D electroconductive scaffolds as conductive nanoparticles tend to agglomerate, a 3D electroactive nanocomposite scaffold was successfully fabricated by electrospinning graphene dispersed PCL solutions [200]. The addition of up to 0.05% conductive graphene into an insulative PCL polymer matrix resulted in an even distribution of graphene particles within the 3D PCL matrix which increased volume conductivity due to the percolation effect [201,202].

Since it has been shown that electrical stimulation can enhance cardiomyocyte function and differentiation capacity [115,203], the possibility of applying external electrical stimulation to PCL+G scaffolds was also examined. As the conductive graphene particles provided local conductive sites within insulative PCL matrix, conventional field stimulation using a conductive solution was not appropriate for these scaffolds. Instead, a point electrical stimulation device was built to provide localized electrical stimulation to

examine signal propagation through PCL+G scaffolds. Since electrical signals in the heart begin in the sinoatrial (SA) node with pacemaker cells and then propagates throughout the myocardium via cell-cell interactions for synchronous contraction [204], localized point stimulation more closely mimics this mechanism by initiating contraction in the cells in contact with the stimulating electrode. Our results demonstrating signal propagation through PCL+G scaffolds containing as low as 0.01% graphene confirms the feasibility of incorporating additional electrical stimulation to these tissues.

To assess the cytocompatibility of PCL+G with stem cell derived cardiomyocytes, scaffolds with 0.01% graphene were chosen to determine whether minimum graphene content is enough to provide functional benefits while maximizing the biocompatibility. Our results demonstrated that 3D PCL+G scaffolds independent of the fiber organization are biocompatible with stem cell derived cardiomyocytes, as demonstrated by their high cellular viability and adherence to the scaffolds [129,205,206]. MES-CM spontaneously contracted, exhibited a positive response to an inotropic agent and expressed classical cardiac specific markers confirming phenotypic characteristics of native cardiomyocytes on graphene scaffolds.

Functional assessment demonstrated similar paced Ca^{2+} transient morphology in mES-CM cultured in all culture conditions. Similar SERCA expression and activity indicated by similar paced transient T_{50} was also demonstrated by all culture conditions. However, caffeine induced transient morphology was significantly altered in the presence of graphene. Specifically, caffeine induced transient T_{50} was significantly decreased in mES-CM cultured on PCL+G scaffolds. This suggests involvement of Ca^{2+} efflux

mechanisms other than sarco/endoplasmic reticulum Ca^{2+}-ATPase (SERCA), which controls up to 90% of Ca^{2+} efflux in mice under normal physiological conditions [207].

The other possible efflux mechanism is the sarcolemnal Na^+/Ca^{2+} exchanger (NCX), which is driven by both Na^+ and Ca^{2+} concentrations. During caffeine treatment, intracellular Ca^{2+} concentration is at its peak, driving NCX forward to expel Ca^{2+} out of the cell [208]. Significantly shorter caffeine induced transient T_{50} and decay time of mES-CM cultured on PCL+G scaffolds with both random and aligned fibers compared to 2D control suggest that graphene plays a role in the expression and organization of NCX in mES-CM, enabling significantly faster free Ca^{2+} expulsion from the cytoplasm [169,209]. This further suggests that more efficient Ca^{2+} homeostasis of mES-CM can be achieved on PCL+G scaffolds. The resulting Ca^{2+} homeostasis mechanism may also explain the significant decrease in spontaneous beating frequency with longer time in culture on PCL+G scaffolds as the gradual decrease in spontaneous beating of stem cell-derived cardiomyocytes indicates further differentiation [165].

Furthermore, culture on PCL+G scaffolds promoted a significantly higher fractional release of approximately 40% compared to that of mES-CM cultured in 2D (approximately 26%). Fractional release is an indicator of excitation-contraction coupling efficiency and the fractional release of mature rat is approximately 60% [173]. A higher fractional release further suggests that calcium-handling function of mES-CM is enhanced with culture on 3D graphene containing scaffolds.

The greatest enhancement in cardiac specific protein expression and contractile behavior was demonstrated by mES-CM cultured on aligned PCL+G scaffold suggesting a synergistic effect from the combination of fiber alignment and incorporation of

graphene into the scaffold. Specifically, up-regulation of Cx43 expression by mES-CM on aligned PCL+G scaffolds suggests enhanced cell-cell coupling [125,197,210], which is likely due to signal propagation facilitated by graphene providing local conductive sites, as suggested in studies performed with carbon nanotubes [183]. Aligned PCL+G scaffolds also stimulated the highest fractional release of all conditions as well as the highest spontaneous beating frequency at day 6 of culture. Cardiomyocyte organization and alignment has been shown to affect electrical function [88] and to optimize force generation while electrical stimulation promotes cardiomyocyte elongation and alignment [116,211]. Hence, the benefits of combining alignment and the presence of graphene would only be further enhanced through the addition of local electrical stimulation.

In summary, this chapter highlights the potential of an electroactive graphene-containing scaffold as a candidate material for engineered cardiac tissue engineering application. The addition of a miniscule amount of graphene nanoparticles does not affect the biocompatibility of 3D scaffolds, yet provided beneficial effects to cardiomyocyte function specifically in calcium-handling behavior. Unlike the scaffolds formed entirely with conductive materials, these scaffolds have local conductive sites provided by graphene nanoparticles within a biocompatible PCL matrix. The changes in cardiomyocyte function on these scaffolds are likely due to local conductive pathways formed by cardiomyocytes that facilitated signal propagation and interaction between them [185,197]. With the development of the point electrical stimulation device, further studies can be performed to investigate whether the combination of graphene and the external electrical stimulation can provide further synergistic effects on mES-CM function. Additionally, cell seeded scaffolds could

be transplanted into a mouse MI-model to evaluate integration into the host as electroconductive scaffold may aid in electrical integration.

CHAPTER 4

MYOCARDIAL INFLAMMATION MODELS

4.1 Introduction

After myocardial infarction (MI), the temporal response includes the initial inflammation phase followed by remodeling during the proliferative and maturation phases [13]. Macrophages are one of the key cell types activated in the initial inflammatory response after injury with CCL2/CCR2 signaling initiating monocyte recruitment and differentiation in the infarct [212].

Macrophage phenotypes can be generally described as more pro-inflammatory in days 1-3, commonly referred to as M1 type, and more anti-inflammatory or pro-healing for days 5-7, described generally as M2 type [142,213-215]. It is recognized that there is a complex spectrum of macrophage phenotypes in the post-MI microenvironment that shifts over time. Various phenotypes, including M2a or M2c, can be characterized by cytokine secretion and cell surface receptor expression [14,216]. It is, however, not known exactly what dictates the shift between macrophage phenotypes. One theory is that M1 and M2 macrophages originated from varying monocyte cell sources [217]. The microenvironment has also been shown to influence macrophage phenotype, indicating plasticity of macrophages [218].

Although macrophages are usually associated with injury, it has been demonstrated that resident cardiac macrophages contribute to cardiac function in the healthy, and steady state condition. Resident cardiac macrophages exhibit an M2-type, pro-healing phenotype, with population expressing various levels of major

histocompatibility complex class 2, CCR2 and Ly6C [218]. Hulsmans et al. demonstrated that resident cardiac macrophages also facilitate electrical signal propagation in the AV node through intricate interactions with cardiomyocytes via connexin43 gap junctions [5]. In fact, they follow the pattern of action potentials of the cardiomyocytes in which they interact. Nevertheless, resident cardiac macrophages are not involved in the immediate inflammatory response post-MI, as they die along with the other cells that populate the infarct. Rather, infiltrating monocytes from the blood differentiate into the macrophages that dictate the initial immune response [219].

Macrophage phagocytic function is known as one regulator of inflammation through clearing of the numerous apoptotic cells such as neutrophils, promoting a shift in macrophages towards anti-inflammatory mediator expression such as IL-10 and TGF-β [220]. Extracellular matrix fragments may also be involved in the promotion of macrophage infiltration and elicitation of a pro-inflammatory microenvironment [221]. It is critical to better understand how macrophages influence the inflammatory response post-MI, as the prolonging of inflammation post-MI is associated with detrimental remodeling and function of the heart [14]. Very recently, inhibition of the innate immune response via treatment with a potent antioxidant called 3-bromo-4,5-dihydroxybenzaldehyde or BDB caused a noticeable improvement in cardiac function, survivability and infarct size due to inhibition of macrophage infiltration and pro-inflammatory cytokine production [222]. Another recent study by Tokutome et al. used nanoparticles (NPs) loaded with an anti-inflammatory drug named Pioglitazone, which targeted monocytes and macrophages. NPs inhibited monocyte recruitment and inflammatory gene expression in macrophages. Instead, NPs promoted a more M2 type macrophage phenotype. These NPs lessened

ischemia-reperfusion injury and significantly reduced mouse mortality [223]. Despite these recent studies, details regarding macrophage subpopulations and their effect on resident surviving cardiomyocytes or on other cell types administered during cell-based therapy remain unclear.

Both the pro- and anti-inflammatory macrophage subsets secrete an array of cytokines that contribute to the post-MI microenvironment. One class of proteins secreted by macrophages after injury is matricellular proteins [224]. Matricellular proteins are nonstructural extracellular matrix proteins, however not much detail is known about their effect on different cell types, including cardiomyocytes. One matricellular protein of interest in the post-MI microenvironment is thrombospondin-1 (TSP-1). TSP-1 is known to be up-regulated at sites of inflammation, including post-MI. TSP-1 is expressed and secreted by infiltrating macrophages and has been shown to be isolated in the infarct border zone [225]. TSP-1 null mice exhibit an exaggerated inflammatory response, with a higher density of infiltrating and activated macrophages and fibroblasts, which causes expansion of the infarct. Because of this, TSP-1 is suggested to form a barrier around the infarct to protect the healthy tissue. TSP-1 is also a strong binder of Ca^{2+} ions, containing over 30 Ca^{2+} binding sites [226]. Ca^{2+} binding of TSP-1 affects its reactivity and interaction at other binding sites [227]. Specifically, the calcium-handling mechanism associated with TSP-1 is store operated Ca^{2+} entry, or SOCE. SOCE has historically been associated with non-electroactive cell types. However, more recently SOCE has been identified in cardiomyocytes during the embryonic and neonatal phase of development [228] as well as in embryonic stem cell derived cardiomyocytes [229]. While healthy adult cardiomyocytes do not exhibit SOCE, stress induces the expression of stromal interaction molecule 1

(Stim1), which is the Ca^{2+} sensing protein in the sarcoplasmic reticulum, in adult cardiomyocytes and therefore initiates SOCE in adult cells under stress [228]. Since TSP-1 is known to bind Stim1 in non-excitable cells, TSP-1 may be a regulator of SOCE in the post-MI microenvironment [230,231].

Another matricellular protein of interest, which was originally identified as a bone matrix protein but is now known to be involved with inflammation through constitutive expression and secretion by macrophages, is osteopontin (OPN) [232,233]. It is highly up-regulated at the infarct border zone post-MI [233] and has also been associated with the development of cardiac disease, specifically cardiac hypertrophy and heart failure [234-238]. This year, Shirakawa et al. demonstrated the relationship between galectin-3 and OPN, which contributes to cardiac repair by involvement in mediating phagocytosis and fibrosis [239]. However, the extent of OPN involvement in the post-MI microenvironment and how OPN is linked to cardiac disease post-MI is not understood. Because cardiac hypertrophy is associated with dysfunction of calcium-handling properties in cardiomyocytes [240], specifically SOCE [228,241-243], OPN could affect cardiomyocyte SOCE response post-MI, and therefore, elicit changes in cardiomyocyte function and further development of cardiac hypertrophy.

In this chapter, two *in vitro* myocardial inflammation models were created using a glass bottom dish. The first is a direct co-culture model in which polarized macrophage subsets are co-cultured with pluripotent stem cell derived cardiomyocytes. The second used macrophage phenotype specific conditioned-media to culture pluripotent stem cell derived cardiomyocytes. These models permit detailed characterization of gene expression by macrophage and cardiomyocyte, expression of matricellular proteins, and

secretion of cytokines. More importantly, the effects macrophages or macrophage-derived factors have on the calcium-handling properties of pluripotent stem cell derived cardiomyocytes were examined. A potential pathway involved in SOCE response of cardiomyocytes with macrophage derived OPN was demonstrated. The results from this *in vitro* study provide insights to better understand the cellular interactions in the post-MI microenvironment, which is otherwise difficult to examine *in vivo*.

4.2 Methods

4.2.1 Mouse Embryonic Stem (mES) Cell Culture and Differentiation

A stable cardiac troponinT-eGFP mES cell line (generous gift from Dr. Yibing Qyang at Yale University) was used. MES cells were cultured on a mouse embryonic fibroblast (Global Stem, MD) feeder layer for 2 days in a DMEM medium supplemented with 15% knockout serum replacement, 1% NEAA, sodium-pyruvate, penicillin/streptomycin (Gibco, NY), 2-mercaptoethanol (Sigma Aldrich, MO) and leukemia inhibiting factor (LIF, 5ng/mL). To differentiate mES cells into cardiomyocytes, mES cells were transferred to and cultured in a feeder-free condition with IMDM medium supplemented with 15% knockout serum replacement, 1% penicillin/streptomycin (GIBCO, NY), 1-Thioglycerol (Sigma Aldrich, MO) and LIF (5ng/mL) for 2 days. Embryoid bodies (EBs) were then formed by a hanging drop method, as described previously [68]. After 2 days, EBs were collected in a differentiation medium containing IMDM medium supplemented with 15% fetal bovine serum, L-glutamine (GIBCO, NY), ascorbic acid and thioglycerol (Sigma Aldrich, MO) and cultured for 8-9 additional days. Spontaneously contracting and GFP positive cells were yielded starting as early as differentiation day 6-7. MES-CM

were purified on day 10-11 of differentiation using a discontinuous Percoll (GE Healthcare) separation technique [57,156,157].

4.2.2 Macrophage Culture

A RAW 264.7 macrophage cell line was used (generous gift from Dr. Dominic Del Re at Rutgers New Jersey Medical School). Macrophages were maintained in an un-polarized state in RPMI medium (GIBCO, NY) supplemented with 10% fetal bovine serum and 1% penicillin/streptomycin (GIBCO, NY).

4.2.3 Macrophage Polarization

Cultured macrophages were serum starved for 24 hours followed by either lipopolysaccharides (LPS, Sigma Aldrich, 100 ng/mL) or IL-4 (Biolegend, 20 ng/mL) supplementation for 24 hours to be activated into a pro-inflammatory or anti-inflammatory phenotype, respectively [244].

4.2.4 2D Myocardial Inflammation Models

4.2.4.1 Indirect Co-culture Model. A schematic of the indirect co-culture model can be seen in Figure 4.1A. MES-CM (2500,000 cells) were seeded on the glass center of the glass bottom culture dish (MatTek). Macrophages were cultured in a 6-well plate (40,000 cells/well), serum starved and polarized for 24 hours as described above. Conditioned-media from macrophage cultures was then centrifuged (3 minutes, 10,000 RPM) to remove any debris or cells. It was then added to mES-CM in 1:1 ratio with

cardiomyocyte differentiation media for 72 hours to examine the effects of macrophage secreted proteins on cardiomyocyte function.

4.2.4.2 Direct Co-culture Model. A schematic of the direct co-culture model can be seen in Figure 4.1B. Initially, 20,000 macrophages are seeded in the outer edges of a glass bottom dish (MatTek) in 0.5 mL of RPMI supplemented media while 250,000 mES-CM are seeded in the glass center region of the dish in 300uL of differentiation media. The use of glass bottom dish allowed for ease of functional analysis. The
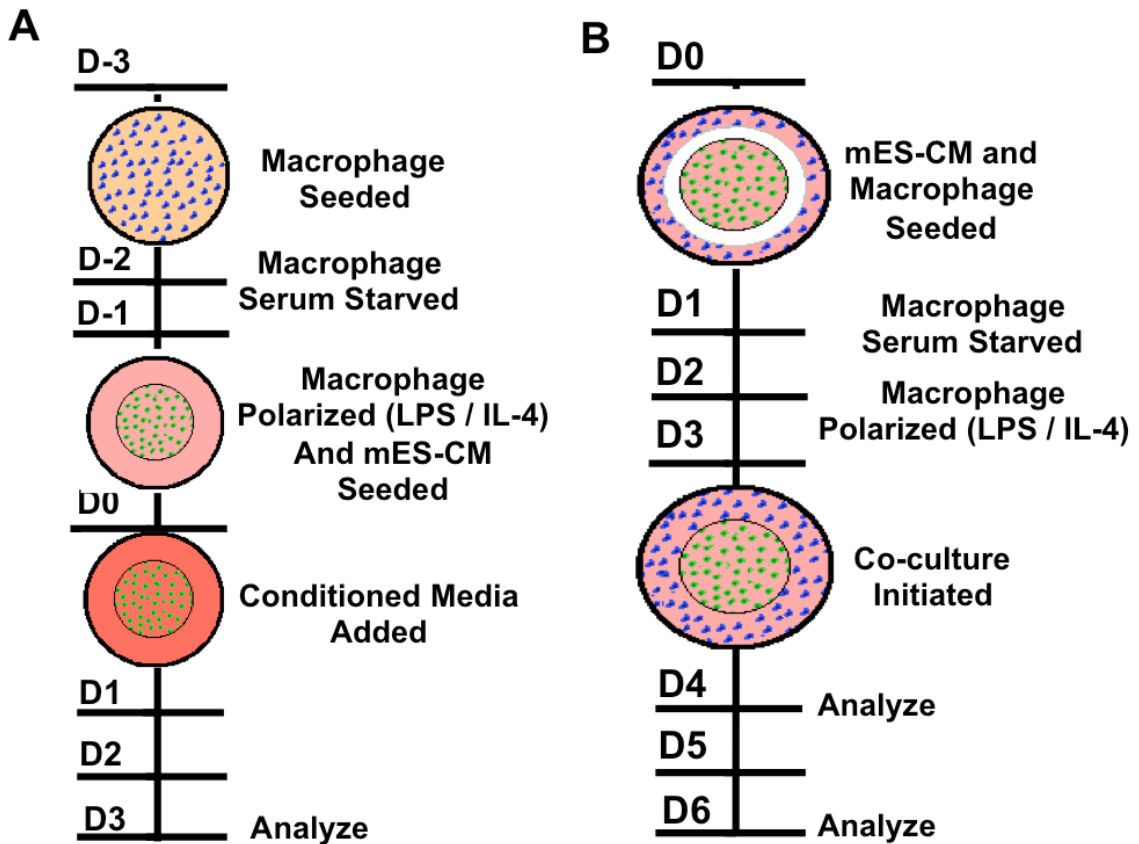
Figure 4.1 Schematic of (A) indirect and (B) direct co-culture of macrophages and cardiomyocytes.
Source: Hitscherich, P. et al. Macrophages Affect Cardiomyocyte Calcium-Handling Function Via Matricellular Protein Secretion. (In preparation, 2018).

following day, macrophage media is replaced with serum free media for 24 hours. Media is replaced again with either serum containing media or LPS or IL-4 supplemented polarization media for another 24 hours. After 24 hours of macrophage polarization, macrophage and cardiomyocyte media is mixed in a 1:1 ratio to initiate co-culture. Samples are then analyzed either 24 or 72 hours later.

4.2.5 Immunofluorescence Imaging

The use of a stable cardiac troponinT-eGFP mES cell line allowed examination of cardiac troponin T expression by mES-CM during culture. GFP expression of mES-CM was visualized using a confocal fluorescence microscope (IX81 DSU, Olympus, Somerset, NJ).

4.2.6 F-actin Imaging

Macrophages in monoculture were fixed overnight using 4% formaldehyde (Sigma Aldrich, MO) after 24 hours of activation. Samples were stained for F-actin using Rhodamine-conjugated phalloidin (1:20, Life Technologies, NY) for 2 hours at room temperature and were counter-stained with DAPI to visualize nuclei before imaging with a confocal fluorescence microscope (IX81 DSU, Olympus, Somerset, NJ).

4.2.7 RT-PCR

Total RNA was extracted and purified from mES-CM and macrophages using the GenElute Mammalian Total RNA Miniprep Kit following the manufacturers instruction. cDNA was created with 200ng of RNA and the High-Capacity cDNA Reverse

Transcription Kit (Applied Biosystems, Grand Island, NY) in the T100 Thermal Cycler (Bio-rad, Hercules, CA) using the following program: 10 min at 25°C, 120 min at 37°C, 5 min at 85°C and then 4°C indefinitely. RT-PCR reactions were then prepared with the SSo Advanced SYBRgreen Mastermix (Bio-rad, Hercules, CA). The primers used in the study are listed in Table A1 (IDT, Coralville, Iowa).[245,246] The qPCR reaction was then run in a CFX Connect Real Time System (Bio-rad, Hercules, CA) for up to 50 cycles. Samples that saw no expression after 50 cycles were considered to have no expression. Changes in expression were represented using the Comparative C_T method as described previously.[247]

4.2.8 Cytokine Secretion

A cytokine array (R&D Systems, Minneapolis, MN) was used to examine inflammatory cytokine secretion in culture medium. Samples examined were from both monoculture polarized macrophages and cardiomyocyte or co-culture media after 72 hours following manufactures instructions. Media was collected and centrifuge (3 min, 10,000 RPM) to remove floating cells and debris. After blocking for 1 hour, nitrocellulose membranes containing 40 different capture antibodies for inflammatory cytokines were incubated with media samples overnight at 4°C. Membranes were then washed and incubated with Streptavidin-HRP. HRP was then activated via a Chemi Reagent before imaging with Chemidoc XRS (Bio-Rad, CA). OPN secretion in monoculture macrophages and conditioned-media environments after 24 or 72 hours of culture, respectively, was quantified using a Mouse/Rat osteopontin Quantikine ELISA (R&D Systems, Minneapolis, MN).

4.2.9 Western Blot Analysis

Cell lysates of macrophages and cardiomyocytes were prepared using a lysis buffer containing RIPA buffer, 1% Triton X100 (Boston BioProducts, MA) and 1% protease inhibitor (Sigma Aldrich, MO). Samples were then diluted 1:1 in Laemmli SDS buffer (Bio-rad, CA) with 5% 2-mercaptoethanol (Sigma Aldrich, MO). Primary antibodies used were rabbit anti-ERK1/2, rabbit anti-phospho-ERK1/2 (1:1000, Cell Signal, Danvers, MA), and rabbit anti-Stim1 (1:1000, Cell Signal). Secondary antibodies used were sheep anti-mouse-HRP and donkey anti-rabbit-HRP (1:1000, GE Healthcare). A minimum of three independent blots was performed for each protein of interest. Protein bands were normalized to the b-actin (1:1000, Sigma Aldrich) loading control and analyzed via densitometry (ImageJ).

4.2.10 Evaluation of Calcium-Handling Properties

After 3 days of co-culture, mES-CM were incubated at room temperature with Rhod-2AM (4 μM) for 30 minutes, followed by a 20 minutes washout (for AM cleavage) in normal Tyrode's solution (NT). Samples were then placed in a heated chamber (35˚C) with a fluorescent inverted microscope (Nikon Eclipse TE200) with an Andor Ixon Charge-Coupled device (CCD) camera (Andor Technology, at 50 frames/s, 512 x 180 pixels) as previously described [160,161]. The intensity of fluorescence was recorded and normalized to the basal diastolic fluorescence levels. Cells were electrically stimulated to examine their response to electrical pacing at 0.5, 1 and 2 Hz frequencies (4.5 ms duration, 150 V, Grass S48 Stimulator, Grass Medical Instruments, West Warwick, RI). Cells were treated with 10 mM caffeine, a ryanodine receptor agonist, to investigate

sarcoplasmic reticulum Ca^{2+} content and fractional Ca^{2+} release. Additionally, for the exploration of store operated Ca^{2+} entry (SOCE), mES-CM were challenged with 10 mM caffeine along with 10 μM cyclopiazonic acid (CPA), a potent sarco/endoplasmic reticulum ATPase inhibitor [248]. The protocol was as follows: 10 sec 1 mM Ca^{2+} NT, 10 sec 0 mM Ca^{2+} NT, 10 sec 1 mM Ca^{2+} NT, 10 sec 0 mM Ca^{2+} NT, 10 sec 0 mM Ca^{2+} NT + 10 μM CPA + 10 mM Caffeine, 10 sec 0 mM Ca^{2+} NT, 10 sec 1 mM Ca^{2+} NT + 10 μM CPA 10 mM Caffeine, 10 sec 0 mM Ca^{2+} NT.

4.2.11   Osteopontin (OPN) Inhibition

OPN was neutralized through the addition of an OPN specific antibody (OPN Ab) (R&D, 6 μg/mL) at the initiation of indirect co-culture. Briefly, conditioned media was collected from polarized macrophages and centrifuged (3 min, 10,000 RPM) to removed cells and floating debris. Macrophage conditioned media was then mixed 1:1 with mES-CM differentiation media before adding OPN Ab (100 μg/mL) to make a final concentration of 6 μg/mL.

4.2.12   OPN Addition

Recombinant mouse OPN (R & D) was added to mES-CM in monoculture by mixing mES-CM differentiation media with 200 μg/mL solution of OPN in 0.1% bovine serum albumin (Sigma Aldrich) to yield a final working concentration of 5 μg/mL.

4.2.13 Statistical Analysis

Results are presented as mean ± standard deviation or as individual data points and an average. Statistical analysis was performed in SPSS (Version 24, IBM) or Prism 7 (GraphPad) using a two-tailed independent samples t-test, one-way ANOVA or their nonparametric counterpart, followed by Tukey or Games-Howell post hoc tests, where appropriate. Statistical significance was accepted for p*<0.05.

4.3 Results

4.3.1 Macrophage Phenotype Characterization

RAW 264.7 macrophages (Figure 4.2A,D) were successfully polarized into either a pro-inflammatory phenotype with treatment of LPS and an anti-inflammatory phenotype with IL-4. LPS treated macrophages demonstrated a more spread out morphology with numerous projections (Figure 4.2B,E). Macrophages treated with IL-4 retained a smaller, rounded morphology (Figure 4.2C,F), similar to untreated controls.

Treatment with LPS for 3 days induced the secretion of pro-inflammatory cytokines including granulocyte colony-stimulating factor (G-CSF), granulocyte-macrophage colony-stimulating factor (GM-CSF), interleukin-1 receptor agonist (IL-1ra), intrleukin-6 (IL-6), regulated on activation normal T cell expressed and secreted (RANTES) and tumor necrosis factor alpha (TNF-α) (Figure 4.3A). Conversely, IL-4 treatment induced secretion of IL-4 and diminished secretion of pro-inflammatory cytokines such as interferon gamma-induced protein (IP-10), RANTES, TNF-α, G-CSF, GM-CSF, IL-1ra and IL-6 (Figure 4.3A).
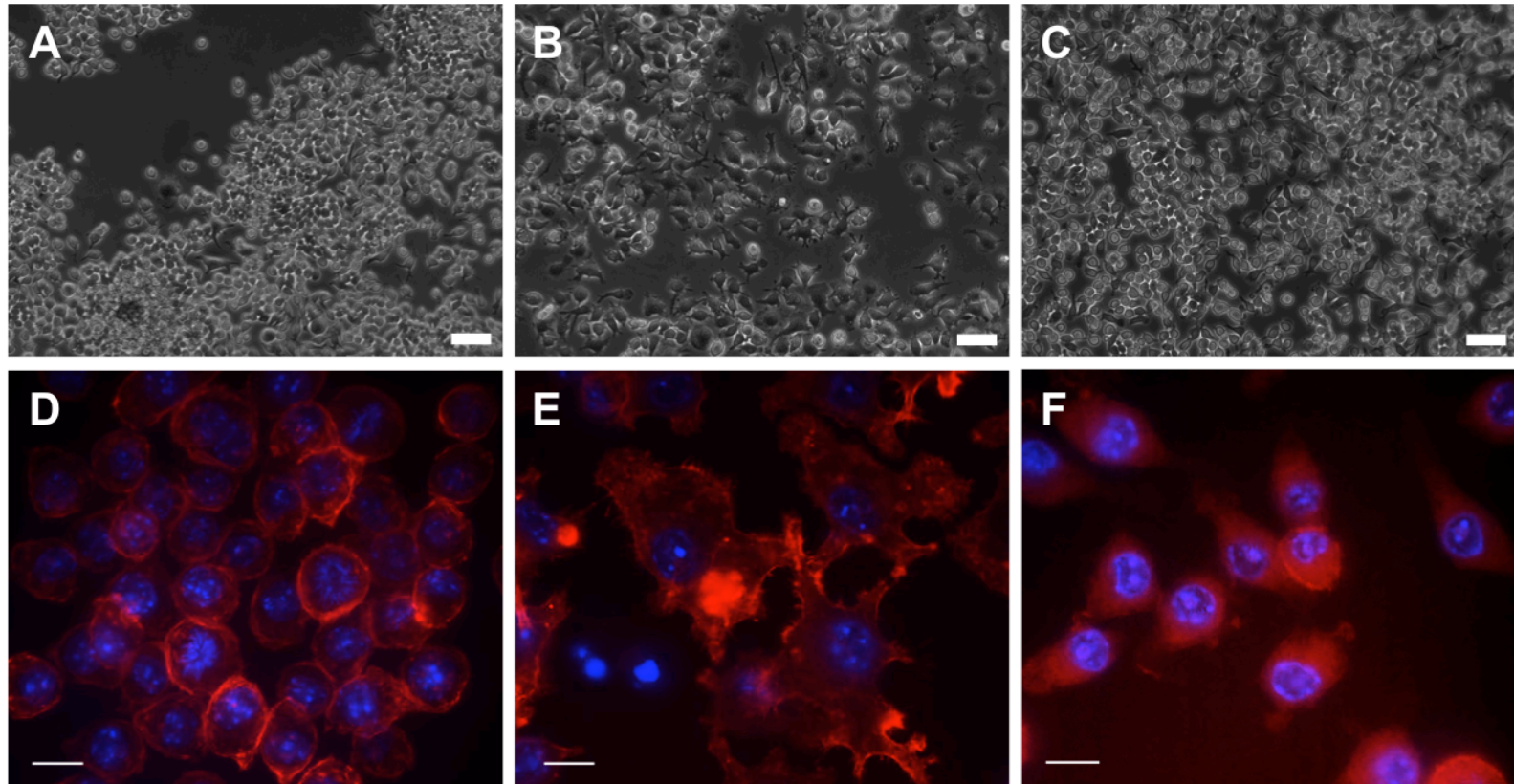
Figure 4.2 (A) Raw264.7 macrophages were polarized towards (B) a pro-inflammatory phenotype with LPS or (C) an anti-inflammatory phenotype with IL-4 (scale bars = 50 μm). F-actin staining with rhodamine-conjugated phalloidin (red) demonstrates the unique morphological features of (D) untreated, (E) LPS treated or (F) IL-4 treated macrophages (scale bars = 10 μm).

Source: Hitscherich, P. et al. Macrophages Affect Cardiomyocyte Calcium-Handling Function Via Matricellular Protein Secretion. (In preparation, 2018).

Gene analysis via RT-PCR also confirmed the expression of genes that are characteristic of either pro- and anti-inflammatory macrophage phenotypes. LPS treated macrophages demonstrated significantly higher expression of pro-inflammatory genes such as TNF-α, IL-1β, Cox2 and Nos2 compared to IL-4 treated macrophages (*p<0.05, Figure 4.3B). On the other hand, IL-4 treated macrophages expressed significantly higher levels of anti-inflammatory genes such as YM1 and ARG1 compared to LPS treated macrophages (*p<0.05, Figure 4.3B).
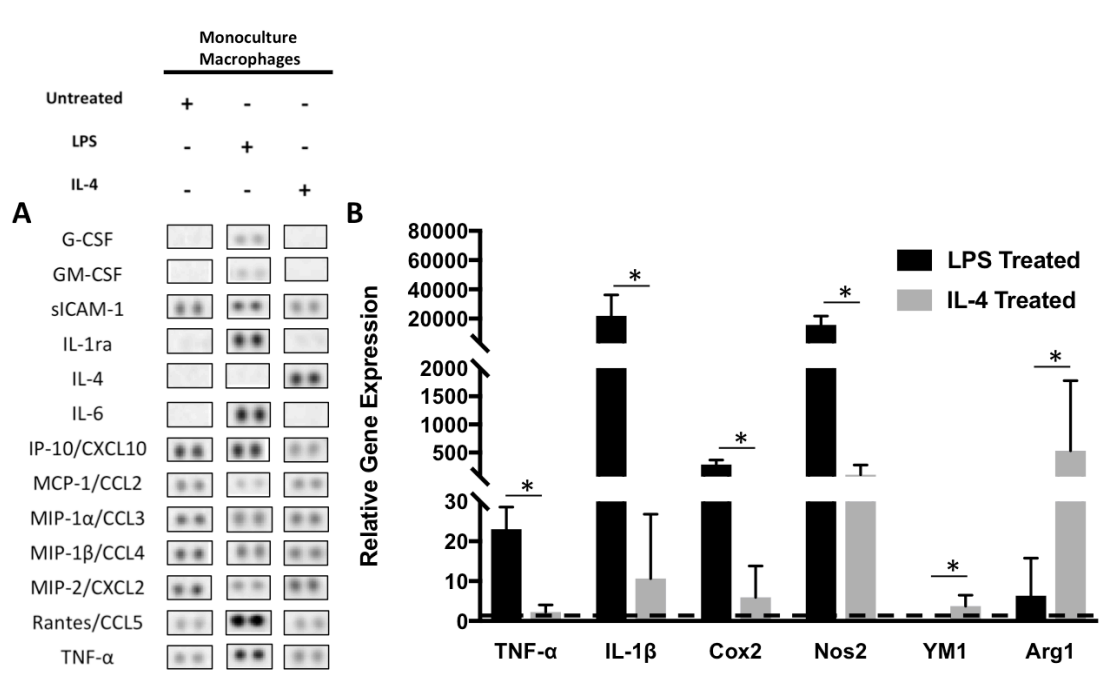
Figure 4.3 (A) Cytokine secretion screen by untreated, LPS and IL-4 treated macrophages after 3 days of monoculture (n=1). (B) Gene expression profiles of LPS and IL-4 treated macrophages after 24 hours of activation relative to untreated macrophages (n≥6, * p<0.05).
Source: Hitscherich, P. et al. Macrophages Affect Cardiomyocyte Calcium-Handling Function Via Matricellular Protein Secretion. (In preparation, 2018).

4.3.2 Indirect Myocardial Inflammation Model

4.3.2.1 mES-CM Characterization. Figure 4.4A-F displays representative images of mES-CM in culture exhibiting cTNT-eGFP expression in all experimental groups after 3 days. RT-PCR results demonstrated a significant down regulation of cTnT (Figure 4.4G) and Serca2 (Figure 4.4H) in mES-CM cultured in LPS-treated macrophage-conditioned media compared to mES-CM cultured in either untreated or IL-4-treated macrophage-conditioned media (*$p<0.05$). However, no significant differences were found in the ratio of Myh6/7 with culture in macrophage-conditioned media (Figure 4.4I). The ratio of Bax/BCL-2, which is a classical apoptosis marker, also remained unchanged in mES-CM cultured in macrophage-conditioned media (Figure 4.4J).

Calcium-handling properties of mES-CM were also explored after 72 hours. MES-CM cultured in LPS-treated macrophage-conditioned media exhibited significantly lower paced and caffeine-induced transient amplitude compared to mES-CM in IL-4-treated macrophage-conditioned media (#$p<0.05$, Table 4.1) and significantly lower paced transient amplitude compared to mES-CM in untreated macrophage-conditioned media (**$p<0.05$, Table 4.1). LPS-treated macrophage-conditioned media also induced significantly longer caffeine-induced transient T_{50} compared to that of mES-CM in monoculture (*$p<0.05$, Table 4.1). Although paced and caffeine-induced transient morphology differed among groups, fractional release, which is the measure of calcium-handling efficiency remained similar among mES-CM in all culture conditions (Figure 4.5A).

MES-CM cultured in IL-4-treated macrophage-conditioned media exhibited significantly higher baseline Ca^{2+} entry compared to mES-CM in monoculture (*$p<0.05$,
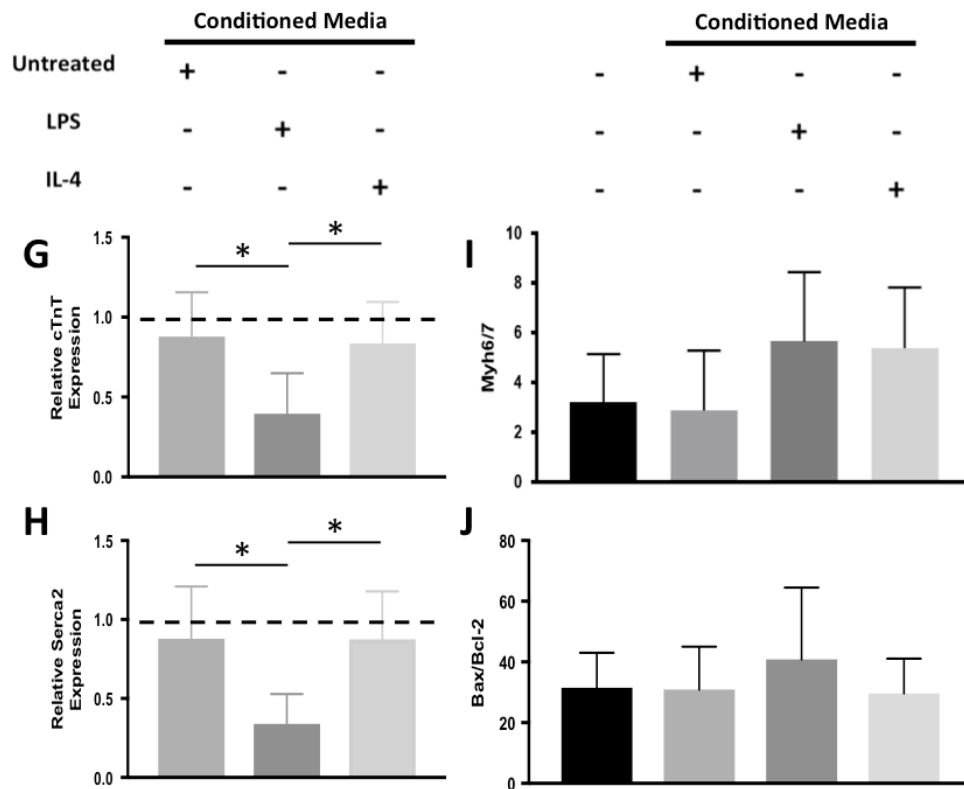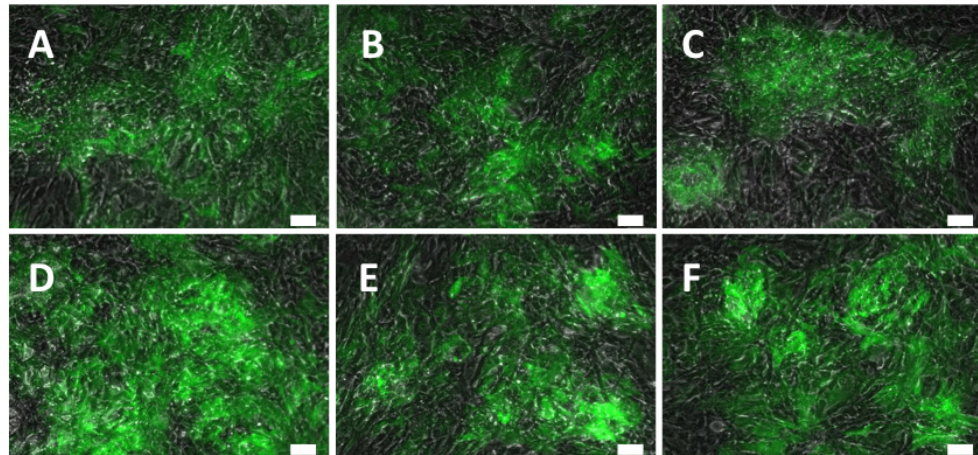
Figure 4.4 Expression of cTnT-eGFP (green) after 72 hours by mES-CM in (A) standard culture, (B) with LPS added, (C) with IL-4 added or in conditioned media culture with (D) untreated, (E) LPS treated or (F) IL-4 treated macrophages (scale bars = 50 μm). RT-PCR of cardiac specific markers such as (G) cTnT and (H) Serca2 as well as the ratio of (I) My6/My7 and apoptosis markers (J) BAX and BCL-2. (n≥5 and *p<0.05)

Source: Hitscherich, P. et al. Macrophages Affect Cardiomyocyte Calcium-Handling Function Via Matricellular Protein Secretion. (In preparation, 2018).
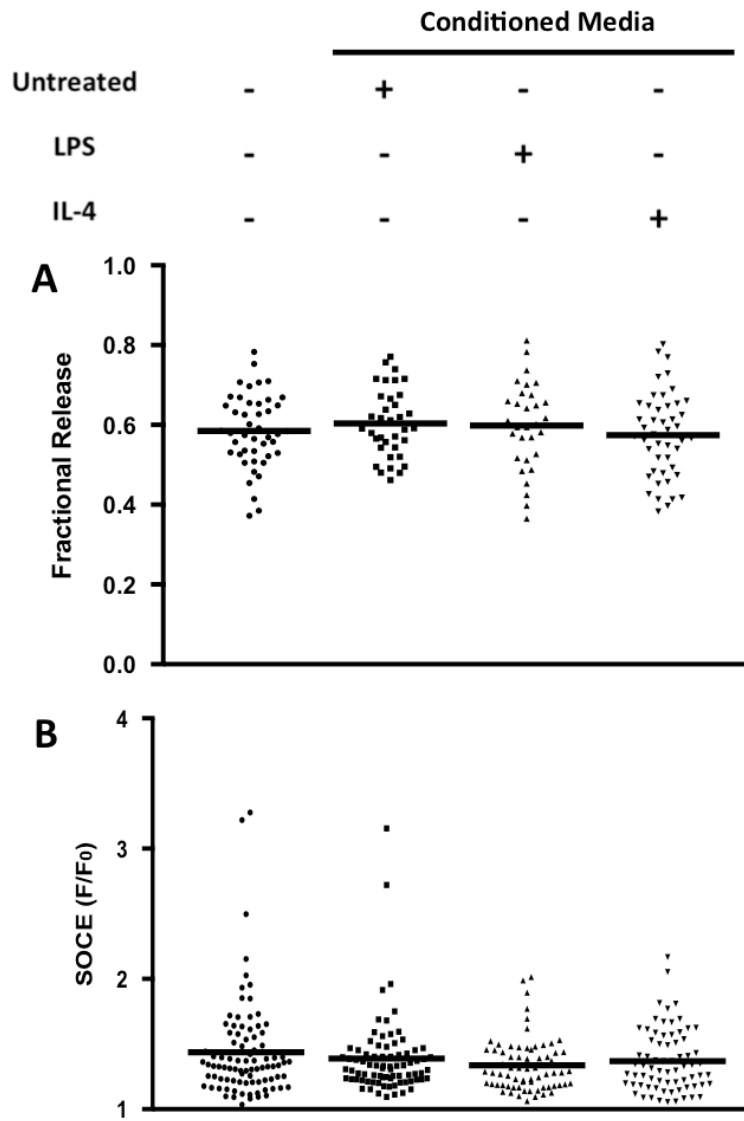
Figure 4.5 (A) Fractional release was calculated as the ratio between paced and caffeine induced transient amplitudes ($n \geq 31$) and (B) store operated Ca^{2+} entry (SOCE) was measured after treatment with caffeine and CPA ($n \geq 70$).

Source: Hitscherich, P. et al. Macrophages Affect Cardiomyocyte Calcium-Handling Function Via Matricellular Protein Secretion. (In preparation, 2018).

Table 4.1). MES-CM in untreated macrophage-conditioned media culture exhibited significantly lower total sarcoplasmic reticulum Ca^{2+} stores compared to mES-CM in monoculture and IL-4-treated macrophage- conditioned media culture (*,#p<0.05, Table 4.1). However, no significant differences in SOCE were found between mES-CM in conditioned media culture (Figure 4.5B).

Table 4.1 Calcium-Handling Properties of mES-CM in Conditioned Media Culture

	mES-CM	Conditioned Media		
		Untreated	LPS Treated	IL-4 Treated
n	44	36	31	46
Amp (F/F_0)	1.51 ± 0.18	1.53 ± 0.21	1.41 ± 0.16 **, #	1.52 ± 0.18
T_{50} (ms)	159.55 ± 84.07	181.26 ± 107.23	180.02 ± 85.07	157.80 ± 81.78
CI Amp (F/F_0)	2.61 ± 0.32	2.55 ± 0.34	2.41 ± 0.40 #	2.71 ± 0.41
CI T_{50} (ms)	813.46 ± 367.06	941.99 ± 245.62	1297.63 ± 816.23 *	925.68 ± 286.22
n	89	80	70	71
Baseline (F/F_0)	1.09 ± 0.03	1.12 ± 0.08	1.10 ± 0.07	1.12 ± 0.07 *
SR Stores (F/F_0)	2.19 ± 0.48	1.98 ± 0.33 *,#	2.16 ± 0.42	2.19 ± 0.55

n, cell number; Amp, Paced Transient Amplitude; T_{50}, Paced Transient T_{50}; CI Amp, Caffeine Induced Transient Amplitude; CI T_{50}, Caffeine Induced Transient T_{50}; Baseline, Baseline Ca^{2+} Entry; SR Stores, Sarcoplasmic Reticulum Ca^{2+} Stores.
*p<0.05 vs. monoculture mES-CM; **p<0.05 vs. mES-CM in untreated conditioned media; #p<0.05 vs. mES-CM in IL-4 treated conditioned media
Source: Hitscherich, P. et al. Macrophages Affect Cardiomyocyte Calcium-Handling Function Via Matricellular Protein Secretion. (In preparation, 2018).
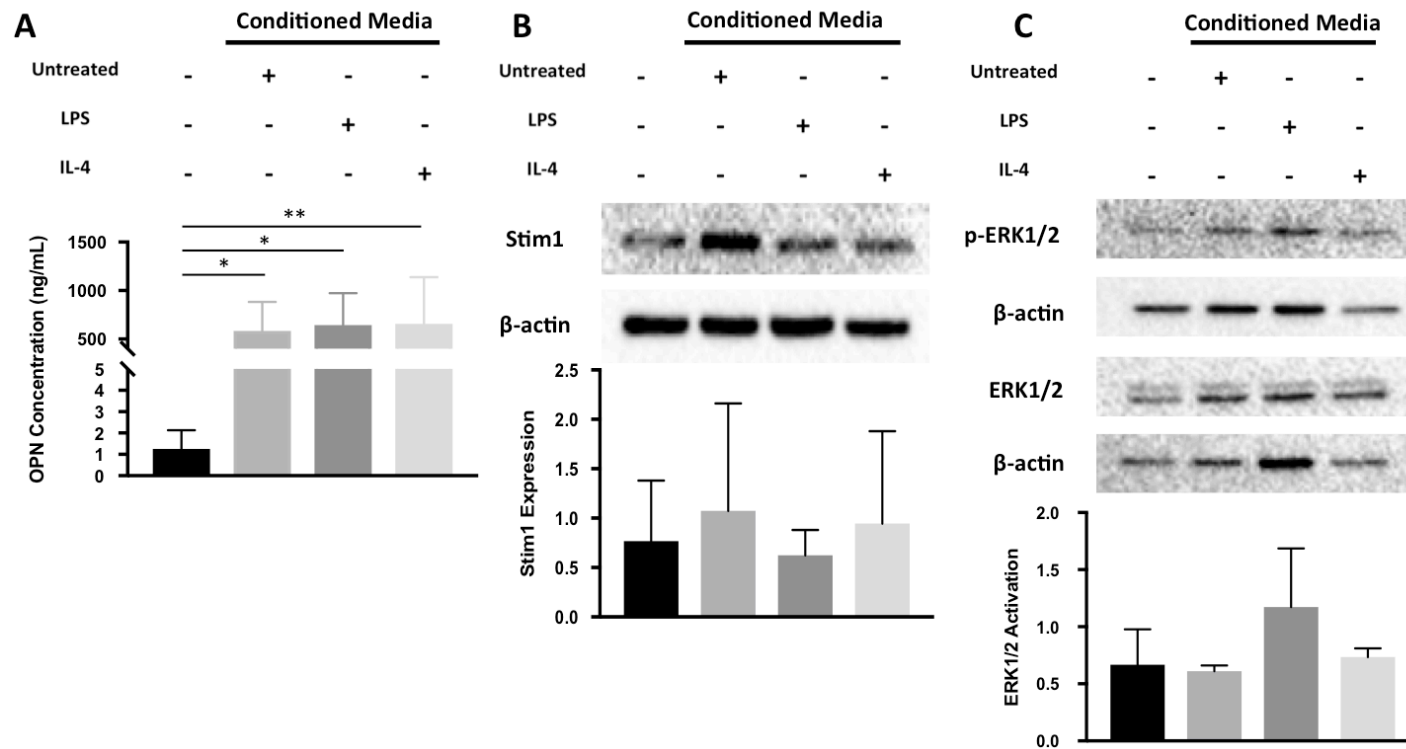
Figure 4.6 (A) Secretion of OPN in mES-CM monoculture and conditioned media cultures were measured after 3 days (n>4, *p<0.05, **p<0.01). (B) Representative blot demonstrating Stim1 expression of mES-CM in monoculture and conditioned media cultures after 3 days, with graphs demonstrating the average of 4 independent trials. (C) Activation of ERK1/2 in mES-CM in monoculture and conditioned media cultures was calculated as the ratio of phosphorylation, included is a representative blot as well as a graph demonstrating the average of 4 independent trials.

Source: Hitscherich, P. et al. Macrophages Affect Cardiomyocyte Calcium-Handling Function Via Matricellular Protein Secretion. (In preparation, 2018).

4.3.2.2 Matricellular Protein Expression and Action. In macrophage-conditioned media culture, significantly higher levels of OPN were present compared to mES-CM in monoculture after 3 days (*p<0.05, **p<0.01, Figure 4.6A). However, similar expression of Stim1, which is the Ca^{2+} sensor and regulator of SOCE, were found in mES-CM in all groups (Figure 4.6B). ERK1/2 phosphorylation was also found to be similar among all groups (Figure 4.6C).

When OPN was neutralized using OPN specific antibody, significant differences were found in SOCE response of mES-CM. Specifically, mES-CM cultured in IL-4-treated macrophage-conditioned media exhibited the lowest SOCE response with OPN inhibition, significantly lower than that of mES-CM in all other conditions without OPN inhibition (p<0.05, Figure 4.7A). MES-CM cultured in LPS-treated macrophage-conditioned media with OPN inhibition also exhibited significantly lower SOCE than mES-CM in monoculture as well as in untreated and IL-4-treated macrophage-conditioned media without OPN inhibition (p<0.05, Figure 4.7A). ERK1/2 phosphorylation was statistically similar among all groups, regardless of OPN inhibition. Although, ERK1/2 phosphorylation was the lowest in mES-CM in IL-4 treated conditioned media with OPN inhibition (Figure 4.7B). Additionally, when 5 μg/mL of recombinant OPN was added to mES-CM in monoculture, SOCE was significantly increased (*p<0.05, Figure 4.7C).
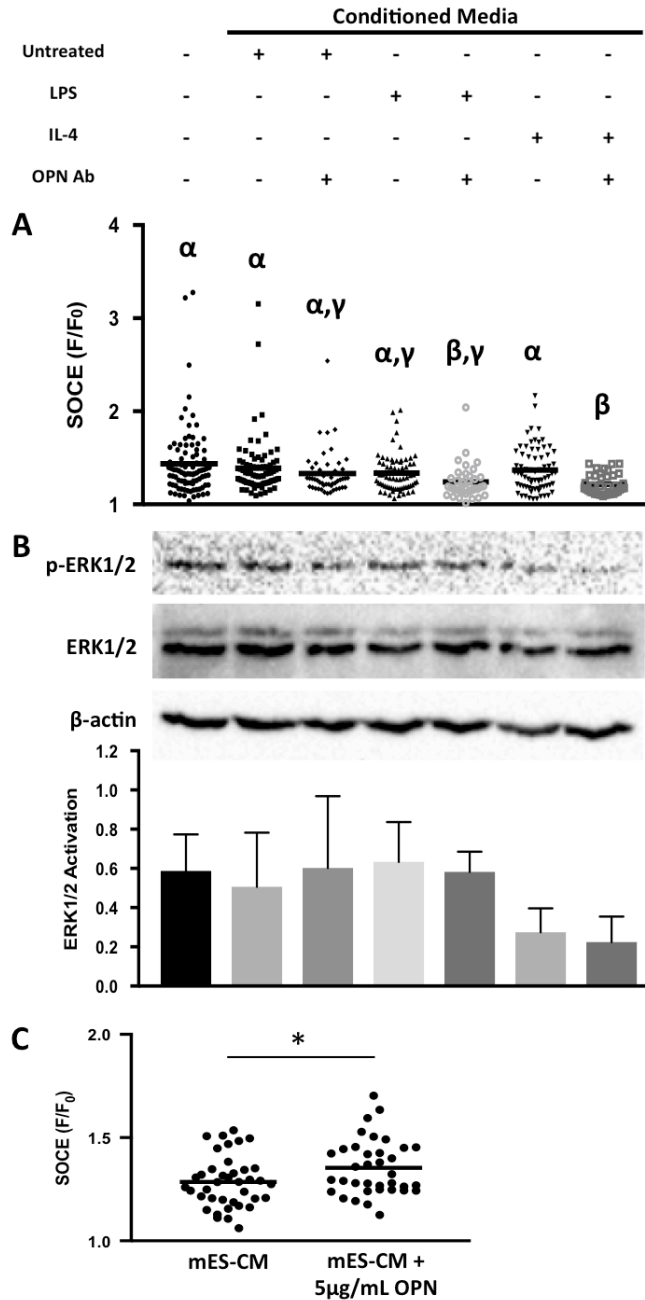
Figure 4.7 (A) Changes in SOCE in mES-CM in conditioned media culture due to OPN inhibition through the addition of an OPN antibody (Ab) were measured after 3 days (n≥38, p<0.05). Similar Greek letters indicate no significant difference between groups. (B) Representative blot of ERK1/2 activation, as well as a graph representing the average of 4 or more independent trials, of mES-CM in conditioned media culture with or without OPN inhibition after 3 days. (C) Changes in SOCE in mES-CM due to the addition of recombinant OPN after 3 days (n≥36, *p<0.05).
Source: Hitscherich, P. et al. Macrophages Affect Cardiomyocyte Calcium-Handling Function Via Matricellular Protein Secretion. (In preparation, 2018).

4.3.3 Direct Myocardial Inflammation Model

4.3.3.1 Macrophage Characterization. In the direct co-culture of macrophages and mES-CM, macrophages were initially seeded in isolation in the outer edge of the dishes. Due to their highly proliferative nature, some macrophages migrated towards mES-CM in the center of the dish to form direct cell-cell interactions with mES-CM. Over the course of 6 days, from initial seeding to day 3 of co-culture, their cell number increased 332.0 ± 65.1 times for untreated, 33.0 ± 4.6 times for LPS treated and 177.8 ± 9.8 times for IL-4 treated macrophages in co-culture. Even in co-culture with mES-CM, macrophages retained similar morphology as compared to those in monoculture after 3 days (Figure 4.8). Both untreated (Figure 4.8A) and IL-4-treated (Figure 4.8C) macrophages remained rounded, while LPS-treated macrophages (Figure 4.8B) were more spread out with projections.

The expression of classical pro-inflammatory genes such as IL-1β and Nos2 was up-regulated in LPS-treated macrophages in co-culture with mES-CM. Similarly, up-regulation of anti-inflammatory genes, such as YM1 and Arg1 were present in IL-4-treated macrophages in co-culture with mES-CM up to 3 days (Figure 4.8D). Pro-inflammatory cytokines, such as G-CSF, IL-1ra, IP-10, Rantes, MIP-2 and TNF-α were present in co-culture of mES-CM and LPS-treated macrophages after 3 days (Figure 4.9A). However, down regulation of pro-inflammatory cytokine secretion as well as up-regulation of IL-4 secretion was seen in co-culture of mES-CM and IL-4-treated macrophages by day 3 (Figure 4.9A). Expression of MCP-1, MIP-1α, MIP-1β, stromal derived factor 1 (SDF-1) and tissue inhibitor of metalloproteinase 1 (TIMP-1) was similar in all groups (Figure 4.9A). Interestingly, mES-CM in monoculture also exhibited low

levels of secretion of pro-inflammatory cytokines such as IP-10 and M-CSF. MES-CM also express high levels of stromal derived factor-1 (SDF-1), tissue inhibitor of metalloproteinase-1 (TIMP-1), macrophage chemotactic protein-1 (MCP-1) and thymus and activation regulated chemokine (TARC) (Figure 4.9B).
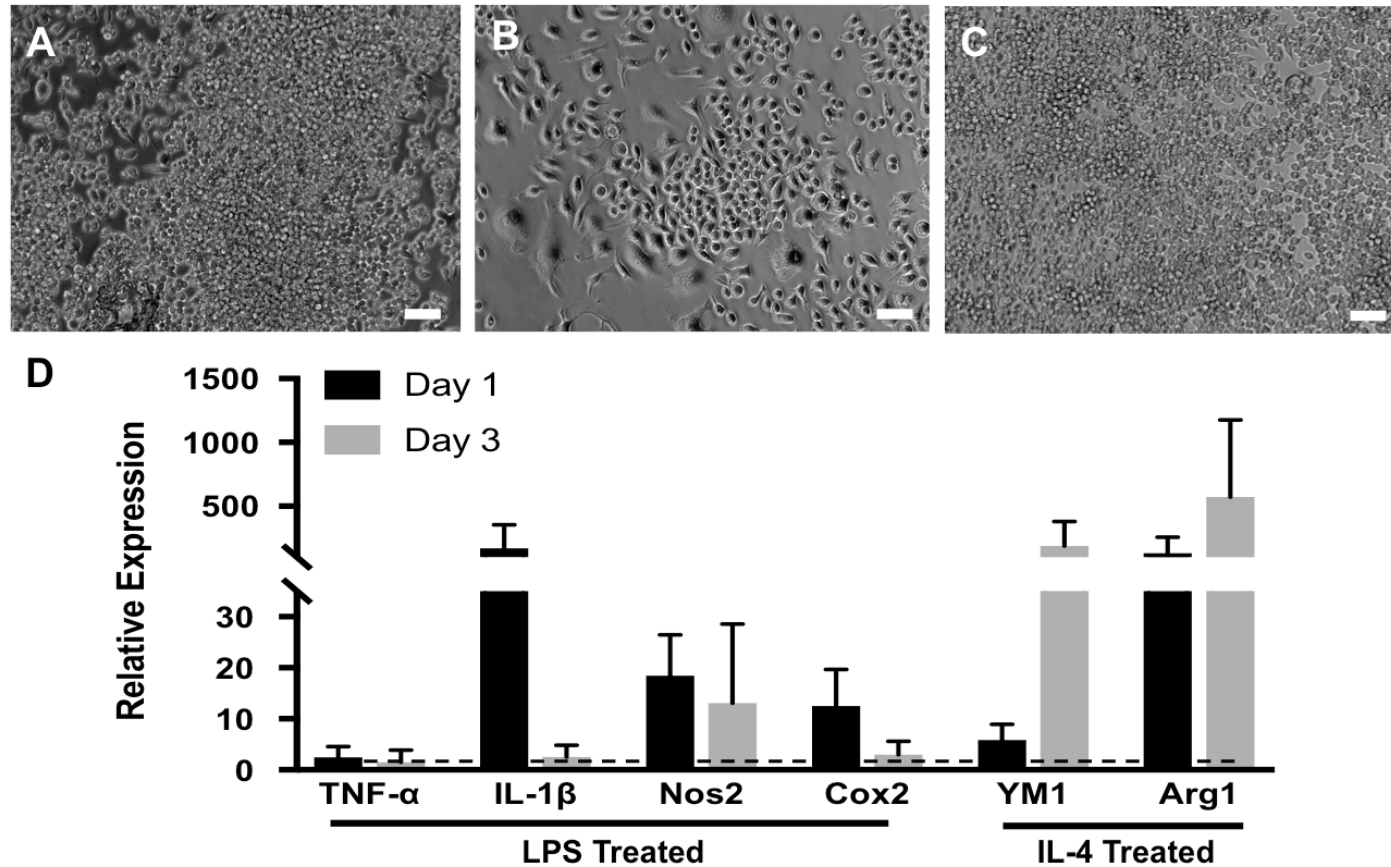
Figure 4.8 (A) Untreated, (B) LPS treated and (C) IL-4 treated macrophages in co-culture with mES-CM (scale bars = 50 μm). (D) Gene expression profiles of LPS and IL-4 treated macrophages in co-culture with mES-CM (n≥3).

Source: Hitscherich, P. et al. Macrophages Affect Cardiomyocyte Calcium-Handling Function Via Matricellular Protein Secretion. (In preparation, 2018).
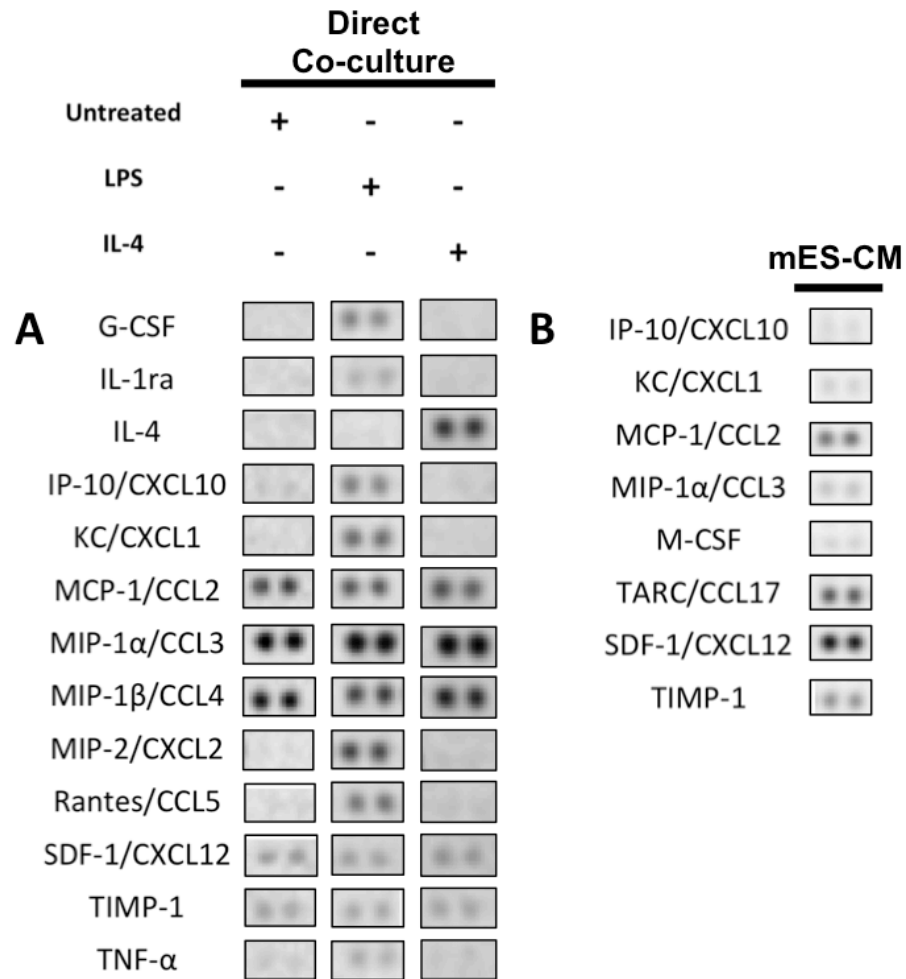
Figure 4.9 Cytokine secretion screen in (A) all direct co-culture conditions and (B) mES-CM in monoculture (n=1).
Source: Hitscherich, P. et al. Macrophages Affect Cardiomyocyte Calcium-Handling Function Via Matricellular Protein Secretion. (In preparation, 2018).

4.3.3.2 mES-CM Characterization. During 3 days of co-culture with macrophages, similar cTnT-eGFP expression was observed in mES-CM independent of macrophage phenotype (Figure 4.10A-D). However, even after only 24 hours of co-culture with macrophage subsets, significant changes in calcium-handling behavior were observed. After 24 hours, mES-CM co-cultured with IL-4-treated macrophages exhibited significantly higher paced transient amplitude compared to mES-CM cultured in all the other conditions (*,**,##$p<0.05$, Table 4.2) and significantly higher caffeine-induced transient amplitude compared to mES-CM in monoculture or untreated macrophage co-culture (*,**$p<0.05$, Table 4.2). No significant differences in paced or caffeine-induced transient T_{50} were found.

After 3 days, mES-CM co-cultured with IL-4-treated macrophages exhibited significantly higher paced transient amplitude compared to mES-CM in LPS-treated macrophage co-culture (##$p<0.05$, Table 4.2). MES-CM co-cultured with untreated macrophages also exhibited significantly higher paced transient amplitude than mES-CM in all other conditions (*,**$p<0.05$, Table 4.2) and significantly longer paced transient T_{50} compared to co-culture with LPS-treated macrophages (**$p<0.05$, Table 4.2). However, mES-CM in co-culture with untreated macrophages also exhibited significantly shorter caffeine-induced transient T_{50} compared to mES-CM in monoculture and co-culture with LPS-treated macrophages (*,**$p<0.05$, Table 4.2).

Additionally, mES-CM co-cultured with untreated and IL-4-treated macrophages exhibited significantly higher fractional release compared to mES-CM in monoculture or LPS-treated macrophage co-culture after 24 hours (**$p<0.05$,#,##$p<0.005$, Figure 4.10E).
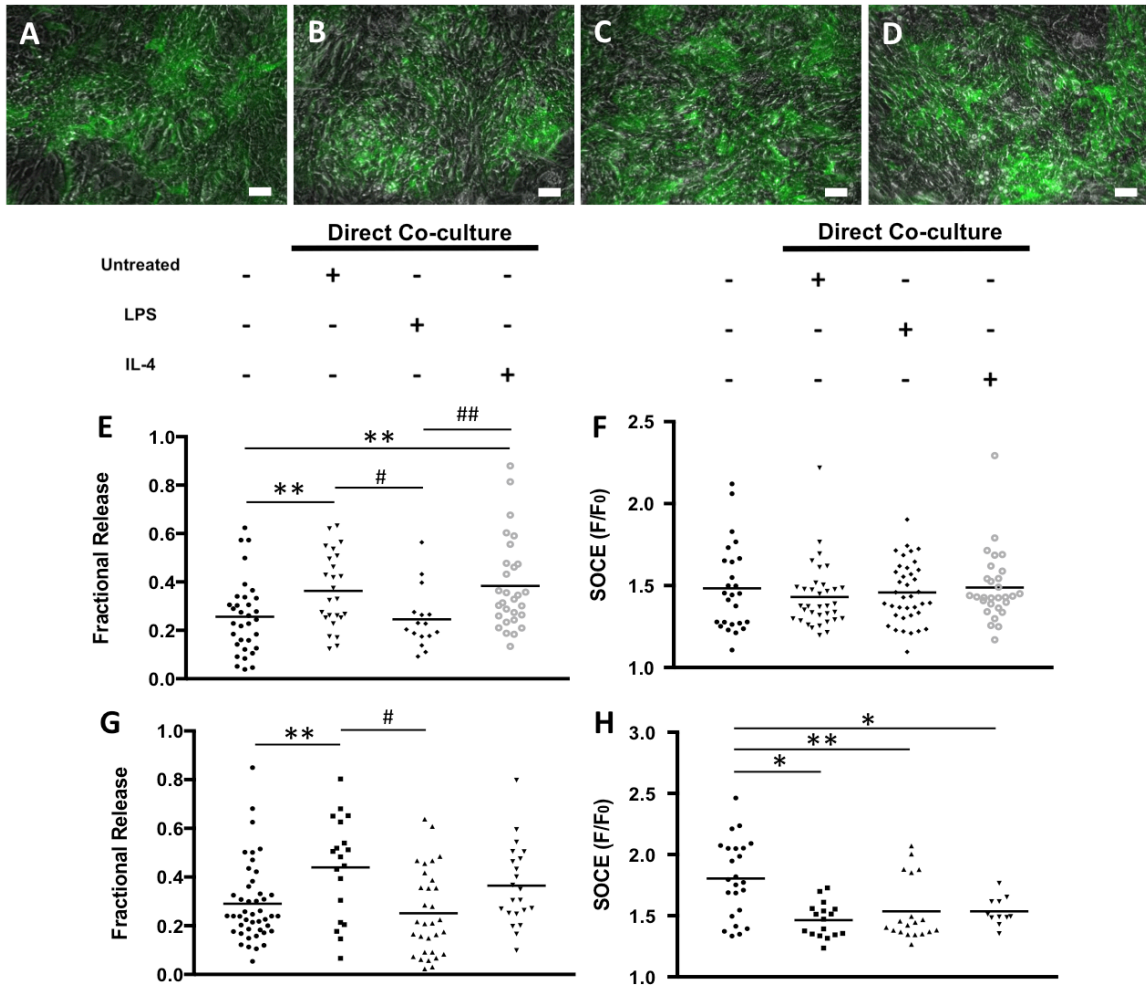
Figure 4.10 Expression of cTnT-eGFP in mES-CM in (A) monoculture and (B) untreated, (C) LPS treated or (D) IL-4 treated macrophage co-culture (scale bars = 50 μm). (E,G) Ca^{2+} fractional release (n≥16) and (F,H) SOCE (n≥11) in mES-CM in monoculture or direct co-culture after 24 or 72 hours, respectively. (*,[#,##] p<0.005, **p<0.05)

Source: Hitscherich, P. et al. Macrophages Affect Cardiomyocyte Calcium-Handling Function Via Matricellular Protein Secretion. (In preparation, 2018).

MES-CM co-cultured with untreated macrophages maintained significantly higher fractional release compared to mES-CM in monoculture and LPS-treated macrophage co-culture up to 3 days (**$p<0.05$,[#]$p<0.005$, Figure 4.10G).

SOCE related properties were also measured in mES-CM in co-culture with macrophage subsets (Table 4.3). After 24 hours, mES-CM co-cultured with LPS-treated macrophages exhibited significantly higher baseline Ca^{2+} entry than mES-CM in co-culture with untreated macrophages (**$p<0.05$) and significantly higher sarcoplasmic reticulum Ca^{2+} stores than all other groups (*,**,[#]$p<0.05$). After 3 days, no significant differences in baseline Ca^{2+} entry were found but mES-CM co-culture with untreated macrophages exhibited significantly lower sarcoplasmic reticulum Ca^{2+} stores compared

Table 4.2 Calcium-Handling Properties of mES-CM in Co-culture

| 24 hours | mES-CM | Direct Co-culture | | |
		Untreated	LPS Treated	IL-4 Treated
n	33	25	16	29
Amp, F/F_0	1.18 ± 0.09	1.31 ± 0.17 *	1.29 ± 0.15	1.48 ± 0.19 *, **, ##
T_{50}, ms	133.6 ± 59.0	138.0 ± 52.5	225.2 ± 124.8	188.9 ± 105.5
CI Amp, F/F_0	1.88 ± 0.42	1.94 ± 0.58	2.24 ± 0.63	2.45 ± 0.58 *, **
CI T_{50}, ms	1817.5 ± 1618.9	1377.6 ± 655.8	1515.7 ± 891.8	1193.9 ± 602.0
72 hours				
n	45	19	31	22
Amp, F/F_0	1.33 ± 0.19	1.63 ± 0.37 *	1.24 ± 0.15 **	1.36 ± 0.14 **, ##
T_{50}, ms	136.9 ± 91.6	180.1 ± 70.3	129.1 ± 47.6 **	169 ± 88.7
CI Amp, F/F_0	2.22 ± 0.41	2.36 ± 0.52	2.11 ± 0.46	2.07 ± 0.35
CI T_{50}, ms	1335.6 ± 762.8	914.1 ± 427.7 *	1376.4 ± 693.2 **	1025.4 ± 287.0

n, cell number; Amp, Paced Transient Amplitude; T_{50}, Paced Transient T_{50}; CI Amp, Caffeine Induced Transient Amplitude; CI T_{50}, Caffeine Induced Transient T_{50}.
*$p<0.05$ vs. monoculture mES-CM; **$p<0.05$ vs. mES-CM in untreated conditioned media; [##]$p<0.05$ vs. mES-CM in LPS treated conditioned media
Source: Hitscherich, P. et al. Macrophages Affect Cardiomyocyte Calcium-Handling Function Via Matricellular Protein Secretion. (In preparation, 2018).

Table 4.3 Calcium-Handling Properties Related to SOCE of mES-CM in Co-culture

24 hours	mES-CM	Direct Co-culture		
		Untreated	LPS Treated	IL-4 Treated
n	≥ 23	≥ 34	≥ 36	≥ 29
Baseline, F/F_0	1.11 ± 0.05	1.10 ± 0.04	1.14 ± 0.06 **	1.13 ± 0.06
SR Stores, F/F_0	2.07 ± 0.46	2.03 ± 0.45	2.39 ± 0.36 *, **, #	2.13 ± 0.42
72 hours (n)				
n	24	≥ 16	19	≥ 10
Baseline, F/F_0	1.18 ± 0.08	1.19 ± 0.09	1.22 ± 0.17	1.13 ± 0.03
SR Stores, F/F_0	2.18 ± 0.36	1.82 ± 0.37 *	1.91 ± 0.46	2.02 ± 0.27

n, cell number; Baseline, Baseline Ca^{2+} Entry; SR Stores, Sarcoplasmic Reticulum Ca^{2+} Stores.
*$p<0.05$ vs. monoculture mES-CM; **$p<0.05$ vs. mES-CM in untreated conditioned media; #$p<0.05$ vs. mES-CM in IL-4 treated conditioned media
Source: Hitscherich, P. et al. Macrophages Affect Cardiomyocyte Calcium-Handling Function Via Matricellular Protein Secretion. (In preparation, 2018).

to monoculture (*$p<0.05$). While no changes in SOCE were observed after the first 24 hours of co-culture (Figure 4.10F), significantly depressed SOCE response was demonstrated after 3 days of co-culture with macrophages independent of their subtypes (*$p<0.005$,**$p<0.05$, Figure 4.10H).

4.3.3.3 Matricellular Protein Expression.   Gene expression of TSP-1 and OPN were examined in macrophages and mES-CM in monoculture as well as in co-culture conditions. TSP-1 expression was over 5 orders of magnitude higher in co-culture macrophages and was significantly increased in IL-4 treated co-culture macrophages compared to monoculture macrophages (*$p<0.05$, Figure 4.11A). However, TSP-1 expression was similar in mES-CM regardless of culture condition (Figure 4.11C). OPN expression was similar in macrophages regardless of co-culture condition and was higher
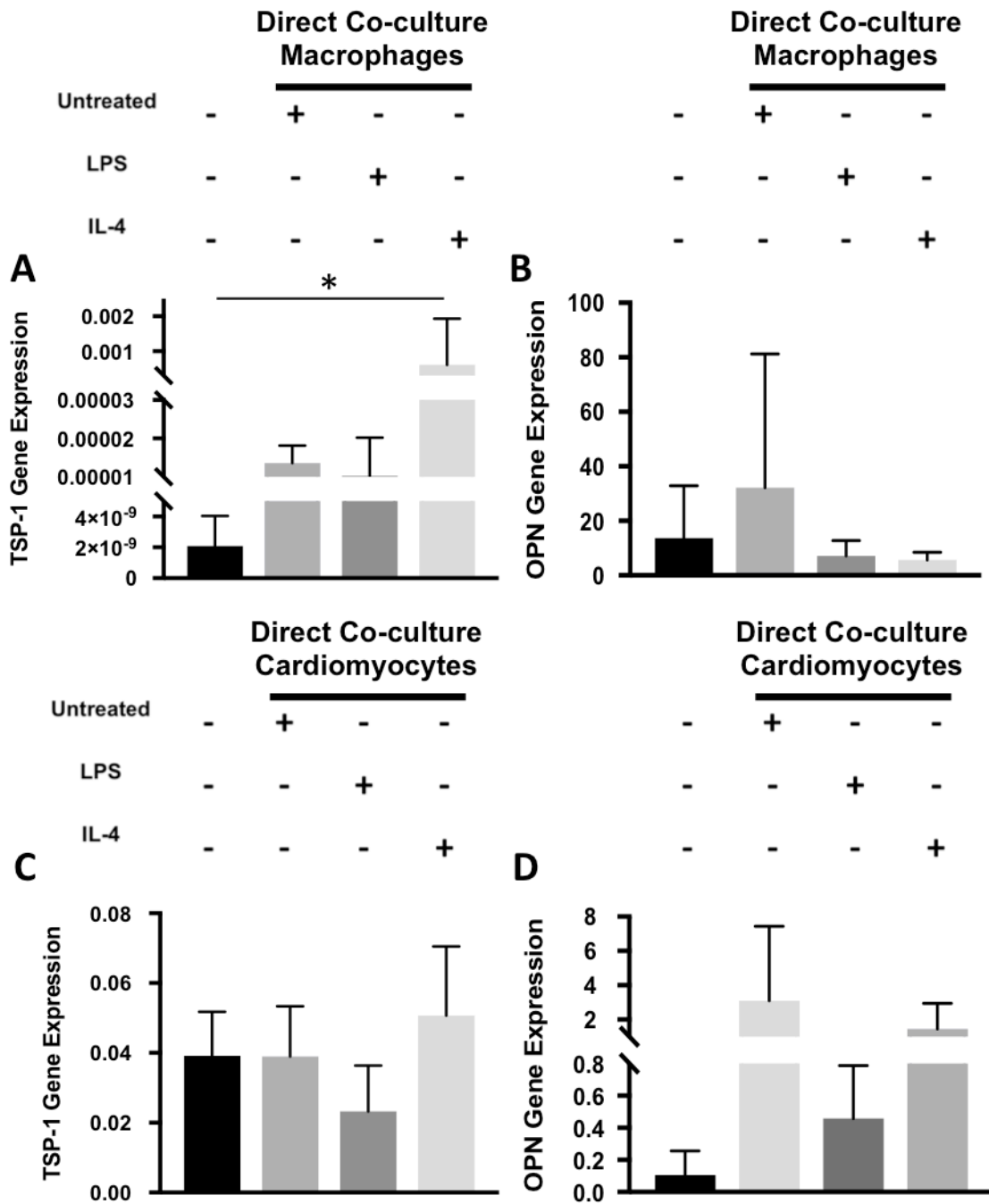
Figure 4.11 Gene expression of (A) TSP-1 and (B) OPN by macrophages in monoculture and direct co-culture with mES-CM after 72 hours. Gene expression of (C) TSP-1 and (D) OPN by mES-CM in monoculture and direct co-culture with macrophages after 72 hours ($n \geq 3$, *$p < 0.05$).

Source: Hitscherich, P. et al. Macrophages Affect Cardiomyocyte Calcium-Handling Function Via Matricellular Protein Secretion. (In preparation, 2018).
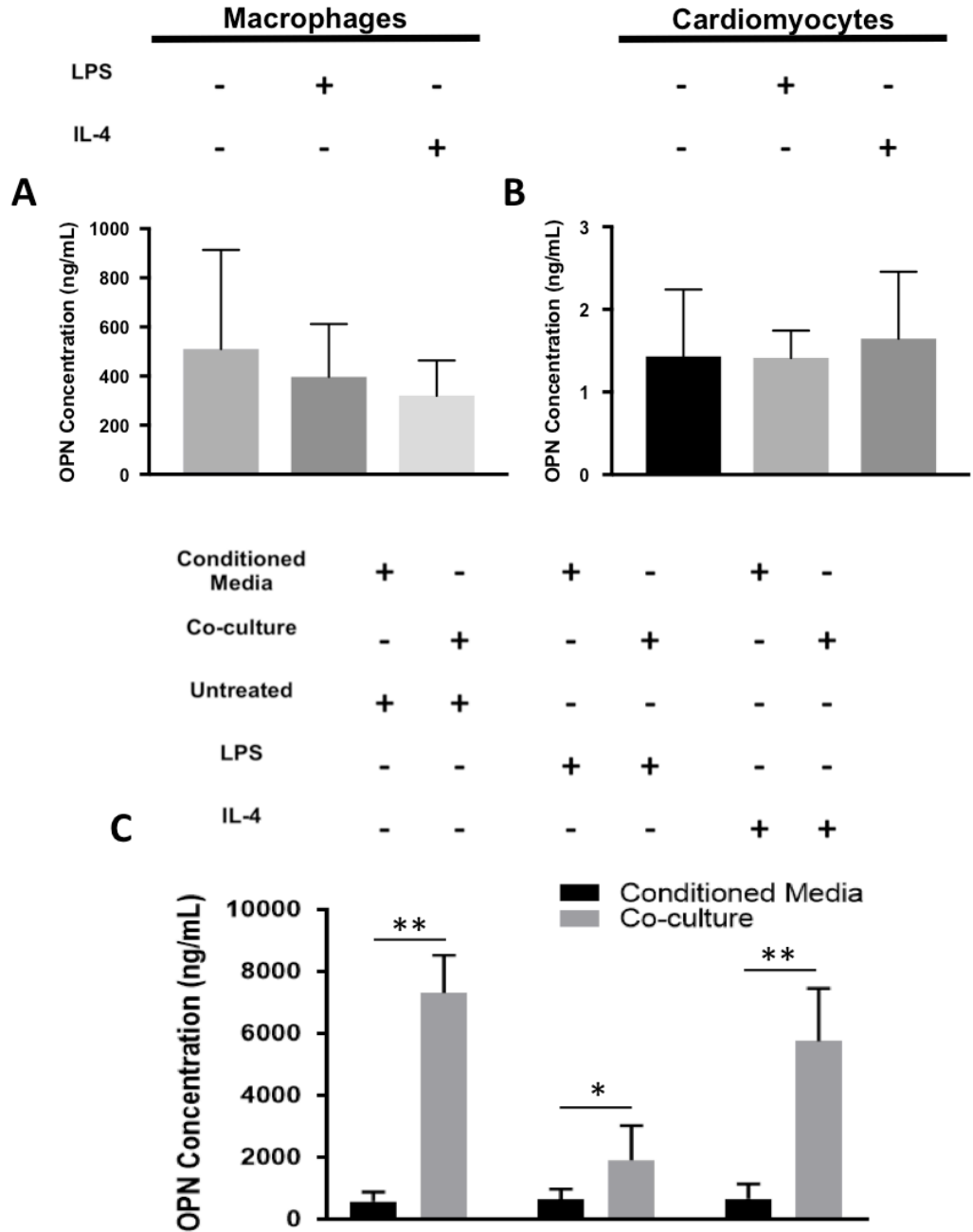
Figure 4.12 OPN secretion in monoculture (A) macrophages and (B) mES-CM. (C) OPN secretion in direct co-culture conditioned compared to corresponding conditioned media groups. (n≥3, *p<0.05, **p<0.001)

Source: Hitscherich, P. et al. Macrophages Affect Cardiomyocyte Calcium-Handling Function Via Matricellular Protein Secretion. (In preparation, 2018).

than TSP-1 expression (Figure 4.11B). MES-CM expressed over four times as much OPN when in co-culture regardless of macrophage phenotype (Figure 4.11D).

All monoculture macrophage populations secreted over 200 ng/mL OPN after 24 hours (Figure 4.12A), while mES-CM groups secreted less than 3 ng/mL over 3 days (Figure 4.12B). Additionally, all co-culture conditions contained over 1800 ng/mL of OPN, significantly higher than the corresponding conditioned media groups ($*p<0.05,**p<0.001$, Figure 4.12C).

4.4 Discussion

Each year, millions of people suffer from MI in the United States. Even those patients who survive MI are left with irreversible damage to the heart and changes in ventricle geometry that result in decreased cardiac performance [249,250]. Despite the immense significance, little is known about the specific roles of key cell types involved in post-MI myocardial survival, remodeling and function. Macrophages are one of the key cell types involved post-MI during the inflammation phase [212]. Very recently, a microfluidic device was created to examine the effect of inflammation on the survival of rat H9c2 cells when in co-culture with LPS treated, pro-inflammatory macrophages [145]. Ai et al. found that pro-inflammatory macrophages increased myocyte apoptosis via mitochondrial damage but did not examine any other phenotypic or functional changes [145]. They only examined the pro-inflammatory microenvironment and therefore were unable to address the influence of temporally changing macrophage phenotypes present in the post-MI microenvironment. In this study, both a indirect and direct myocardial inflammation model was created, to simulate the post-MI microenvironment and to better understand

how distinct macrophage subsets affect pluripotent stem cell derived cardiomyocyte phenotype and function. This study specifically focuses on the effect of macrophages on calcium-handling function of cardiomyocytes to identify a potential mechanism through which macrophages and cardiomyocytes interact after injury.

Macrophages of two different subsets were successfully derived as confirmed by their gene expression and cytokine secretion. Polarized macrophage subsets exhibited distinct morphologies with the pro-inflammatory subset exhibiting a more round, spread out morphology consistent with previously described work using bone marrow derived macrophages [251]. LPS treated macrophages expressed known sets of pro-inflammatory makers such as TNF-α, IL-1β, Nos2 and Cox2 [244]. IL-4 treated macrophages, however, expressed significantly higher levels of characteristic anti-inflammatory markers, including YM1 and ARG1 [244], with significantly lower levels of pro-inflammatory markers as expected. LPS treatment up-regulated pro-inflammatory cytokine secretion after 24 hours consistent with a previously described studies using bone marrow derived macrophages and RAW264.7 cells [145,216,252,253]. LPS treated macrophage secretion of pro-inflammatory cytokines such as MCP-1, MIP-1α and RANTES match with the cytokines found in serum of patients up to 7 days post-MI [254], suggesting the translational potential of the model. Alternately, IL-4 treatment induced the down-regulation of pro-inflammatory cytokine secretion as well as up-regulation of IL-4 secretion [255].

To explore the effects of macrophage derived factors on cardiomyocyte function, conditioned media from polarized macrophage subsets was first used to culture mES-CM. Our results suggest that differentiation and maturation of mES-CM is not affected by macrophage-secreted factors as evidenced by similar expression of Myh6/7 ratio in all

96

conditioned media groups. Moreover, similar BAX and BCL-2 expression suggested that macrophage-derived factors do not affect mES-CM apoptosis in contrast to a recent study that reported increased cardiomyocyte apoptosis when in indirect co-culture with pro-inflammatory macrophages [145].However, cardiomyocyte culture with pro-inflammatory macrophage-conditioned media led to a significant down-regulation of Serca2, which is the principle regulator of cytoplasmic Ca^{2+} efflux [256]. Down regulation of Serca2 was correlated to the significant changes in sarcoplasmic reticulum calcium-handling, namely caffeine-induced transient T_{50}. This change in Serca2 expression suggests that a prolonged or exaggerated pro-inflammatory environment could contribute to Serca2 down-regulation, which can progress into the development of heart failure post-MI [257]. Moreover, as Serca2 up-regulation post-MI may aid in preservation of ventricular function [258], our results suggest that timely resolution of inflammation may improve ventricular function through increased Serca2 expression.

Another calcium-handling mechanism known to be up-regulated in response to stress or inflammation is SOCE[243,259,260]. Traditionally found in non-electroactive cell types, SOCE is associated with changes in sarcoplasmic reticulum Ca^{2+} stores. While there exists some debate over whether SOCE is present in healthy adult cardiac tissue, it has been identified in cardiomyocytes during the embryonic and neonatal phase of development [228] as well as in embryonic stem cell derived cardiomyocytes [229]. In our macrophage-conditioned media treated mES-CM group, no significant SOCE differences were detected. Because stem cell derived cardiomyocytes were used in our study, it is plausible that the innate presence of SOCE in these cells did not allow for the demonstration of macrophage-derived factors' effect on SOCE response.

One of the proteins known to be up-regulated in response to inflammation is OPN [261]. OPN is secreted by macrophages [233,235-237] and while knockout studies suggest that OPN plays a crucial role in the healing process immediately after MI [238], it is also associated with the development of cardiac hypertrophy and the regulation of Ca^{2+} homeostasis [233,235-237]. OPN is a matricellular protein, which is a non-structural protein that localizes at the infarct border zone [233,234,262]. Matricellular proteins can act as cell-matrix interaction mediators or as cytokines to initiate cellular processes [263]. OPN is known as a promiscuous cytokine, interacting with multiple types of integrins as well as other cell surface receptor like CD44, which are implicated in the cardiac inflammatory response [221,264-266]. OPN binding initiates multiple mitogen-activated protein kinase (MAPK) pathways within the cells ultimately regulating ERK1/2 activation [235,264,266]. ERK1/2 is also known to regulate SOCE by regulating the phosphorylation of stromal interaction molecule 1 (Stim1), the calcium sensor on the SR that regulates SOCE [267,268]. Because of this it was hypothesized that SOCE could be regulated by OPN via ERK1/2 however, the link between OPN and SOCE has not previously been demonstrated in cardiomyocytes.

In this study, the effect of OPN on mES-CM calcium-handling behavior was explored. Results confirmed that OPN was mostly secreted by macrophages independent of their phenotype with negligible secretion by mES-CM. The concentration of OPN in all macrophage-conditioned media groups, although significantly higher than monoculture mES-CM, was within a normal range of serum OPN concentration seen in patients [269], which may be below the concentration threshold for causing significant changes in our experimental groups. However, OPN inhibition elicited significant

changes in mES-CM SOCE response, especially with culture in LPS- and IL-4-treated macrophage-conditioned media, suggesting OPN promotes SOCE response in mES-CM. Furthermore, the addition of recombinant OPN at a concentration similar to plasma OPN concentrations in patients from day 3 to day 7 post-MI with successful reperfusion [269], induced significant up-regulation of SOCE in mES-CM. These results demonstrate for the first time that macrophage secreted OPN is sufficient to elicit increases in cardiomyocyte SOCE response.

Since macrophages are now known to connect with cardiomyocytes via gap junctions [5] contributing to steady state cardiac function, co-culture of macrophages and mES-CM was also performed to determine the effects of direct cell-cell interaction on cardiomyocyte calcium-handling function. Maintenance of macrophage subset phenotype in co-culture was first confirmed by morphology and gene expression, which remained similar to macrophages in monoculture. Interestingly in direct co-culture condition, the secretion of TIMP-1 and SDF-1 were detected. Since the secretion of TIMP-1 and SDF-1 was demonstrated by mES-CM in monoculture and not by macrophages in monoculture, it is likely that mES-CM are the main source of TIMP-1 and SDF-1 in the co-culture conditions. SDF-1 is secreted by cardiomyocytes post-MI exhibiting a paradoxical role by both promoting cardiomyocyte apoptosis and being considered cardioprotective [270-272]. TIMP-1 expression in our mES-CM cultures could be from nonmyocytes, e.g. cardiac fibroblast-like cells, as TIMP-1 is known to be secreted by macrophages and fibroblasts in the post-MI microenvironment [273]. It is demonstrated that TIMP-1 is involved with left ventricular remodeling as well as cell signaling [273]. A high level of TARC secretion was also demonstrated by mES-CM in monoculture. Although

TARC is known to be associated with inflammation and may be involved with coronary artery disease, it is not known whether or not cardiomyocytes secrete TARC [274].

The initial seeding density ratio of mES-CM to macrophages was 10:1 but after 3 days of co-culture, the resulting densities change dependent on macrophage phenotype. Based on quantification data of macrophage infiltration in a mouse MI model by Vandervelde et al., macrophage density changes can be estimated as 180 million/cm^3 to 400 million/cm^3 to 320 million/cm^3 on day 3 to 4 to 7, respectively [275]. Taking into account the healthy, normal cardiomyocyte density of an adult heart at about 28 million cells/cm^3,[18] the ratio of cardiomyocytes to macrophages present in the infarct border zone could be estimated at 1:6, 1:14 and 1:11 from day 3 to 4 to 7, respectively. In our direct co-culture model, the LPS treated condition exhibited a cardiomyocyte to macrophage ratio of about 1:4, similar to day 3 post-MI, when pro-inflammatory macrophages are known to inhabit the infarcted myocardium. Additionally, direct co-culture with IL-4 treated macrophages demonstrated a cardiomyocyte to macrophage ratio of about 1:18 at day 3 of co-culture, similar to post-MI day 4 and 7, when the shift towards a pro-healing and anti-inflammatory phenotype of macrophages is present in the infarct. This suggests relevant cell-cell ratios between cardiomyocytes and macrophages in our direct co-culture model.

It was demonstrated that the expression of cTnT by mES-CM is not affected by the presence of macrophages independent of their phenotype in co-culture. Conversely, Ca^{2+} fractional release in mES-CM was significantly affected by the presence of macrophages after only 24 hours of co-culture. Specifically, co-culture with anti-inflammatory macrophages, either untreated or IL-4 treated, elicited enhanced Ca^{2+}

cycling efficiency, as demonstrated by a significantly higher fractional release [173]. Increased fractional release was maintained in those culture conditions for up to 72 hours. Further investigation of SOCE response demonstrated no change after 24 hours, but direct co-culture with all macrophage subsets led to significant down-regulation of SOCE after 3 days of culture. These results suggest that direct cell-cell interaction between activated macrophages and cardiomyocytes was necessary to significantly affect cardiomyocyte calcium-handling function.

Again, because matricellular proteins TSP-1 and OPN are up-regulated post-MI and are associated with regulation of Ca^{2+} homeostasis [225,231,233,235], their expression was examined in co-culture. However, very low TSP-1 expression in all conditions and inconsistent up-regulation in all co-culture conditions, suggests that it is less likely to be directly involved in cardiomyocyte calcium-handling behavior. However, despite significantly elevated levels of OPN, the promotion of SOCE was completely reversed when direct contact between mES-CM and macrophages was present. This suggests that while macrophage secreted OPN may promote SOCE, direct contact with macrophages significantly suppresses SOCE in mES-CM.

OPN has been explored as a potential biomarker for the prediction of adverse events and outcomes related to vascular conditions [276] as well as prediction of death in patients suffering chronic heart failure [277]. Our results further support the use of OPN as a marker of cardiac diseases and suggests macrophage secreted OPN could play an important role in the disruption of Ca^{2+} homeostasis through the promotion of SOCE leading to long-term pathological hypertrophy development if not regulated properly. Further exploration of the complicated crosstalk between activated macrophages and

mES-CM, as well as the effects on adult myocytes or human derived cell types would be interesting. These model can also be expanded to include additional features of the post-MI microenvironment, namely hypoxia or reactive oxygen species, in order to better recapitulate the native post-MI microenvironment. Nevertheless, this study demonstrated for the first time, novel *in vitro* myocardial inflammation models dedicated to understanding the effects of activated macrophage subsets on cardiomyocyte calcium-handling function and its relationship to macrophage secreted matricellular proteins.

CHAPTER 5

CONCLUSIONS AND FUTURE DIRECTIONS

The objective of this dissertation was to present insights into cardiac regenerative medicine gleaned through the exploration of *in vitro* models of healthy and diseased cardiac tissues. To accomplish this goal, the study was divided into two separate aims.

Aim 1 was to develop functional *in vitro* cardiac tissues. This was accomplished through the use of two types of electroactive biomaterials, which were electrospun into highly aligned and anisotropic scaffolds, mimicking the native myocardial tissue architecture. The first was PVDF-TrFE, a piezoelectric material, which is known to generate electrical charge via mechanical deformation. It was hypothesized that the contraction of mES-CM cultured on the scaffold could deform the scaffold enough to generate changes in electrical charge. This would in turn, stimulate the seeded cardiomyocytes, promote differentiation and enhance function. When mES-CM were cultured on PVDF-TrFE, not only did they attach and express cardiac specific markers, but also followed the topographical cues and formed highly aligned and anisotropic tissues that spontaneously contracted. MES-CM cultured on PVDF-TrFE scaffolds could also be electrically paced, responded to ryanodine receptor and β-adrenergic stimulation. Additionally, mES-EC, a vascular cell type, were cultured on PVDF-TrFE scaffolds. Not only did mES-EC remain viable when cultured on PVDF-TrFE scaffold but also were able to maintain their mature phenotype including the ability to uptake LDL and expressed EC specific markers. Taken together, results indicate that PVDF-TrFE offers a promising base for cardiac tissue engineering applications.

103

The second electroactive material was a novel, conductive graphene composite scaffold. PCL+G scaffolds exhibited even distribution of graphene particles forming local conductive networks, which increased the overall conductivity of the scaffold with as little as 0.005% graphene content. When mES-CM were seeded on PCL+G scaffolds, they not only attached, but grew into the scaffolds. They exhibited classical cardiac specific markers, well-registered sarcomeres and spontaneously contracted for up to two weeks in culture. The combination of graphene and highly aligned fiber orientation elicited the most efficient calcium-handling properties in mES-CM, with an average fractional release of over 40% and significantly shortened caffeine induced transient decay. Taken together, results confirm the biocompatibility of conductive PCL+G scaffold and its potential to promote the enhanced function of *in vitro* cardiac tissues.

It is, however, important to note the limitations associated with the aforementioned tissue models. First, functional analysis was also performed on a single cell basis, requiring dissociation of mES-CM from scaffold-based tissues for examination. Although dissociation treatments were kept consistent across all sample groups, it would be beneficial to examine functional properties in intact tissues. Additional functional measures, such as twitch force, could also be explored for further characterization of mES-CM derived cardiac tissues.

Future studies that could be explored for Aim1 include the addition of external stimulation. For PVDF-TrFE, the addition of mechanical stretching could enhance the piezoelectric activity of the material. For PCL+G based tissues, further exploration of the novel point electrical stimulation device could elucidate the benefits of cardiomyocyte culture on scaffolds with electroactive networks. Future studies also include a transition

to *in vivo* mouse MI models. It is important to examine the functional integration of electroactive biomaterials *in vivo* for clinical applications. It is yet to be determined whether electroactive biomaterials elicit any arrhythmia or changes in electrical activity of the cells upon implantation.

The limitation for PVDF-TrFE scaffolds is their non-biodegradability. It would be interesting to explore whether that plays a role in the regulation of inflammation post-MI through a graft-versus-host reaction. It would be necessary to explore biodegradable piezoelectric biomaterials in the future. In addition, long-term *in vivo* studies examining the effects of graphene particles and whether they are retained on the scaffolds awaits further investigation.

In Aim 2 an *in vitro* myocardial inflammation model was developed in order to better understand the post-MI microenvironment. First, it was confirmed that activated subpopulations of macrophages could be generated. Macrophages were successfully polarized towards either a pro- or anti-inflammatory phenotype as evidenced by gene expression and cytokine secretion. Secreted factors from macrophage subpopulations were then used to culture mES-CM in an indirect co-culture model. Some significant changes were seen in the pro-inflammatory conditioned media group, including decreased cTnT and Serca2 expression. However, calcium-handling properties such as fractional release and SOCE were unchanged despite significantly higher levels of OPN, a matricellular protein hypothesized to cause significant changes in mES-CM calcium-handling function. Inhibition of OPN significantly decreased SOCE in LPS and IL-4 treated conditioned media groups and reduced ERK1/2 activation in those conditions. Furthermore, the addition of recombinant OPN at a concentration similar to plasma OPN

concentrations in patients' post-MI induced significant up-regulation of SOCE in mES-CM. Together, these data suggest for the first time a possible connection between OPN and SOCE in cardiomyocytes potentially through the regulation of ERK1/2.

To determine the effects of direct cell-cell interaction on mES-CM calcium-handling function a direct co-culture model was created with polarized macrophage subpopulations. Direct co-culture demonstrated that macrophage subsets had distinct effects on mES-CM calcium-handling function that changed over time. Specifically, mES-CM co-cultured with untreated and IL-4 treated macrophages exhibited significantly higher fractional release after 24 hours. However, only mES-CM co-cultured with untreated macrophages kept the significantly increased fractional release by day 3. Additionally, SOCE response was unchanged after 24 hours but after 3 days, all co-culture conditions induced a significant depression of SOCE in mES-CM despite the significant up-regulation of OPN secretion in all co-culture conditions. This suggests that while macrophage secreted OPN may promote SOCE, direct contact with macrophages significantly suppresses SOCE in mES-CM.

In summary, Aim 2 demonstrated direct cell-cell interaction with macrophages was necessary to elicit significant changes in mES-CM calcium-handling function. Additionally, it revealed a novel pathway involved in calcium-handling function of cardiomyocytes in the post-MI microenvironment. OPN has been explored clinically as a marker for myocardial injury and as a potential therapeutic target for post-MI remodeling. Results from Aim 2 further confirm OPN as an important regulator of cardiomyocyte calcium-handling function. Furthermore, OPN, if not regulated properly post-MI, could play an important role in the disruption of Ca^{2+} homeostasis, through

regulation of SOCE, leading to long-term pathological development and ultimately heart failure.

While RAW264.7 cells were used in this study, further studies can be extended using other macrophages including primary bone marrow derived macrophages to better recapitulates the native microenvironment within the heart post-MI. The use of mouse derived cells limits the translation of the research and it would be necessary to repeat the studies with human derived cells to examine species dependency. Additionally, for Aim 2, because stem cell derived cardiomyocytes do remain immature post-differentiation, it would be interesting to study the effects of activated macrophage subsets on adult cardiomyocytes to explore changes in their calcium-handling behavior as well.

Future studies for Aim 2 include further investigation of OPN and its effect on cardiomyocyte function and the development of maladaptive cardiac dysfunction and disease in an *in vivo* MI animal model. Because OPN is present in numerous tissues in the body and knock-out mice have demonstrated detrimental post-MI healing, methods for temporal and spatial regulation of OPN should be explored. One potential option is the use of an injectable hydrogel exhibiting release of an OPN inhibitor or exhibiting a mimic for OPN antibody. Additionally, the *in vitro* model could be enhanced through the addition of other characteristic of the post-MI microenvironment, such as induction of reactive oxygen species or mimicking the hypoxic environment of the infarct.

In conclusion, the presented results expand the current state of research in cardiac regenerative medicine by 1) demonstrating the potential of two electroactive biomaterials for the formation of functional cardiac tissues and by 2) creating a simplified *in vitro*

inflammation model of the highly complex post-MI microenvironment which could illuminate novel targets for the enhancement of post-MI remodeling and healing.

APPENDIX A

RT-PCR PRIMERS

Table A.1 contains the forward and reverse primer sequences for all genes analyzed via

RT-PCR. [245,246,278-285]

Table A.1 List of RT-PCR Primers

Gene	Forward	Reverse	Source
Matricellular Proteins			
OPN	CTTTCACTCCAATCGTCCCTAC	GCTCTCTTTGGAATGCTCAAGT	278
TSP-1	GTGTTTGACATCTTTGAACTC	CCAAAGACAAACCTCACATTC	279
Cardiac Specific Markers			
cTnT	GAGACAGAGGAGGCCAACGTA	CTTTCCTTCTCCCGCTCAT	280
Serca2	TGCCTGGTAGAGAAGATGAA	CCCTTCACAAACATCTTGCT	281
My6	CTCCTTGTCATCAGGCAC	ACATTCTTCAGGATTCTCTG	282
My7	CTTCTCAGACTTCCGCAG	TTCCTTACTTGCTACCCTC	282
Apoptosis Markers			
Bax	TGCAGAGGATGATTGCTGAC	GATCAGCTCGGGCACTTTAG	283
BCL-2	ACAACCGCGAGCCAGGTA	CAGGGCATAGAACTCGGAAG	283
Pro-inflammatory Markers			
TNF-α	CGTCAGCCGATTTGCTATCT	CGGACTCCGCAAAGTCTAAG	284
IL-1β	GCCCATCCTCTGTGACTCAT	AGGCCACAGGTATTTTGTCG	284
Nos2	GAGCGAGGAGCAGGTGGAAGACTA	GCGCTGCCCTTTTTTGCCCCATAG	285
Cox2	TTCACCCGAGGACTGGGCCATGGA	GCCCCACAGCAAACTGCAGGTTCT	285
Anti-inflammatory Markers			
YM1	GAAGCCCTCCTAAGGACAAAC	GCAGCCTTGGAATGTCTTTCT	285
Arg1	AGGCCCTGCAGCACTGAGGAA	GCCAGGTCCCCGTGGTCTCTCA	285
Pluripotent Markers			
Nanog	GTCTGCTACTGAGATGCTCTG	CTTGCACTTCATCCTTTGG	245
Oct3/4	CATACTGTGGACCTCAGGTT	CTCACACGGTTCTCAATGCT	245
Sox2	CAAGACGCTCATGAAGAAGG	AGTGGGAGGAAGAGGTAACC	245
Mesoderm Markers			
Hand1	GCTACGCACATCATCACCAT	GATCTTGGAGAGCTTGGTGT	245
rachyury	CTGCCTACCAGAATGAGGAG	GAGAACCAGAAGACGAGGAC	245
Twist2	AGAGCGACGAGATGGACAAT	TGTTCTGAGAGTTCCGGTC	245
Endoderm Markers			
PDX1	CTTTCCCGTGGATGAAATCC	GTCAAGTTCAACATCACTGCC	246
Sox17	CCATAGCAGAGCTCGGGGTC	GTGCGGAGACATCAGCGGAG	246
Pax4	ACCAGAGCTTGCACTGGACT	CCCATTTCAGCTTCTCTTGC	246
Ectoderm Markers			
Fgf5	ATGAGCCTGTCCTTGCTCTT	TCGTGGGAGCCATTGACTTT	245
Otx2	GACGTTCTGGAAGCTCTGTT	ATGGTTGGGACTGAGGTACT	245
Sox1	CCAAGAGACTGCGCGCGCTG	GGGTGCGCCGGGTGTGCGTG	245
Housekeeping Gene			
β-actin	GATCTGGCACCACACCTTCT	GGGGTGTTGAAGGTCTCAAA	285

APPENDIX B

SELF ASSEMBLING PEPTIDE HYDROGELS

In Appendix B, mouse embryonic stem (mES) cells will be characterized in a self-assembling peptide hydrogel (SAPH) [107].

B.1 Introduction

Embryonic stem cells (ESCs) can be successfully differentiated into cells of all three germ layers and have unlimited proliferation potential, making them an ideal cell source for regenerative medicinal applications [245]. However, most early and current clinical trials related to regenerative cell injection or transplantation utilize adult autologous stem cells. As a result, these studies have failed to demonstrate complete tissue regeneration due to the inability of adult stem cells to differentiate into cells of interest, such as cardiomyocytes [86]. Currently, The U.S. National Library of Medicine's ClinicalTrials.gov website lists only 17 clinical trials involving embryonic stem cells or cells derived from their progenitors. In fact, the first clinical trial involving pluripotent stem cells or cells derived from them was completed less than a decade ago [286]. This lack of approved trials is due to the safety concerns associated with pluripotent stem cell derived cells [286]. For this reason, it is critical to develop a niche in which these cells can be matured into homogeneous somatic cell populations that maintain their mature phenotype post-implantation.

It has been also demonstrated that even if there were success *in vitro* with differentiating a mature population of somatic cells from pluripotent stem cell sources, there are still issues associated with the delivery including massive cell death after

injection [287] and limited retention or homing of the cells to the site of injury, limiting the potential benefits of these therapies [288]. Because of this, researchers have begun to explore different materials, such as hydrogels, to address some of these hurdles.

Self-assembling peptide hydrogels (SAPHs) are thixotropic —they liquefy under shear force and reassemble when the force is removed [108,109,289]. This property allows them to flow during injection and then be reconstituted at the site of injection. This property may also protect the cells suspended in the 3D hydrogel during injection, promoting cell survival. They can also be tailored to include specific sequences, such as a cell adhesion sequence like RGD. This could potentially increase retention of cells at the site of injury. In this study, ESCs are cultured in SAPH to examine spatiotemporally directed differentiation. Such cell-hydrogel combinations have great potential for site-directed delivery via transcatheter implantation or direct injection into the desired site.

B.2 Methods

B.2.1 Peptide Synthesis

Peptides were synthesized using solid-phase peptide synthesis with acetyl N-terminal and amide C-terminal protective groups, using methods described elsewhere [111,289] having a sequence of K-SLSLSL-RG-SLSLSL-K-G-RGDS, termed SLac. Peptide was the lyophilized before dissolution in 298 mM sucrose in water (Sigma Aldrich).

B.2.2 mES Cell Seeding in SAPH

MES were trypsinized (Gibco, Grand Island, NY) and then resuspended in LIF and serum-free mES cell medium at a density of 2×10^6 cells/mL. Cell solution was then

mixed with equal volume of 1% SLac peptide generating a 0.5% SLac SAPH with a density of 1 x 10^6 cells/mL. SAPH+mES were incubated for 15 minutes at 37 °C before LIF free mES cell medium was added. SAPH+mES were maintained for up to 28 days.

B.2.3 SAPH+mES Characterization

B.2.3.1 Cluster Measurement. Cell clusters within SAPH+mES were imaged in phase contrast using confocal fluorescence microscope (IX81 DSU, Olympus, Somerset, NJ) and cluster diameters were measured using ImageJ software.

B.2.3.2 Cell Viability. A LIVE/DEAD Viability/Cytotoxicity kit (Life Technologies, NY) was used to determine viability of cells on scaffolds after 3 and 6 days of culture. Briefly, scaffolds were rinsed with warm PBS and then stained with 0.2 M ethidium homodimer and 0.005 M calcein for 30 minutes at 37 °C. Immunofluorescent images were obtained using a confocal fluorescence microscope (IX81 DSU, Olympus, Somerset, NJ) and the ratio of live/dead cells to the total number of cells was analyzed using ImageJ software.

B.2.3.3 RT-PCR. Total RNA was extracted from SAPH+mES using TRIzol (Invitrogen, Carlsbad, CA) as previously described [290]. Briefly, frozen tissues were thawed and homogenized in 1mL of TRIzol using a 20-G needle and syringe until totally dissolved, then incubated at room temperature for 5 minutes. Chloroform, 200 uL, was then added to mixture before shaking vigorously for 25 seconds followed by 2-minute incubation at room temperature. Samples are then centrifuged for 15 minutes at 12,000

RPM to generate a dual phase solution. The top phase is collected and then purified using the GenElute Mammalian Total RNA Miniprep Kit following manufacturers instruction. CDNA was created with 500ng of RNA and the High-Capacity cDNA Reverse Transcription Kit (Applied Biosystems, Grand Island, NY) in the T100 Thermal Cycler (Bio-rad, Hercules, CA). RT-PCR reactions were then prepared with the SSo Advanced SYBRgreen Mastermix (Bio-rad, Hercules, CA) and the primers listed in Table A1 (IDT, Coralville, Iowa).[245,246] The qPCR reaction was then run in a CFX Connect Real Time System (Bio-rad, Hercules, CA). Fold change increases in expression over mES cells in standard culture were calculated using the Comparative C_T method as described previously.[247]

B.2.4 Statistical Analysis

Results are presented as mean ± standard deviation. Statistical analysis for gene expression was performed using a one-way ANOVA followed by Tukey post-hoc tests where appropriate. Statistical analysis for cluster diameter was performed using a two-tailed independent samples t-test or its no- parametric equivalent Mann Whitney U test. Statistical significance was accepted for $p < 0.05$.

B.3 Results and Discussion

MES were distributed in SLac and cultured for up to 28 days in LIF free media, allowing for stem cell differentiation. MES cells, which were initially distributed in the peptide, demonstrated high cellular viability (Figure B.1A). Interestingly, by 7 days, mES cells start to form clusters and large viable mES cell clusters are apparent in the peptide
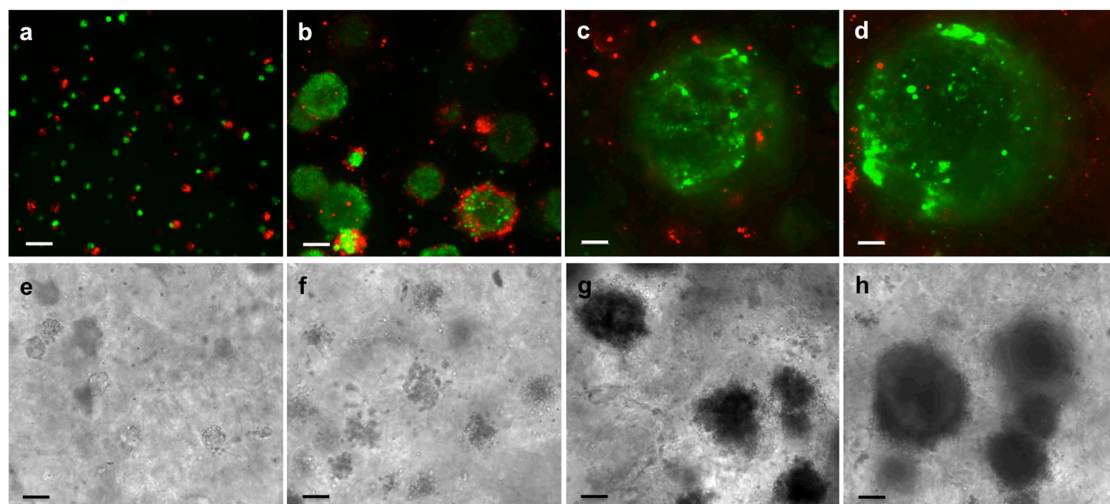
Figure B.1 mES cell viability in SLac peptide hydrogels was assessed via Live/Dead assay (Live (green), dead (red)) at (a) day 0, (b) day 7, (c) day 14 and (d) day 28. Clusters within SLac SAPH were imaged after (e) 3, (f) 7, (g) 14 and (h) 28 days of culture. Scale bars = 50 μm.

Source: Hitscherich, P. et al. Injectable Self-Assembling Peptide Hydrogels for Tissue Writing and Embryonic Stem Cell Culture. J. Biomed. Nanotech. 14, 802-807, (2018).

(Figure B.1B,F). Cluster size significantly increased at each time point (Figure B.2) and demonstrated high cellular viability for up to 4 weeks (Figure B.1D,H).

Gene expression profiles of mES cells cultured in SLac peptide were also examined up to 28 days in culture. Expression of classical pluripotency markers such as Nanog, Oct3/4, and Sox2 were examined.[245] Expression of Oct3/4 was highest at 7 days while expression was significantly lower by day 28. Sox2 peaked at 14 days of culture with expression being significantly lower again at 4 weeks while Nanog expression remained similar throughout the 4 weeks of culture (Figure B.2A). This demonstrates that over the course of culture, mES cells began to differentiate, losing their pluripotent gene expression profile by day 28. All mesoderm markers analyzed remained statistically similar throughout the culture time; however, there was an increasing trend for Brachyury and Twist2 (Figure B.2B).[245] Similarly, endoderm markers were up-regulated. However,

expression of PDX1, Sox17, and Pax4 did not change significantly over the culture period (Figure B.2C).[246] Finally, ectoderm markers, including Fgf5 and Sox1, remained statistically similar with an increasing trend for up to 4 weeks while Otx2 was significantly down-regulated from day 3 to day 28 (Figure B.2D).[245] These results demonstrate differentiation of mES cells into cells of all 3 germ layers, opening up the possibility of SAPH to be used as a platform for pluripotent stem cell differentiation. SAPH versatility also allows for the tailoring of peptide sequences to tissue or cell specific sequences, including pro-angiogenic functionality [111].
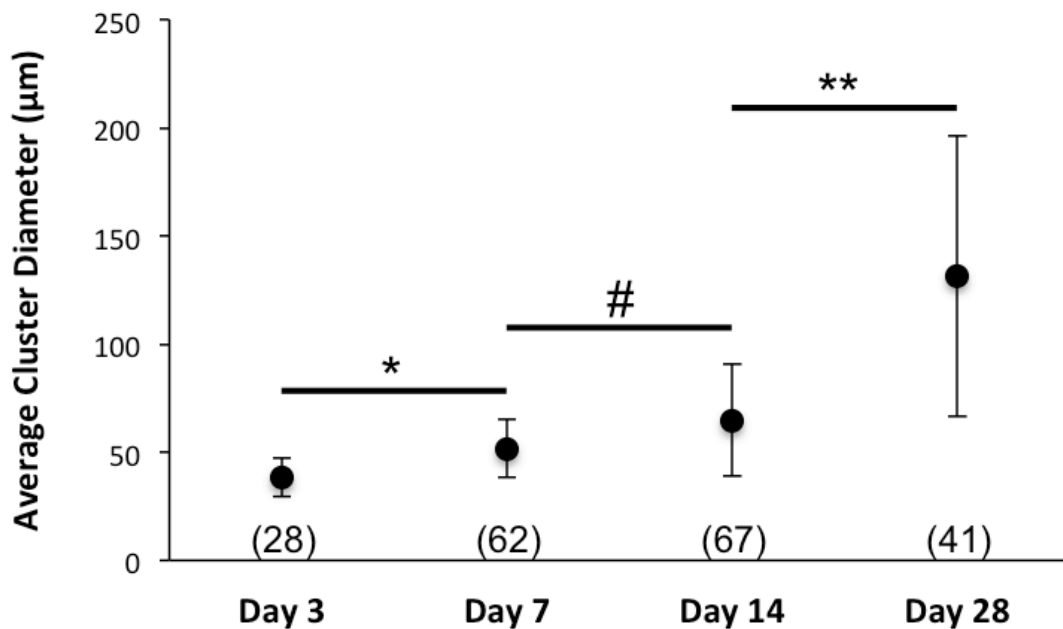
Figure B.2 Diameter of mES cell clusters in SAPH cultured for up to 28 days. (*,#,**, p<0.005)

Source: Hitscherich, P. et al. Injectable Self-Assembling Peptide Hydrogels for Tissue Writing and Embryonic Stem Cell Culture. J. Biomed. Nanotech. 14, 802-807, (2018).
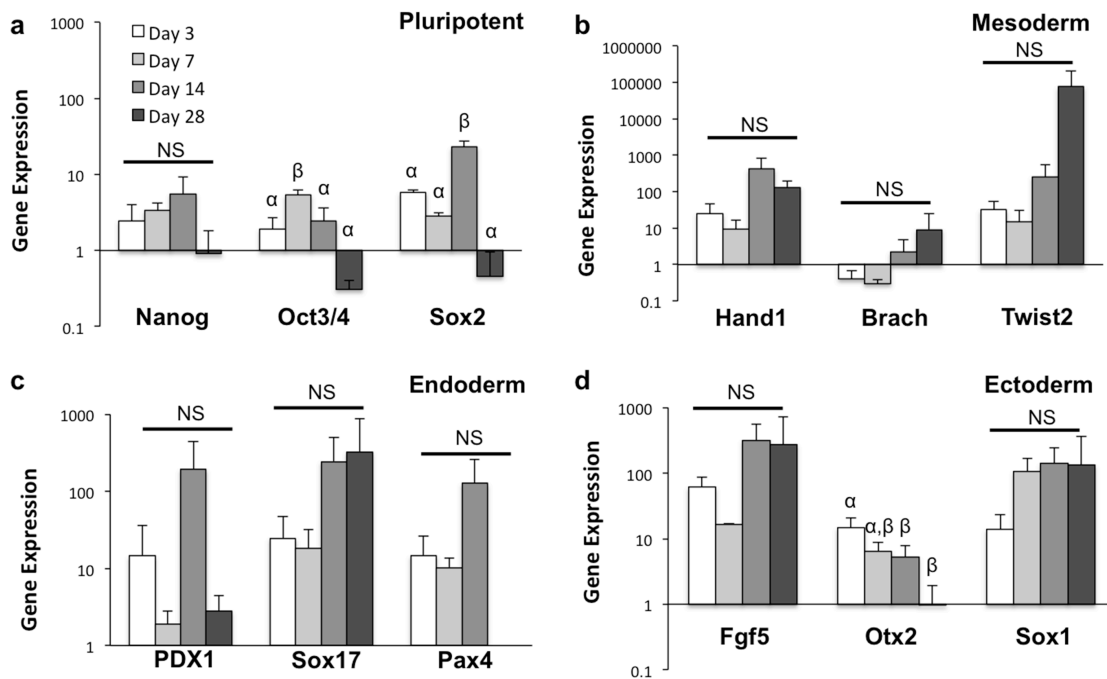
Figure B.3 Gene expression profiles of mES cells cultured in SAPH were analyzed up to 28 days using characteristic (a) pluripotent, (b) mesoderm, (c) endoderm and (d) ectoderm markers. N=3 for all groups. Similar Greek letters indicate no significant difference between days. (*p<0.05)

Source: Hitscherich, P. et al. Injectable Self-Assembling Peptide Hydrogels for Tissue Writing and Embryonic Stem Cell Culture. J. Biomed. Nanotech. 14, 802-807, (2018).

APPENDIX C

CELL CULTURE MEDIUM RECIPES

This appendix includes the culture medium recipes for all of the presented studies.

C.1 Mouse Embryonic Fibroblast (mEF) Culture Medium

1. 500mL, DMEM, high glucose (GIBCO 11965-084)

2. 58mL, FBS (Atlanta Biologicals S11550)

3. 5.8mL, 100 x Penicillin/streptomycin (GIBCO 15140)

4. 5.8mL, 100 x NEAA (GIBCO 11140)

5. 5.8mL, 100 x Na-pyruvate (GIBCO 11360)

C.2 Mouse Embryonic Stem (mES) Cell Culture Medium

1. 500mL DMEM, High Glucose (GIBCO 11965-084)

2. 90mL KN Serum Replacement (GIBCO 10828)

3. 6.25mL 100x Penicillin/streptomycin (GIBCO 15140)

4. 6.25mL 100x NEAA (GIBCO 11140)

5. 6.25mL 100x Na-Pyruvate (GIBCO 11360)

6. 4.4uL 2-Mercaptoethanol (Sigma M6250)

7. LIF final Concentration is 5ng/mL in 50 mL aliquot (R&D 8878-LF)

C.3 mES Adaptation Culture Medium

1. 500 mL IMDM (GIBCO 12440-053)

2. 90 ml, KO Serum Replacement (GIBCO 10828)

3. 6 mL, 100 x Penicillin/streptomycin (GIBCO 15140)

4. 4.7 uL, 1-Thioglycerol (Sigma M6145)

5. LIF final Concentration is 5ng/mL in 50 mL aliquot (R&D 8878-LF)

C.4 mES Differentiation Culture Medium

1. 85 mL, IMDM (GIBCO 12440-053)

2. 15 mL, FBS (Atlanta Biologicals S11550)

3. 1 mL, 100 x Penicillin/streptomycin (GIBCO 15140)

4. 5 mg, L-Ascorbic acid: Final concentration is 5 μg/ml (Sigma Aldrich A4544)

5. 0.78 uL 1-Thioglycerol (Sigma M6145)

C.5 Serum Free Macrophage Culture Medium

1. 50 mL, RPMI (Gibco 31800-022)

2. 0.5 mL, 100x Penicillin/streptomycin (GIBCO 15140)

C.6 Complete Macrophage Culture Medium

1. 178 mL, RPMI (Gibco 31800-022)

2. 20 mL, FBS (Atlanta Biologicals S11550)

3. 2 mL, 100x Penicillin/streptomycin (GIBCO 15140)

APPENDIX D

DETAILED MOUSE EMBRYONIC STEM CELL CULTURE AND

DIFFERENTIATION

This appendix describes the detailed protocol for mouse embryonic stem (mES) cell

culture and differentiation into cardiomyocytes.

D.1 Mouse Embryonic Fibroblast (mEF) Plating

1. Coat 6 well plate with 0.1% gelatin (Sigma Aldrich G9391) for 1 hour in the incubator.

2. Thaw a mEF vial (ThermoFisher Scientific A34959) in hands, transfer to clean 15 mL tube and add double volume of mEF medium.

3. Centrifuge at 1000 rpm for 5 minutes and then decant old medium.

4. Remove excess gelatin from plate and add 1 mL of mEF medium to each well.

5. Suspend mEF in 6 mL of mEF medium and distribute 1 mL of cell suspension in each plate well.

6. Bring plate to incubator and move the plate 7 times up and 7 times to the side in order to evenly distribute cells.

7. Make sure to change medium every other day and to use wells and plates by day 14.

D.2 Mouse Embryonic Stem (mES) Cell Passage

1. Trypsinize with 500 uL of 0.05% (Gibco 25300-054) and 500 uL of .25% trypsin (Gibco 25200-056) for about 3 minutes.

2. Rinse well with trypsin solution and then transfer to clean 15 mL tube.

3. Add 1 mL of fresh mES-LIF medium directly to the cells in the tube and then use another 1 mL of fresh medium to rinse the dish again.

4. Centrifuge at 1000 rpm for 5 minutes.

5. Decant off old medium and suspend in 2 mL of mES-LIF medium.

6. After counting, take 0.04 million cells and plate in a new mEF-covered well with 3 mL of mES+LIF medium.

D.3 mES Adaptation

1. Coat tissue culture treated p35 dishes with 0.1% gelatin for 1 hour in the incubator.

2. Pre-plate mES in tissue culture treated p35 uncoated dish for 30 minutes in incubator.

3. Remove excess gelatin and seed 0.15 million pre-plated mES into each gelatin coated dishes with 2mL of Adaptation+LIF medium.

4. Place in incubator and move in "figure 8" shape in order to evenly distribute the cells within the plate.

D.4 Embryoid Body (EB) Formation

1. Trypsinize as described for mES using differentiation medium.

2. Count cells to determine how many differentiation plates can be made.

   a. Each drop is 15uL and must contain 1000 cells.

   b. Must use the multi pipette with 10 filtered 100uL tips.

   c. Must make 20 – 25 rows of hanging drops/dish.

   d. Calculate amount of suspension needed

      i. 15uL/drop * #rows * 10drops/row = _____ uL/plate

      ii. _____ uL/plate * # of plates = _____ uL suspension

   e. Calculate number of cells needed

      i. 1000cells/drop*10drops/row*# rows = _____ cells/plate

      ii. _____ cells/plate * # of plates = _____ cells

3. Suspend the correct amount of cells in the correct amount of medium to create the suspension and make sure to mix very well.

4. Add 10-12 mL of 0.01% gelatin in the bottom surface of the 150 mm untreated culture dish to keep the hanging drops hydrated.

5. Pour the suspension into a reagent reservoir. Be sure to not disturb the reservoir once the suspension is poured.

6. Flip the lid of the 150 mm untreated culture dish and distribute the suspension in drops on the lid one row at a time. Be careful to allow enough room between drops to keep them from merging.

7. Invert the lid carefully and replace on the gelatin-coated bottom.

8. Culture for 2 days.

D.5 EB Collection

1. Can only use a total of 5mL of differentiation medium per 150 mm plate. This includes the hanging drops themselves.

    a. 15uL/drop * #rows * 10drops/row = _____ uL

    b. Use the remaining amount of medium to collect EBs and wash the plate.

2. Collect EBs from three 150 mm dishes into one 100 mm tissue culture dish.

3. Allow the cells to differentiate for up to 10 days without medium change for mES-CM differentiation.

APPENDIX E

MOUSE EMBRYONIC STEM CELL DERIVED CARDIOMYOCYTE

PURIFICATION

This appendix includes the recipes of all solutions necessary for as well as a detailed protocol of mouse embryonic stem cell-derived cardiomyocyte (mES-CM) purification.

E.1 Reagent Recipes

E.1.1 Collagenase I/II Solution

1. 30 mg Collagenase I (Worthington Chemical LS004196)

2. 30 mg Collagenase II (Worthington Chemical LS004176)

3. 0.6 mL HBSS (Sigma Aldrich H1387)

E.1.2 DNAse1 Solution

1. 30 mg DNAse1 (Roche 10-104-159-001)

2. 3 mL MilliQ water

E.1.3 10X Clear ADS Buffer

1. 500 mL of MilliQ water

2. 34 g NaCl (Sigma Aldrich S5886)

3. 23.8 g HEPES (Sigma H4034)

4. 0.69 g NaH_2PO_4 (Sigma Aldrich S9638)

5. 3 g Glucose (Sigma Aldrich G7528)

6. 2 g KCl (J.T. Baker 3040-01)

7. 1.025 g MgSO$_4$-7H$_2$O (Sigma Aldrich 63138)

8. Adjust pH to 7.4

E.1.4 Percoll Stock Solution

1. 5 mL 10X Clear ADS Buffer

2. 45 mL Percoll Solution (Sigma Aldrich P4937)

E.1.5 1X Red ADS Buffer

1. 5 mL 10X clear ADS

2. 45 mL Sterile MilliQ water

3. Phenyl Red powder (Sigma Aldrich P5530)

E.1.6 Top Gradient
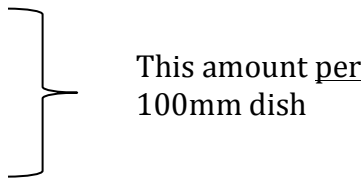
1. 22.5mL Percoll Stock Solution

2. 27.5mL 1X Clear ADS Buffer

E.1.7 Bottom Gradient

1. 25mL Percoll Stock Solution

2. 14mL 1X Red ADS Buffer

E.2 mES-CM Purification

E.2.1 Embryoid Body (EB) Digestion Protocol

1. Prepare digestion solution as follows:

   a. 100 μl Collagenase I

   b. 100 μl Collagenase II   } This amount per 100mm dish

   c. 325 μl Differentiation Medium

2. Add DNAse1 to solution at 10 μl per 1ml digestion solution.

3. Aspirate medium out of a 100 mm differentiation dish and pipette about 500 uL of digestion solution into the dish, and gently scrape cells off with a cell scrapper. Note: cells will come off in sheets.

4. Transfer cells from the dish into a 15 mL tube using a 5 mL pipette.

5. Repeat for all 100 mm dishes.

6. Mix digestion solution and cells 10 times with 5 mL pipette to begin breaking up cell clusters.

7. Incubate at 37°C in the water bath for 70 minutes in 20, 15, 15, 20 minute intervals. Gently dissociate the cells with a 5mL pipette about 10 times.

8. Spin cells at 1000 rpm for 5 minutes and discard the supernatant.

9. Suspend cells in 5 mL Differentiation Medium and count the cells, "initial cell count".

10. Spin cells again at 1000 rpm for 5 minutes and discard supernatant.

11. Suspend in 2 mL of 1X Red ADS buffer per tube for Percoll separation.

E.2.2 Percoll Separation Protocol

1. Add 4 ml of top gradient to a 15 ml tube.

2. Gently add 3 ml of bottom gradient underneath the top gradient by very slowly pipetting to maintain a clear interface between top and bottom gradients.

3. Gently pipette 2 ml of the cells suspended in 1x red ADS to the top of the top gradient.

4. And image of the gradients can be seen below:
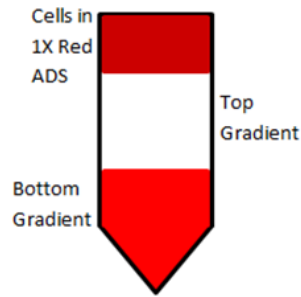
5. Spin at 4000 rpm for 30 min with <u>NO</u> deceleration.

6. Cardiomyocytes will be located in the bottom portion. The top contains other cell types:
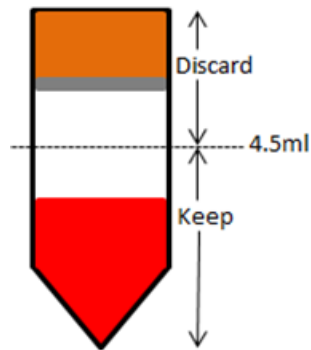
7. Remove the top half portion and discard.

8. Add 10 ml PBS to the bottom half in the tube and spin at 2000 rpm for 5 min to remove the Percoll gradient and discard supernatant.

9. Suspend in differentiation media and count cells.

10. Use as needed.

APPENDIX F

SINGLE CELL CALCIUM-HANDLING ANALYSIS

This appendix describes the recipes of all solutions necessary for as well as a detailed protocol of single cell calcium-handling analysis.

F.1 Reagent Recipes

F.1.1 Normal Tyrode's (NT) Solution

1. 15.896 g NaCL (136mM, Sigma Aldrich S5886)

2. 0.805 g KCl (5.4mM, J.T. Baker 3040-01)

3. 0.091 g NaH_2PO_4 (0.33mM, Sigma Aldrich S9638)

4. 0.407 g $MgCl_2$ (1mM, Sigma Aldrich M4880)

5. 4.766 g HEPES (10mM, Sigma Aldrich H4034)

6. 2 L MilliQ water

7. Adjust pH to 7.4

F.1.2 Modified NT Solution (Mod NT)

1. 1 L NT

2. 1.8 g glucose (Sigma Aldrich G7528)

3. 1 mL of 1 M $CaCl_2$ (Sigma Aldrich C5080)

F.1.3 Calcium Free Mod NT (CF-Mod NT) Solution

1. 1 L NT

2. 1.8 g glucose (Sigma Aldrich G7528)

F.1.4 Caffeine (Caff) Solution

1. 50 mL NT

2. 97 mg caffeine (10 mM, Sigma Aldrich C-8960)

3. Sonicate until dissolved

F.1.5 Isoproterenol (Iso) Solution

1. 5 uL of 10 mM stock solution (Sigma Aldrich I6504)

2. 50 mL of Mod NT solution (1 uM)

F.1.6 Store Operated Calcium Entry (SOCE) Solution

1. 50 mL calcium free Mod NT

2. 50 uL 10 mM stock cyclopiazonic acid (CPA) solution (Sigma Aldrich C1530)

3. 97 mg caffeine (10 mM, Sigma Aldrich C-8960)

F.1.7 Calcium Free SOCE (CF-SOCE) Solution

1. 50 mL Mod NT

2. 50 uL 10 mM stock cyclopiazonic acid (CPA) solution (Sigma Aldrich C1530)

3. 97 mg caffeine (10 mM, Sigma Aldrich C-8960)

F.2 Calcium-Handling Analysis

F.2.1 Normal Calcium-Handling Analysis

1. Incubate mES-CM with Rhod-2AM (4 µM, Invitrogen R1245MP) for 30 minutes.

2. Replace solution with Mod NT for 20 minutes for AM cleavage.

3. Under constant perfusion with Mod NT, stimulate cells at 0.5, 1 and 2 Hz frequencies (4.5 ms duration, 150 V, Grass S48 Stimulator, Grass Medical Instruments) for 30 seconds.

4. Stop stimulation for a minimum of 5 seconds.

5. Switch perfusion solution to Caff solution for a minimum of 5 seconds.

6. Switch perfusion solution back to Mod NT for 10 seconds.

F.2.2 Iso Challenge

1. Incubate mES-CM with Rhod-2AM (4 μM, Invitrogen R1245MP) for 30 minutes.

2. Replace solution with Mod NT for 20 minutes for AM cleavage.

3. Under constant perfusion with Mod NT, spontaneously contracting cells were recorded for at least 60 seconds.

4. Switch perfusion solution to Iso solution for at east 60 seconds until frequency increase plateaus.

F.2.3 SOCE

1. Incubate mES-CM with Rhod-2AM (4 μM, Invitrogen R1245MP) for 30 minutes.

2. Replace solution with Mod NT for 20 minutes for AM cleavage.

3. Under constant perfusion with Mod NT, stimulate cells at 0.5 Hz frequency (4.5 ms duration, 150 V, Grass S48 Stimulator, Grass Medical Instruments) in order to choose cells to examine.

4. Perfuse cells with Mod NT solution for 10 seconds.

5. Perfuse cells with CF-Mod NT solution for 10 seconds.

6. Perfuse cells with Mod NT solution for 10 seconds.

7. Perfuse cells with CF-Mod NT solution for 10 seconds.

8. Perfuse cells with CF-SOCE solution for 10 seconds.

9. Perfuse cells with CF-Mod NT solution for 10 seconds.

10. Perfuse cells with SOCE solution for 10 seconds.

APPENDIX G

DETAILED RT-PCR PROTOCOL

This appendix describes the detailed protocol for RNA extraction, cDNA creation and RT-PCR.

G.1 Reagents

1. B-mercaptoethanol (Sigma Aldrich M6250)

2. RNA Isolation Kit (Sigma Aldrich RTN350)

    a. Lysis Buffer (L8285)

    b. Wash Buffer I (W3136)

    c. Wash Buffer II (W3261)

    d. Elution Solution (E8024)

3. Nuclease Free Water (Invitrogen 10977-015)

4. Ethanol (Fisher S25309)

5. cDNA Kit (Applied Biosystems 4368814)

    a. 10X RT Buffer

    b. 25X dNTP Mix

    c. 10X RT Random Primers

    d. Multiscribe RT

6. Sybrgreen Supermix (Applied Biosystems A25743)

G.2 Protocols

G.2.1 Sample Preparation

1. Determine approximate number of cells and make enough Lysis Buffer for all samples

   a. Up to 5 x 10^6 cells – 250 µL Lysis Buffer

   b. Over 5 x 10^6 cells – 500 µL Lysis Buffer

2. Completely aspirate culture medium.

3. Add appropriate amount of Lysis buffer to the dish.

4. Collect the lysate using a cell scraper.

5. Pipette the lysate into a micro-centrifuge tube.

6. Vortex to mix and ensure that no visible clumps are present for at least 1 minute.

7. Lysates can be used directly for RNA extraction or stored at -80 °C at this point.

G.2.2 RNA Extraction

1. Add 1:1 volume of 70% Ethanol to the homogenized lysate and mix well by pipetting.

2. Transfer up to 700 µL including any precipitates into the RNA filter column.

3. Centrifuge for 30 sec at >8000 g (10,000 rpm). Discard the flow through by decanting into waste beaker.

4. If the sample exceeds 700 µL, centrifuge successive aliquots in the same RNA filter column. Discard the flow through.

5. Add 500 uL of Wash Buffer I to the RNA filter column. Close the lid, centrifuge for 30 sec at >8000 g (10,000 rpm). Discard the flow through and collection tube.

6. Move RNA filter column to new collection tube.

7. Add 500 uL of Wash Buffer II to the RNA filter column. Close the lid, centrifuge for 30 sec at >8000 g (10,000 rpm) to wash the spin column membrane. Discard the flow through.

8. Add 500 uL of Wash Buffer II to the RNA filter column. Close the lid, centrifuge for 2 min at >8000 g (10,000 rpm) to wash the spin column membrane. Discard the flow through.

9. Close the lid and centrifuge for 1 min at full speed (14,000 RPM) to dry the column.

10. Place the RNA filter column in a new collection/recovery tube.

11. Add 35 uL of Nuclease Free water directly on top of the membrane.

12. The lid will not close at this point. Centrifuge for 1 to 1.5 min at 10,000 rpm to elute the RNA.

13. If expected RNA yield is >30 μg, then repeat with additional 30-50 uL of water.

14. Discard the column, put the cap back on the collection tube and save the sample over ice for use within 2hrs. For long term use save at -80 °C.

G.2.3 RNA Quantification

G.2.3.1 Method I

1. Use NanoDrop in ICPH lab. Blank with Nuclease Free water and then measure "RNA-40" for each sample. Record 260/280, 260/230 and concentration.

2. Dilute sample with Nuclease Free Water in order to generate a concentration that would have 200 ug in each cDNA reaction.

G.2.3.2 Method II

1. Open the InfinitePro software and go the Applications bar using the Tecan 16 Flat Black plate.

2. Set to needed type (RNA)

3. Add 2ul drops of nuclease free water to each well for blanking. Close the lid. Open the machine (Infinite M200 Pro) and put in the plate.

4. After blanking is done, the plate will come out

5. Use Kim Wipe to clean both sides.

6. Add 2ul of your sample to one of the wells. Highlight on the software the wells that will be used.

7. Load the plate into the machine and press the start button in the top left corner (blue play button).

8. A window of Microsoft Excel will open containing both purity and concentration for each sample.

9. Use the concentration data to dilute sample with Nuclease Free Water in order to generate a concentration that would have 200 ug in each cDNA reaction.

G.2.4 cDNA Synthesis

1. Allow the kit components to thaw on ice (Applied Biosystems 4368814).

2. Prepare 2X RT master mix. This amount is required per reaction. For every 7 reactions make one extra.

   a. 10X RT Buffer   2 uL

   b. 25X dNTP Mix (100 mM)   0.8 uL

   c. 10X RT Random primers   2 uL

   d. Multiscribe RT   1 uL

   e. Nuclease free water   4.2 uL

   TOTAL   **10 uL**

3. Place the 2X RT master mix on ice and mix gently by flicking the tube with your finger.

4. Pipette 10 uL of 2X RT master mix into each well of a 96 well plate.

5. Pipette 10 uL of RNA sample into their respective well and pipette up and down 2-3 times gently to mix.

6. Seal the plates with clear adhesive tape.

7. Keep the tubes on ice till you are ready to load on the thermal cycler.

8. Program the thermal cycler as follows:

   a. Step 1 – 10 minutes at 25°C

b. Step 2 – 120 minutes at 37°C

    c. Step 3 – 5 minutes at 85°C

    d. Step 4 – Infinity at 4°C

9. Load the reactions into the T100 Thermal Cycler (Bio-rad).

10. Set the reaction volume to 20 uL.

11. Start the reverse transcription run.

12. After the run is over, dilute each reaction 1:4 with Nuclease Free water, making the final volume 80uL.

13. Aliquot samples here into 1, 2 or 3 gene aliquots (19uL/gene) according to the expected usage as cDNA is good for only one freeze and thaw cycle.

14. Store samples at 4-6 °C for short-term use (24 hrs) or in -80 °C for long-term storage (up to a year).

G.2.5 RT-PCR Protocol

1. Make a layout of the plate.

2. Thaw all components over ice.

3. Run all samples in triplicates and always include a control on every plate, for every gene for comparison.

4. Set up the reaction Master Mix as follows: This is determined with each individual kit but an example of one recipe is listed below:

    a. SYBRgreen Supermix (Applied Biosystems A25743)   10 uL

    b. Forward primer (10 uM)   2 uL

    c. Reverse primer (10 uM)   2 uL

5. Make master mix for each gene, adding one extra reaction to account for loss with pipetting.

6. The volume/reaction is 20 uL.

7. Add 14ul of the appropriate Master Mix by pipetting carefully along the wall of the well.

8. Add 6ul of the appropriate cDNA samples to each well, pipetting up and down 3-4 times to mix components.

9. Open Bio-rad CFX Manager software and load the plate on the CFX Connect RT System (Bio-rad).

10. Start a new protocol.

11. This is determined by the Sybrgreen mix (Applied Biosystems A25743) as follows:

    a. 2 minutes @ 50°C

    b. 2 minutes @ 95°C

    c. 15 seconds @ 95°C

    d. 15 seconds @ 57°C

    e. 1 minute @ 72°C

        i. Cycle c, d and e for 50 cycles

12. Read the C_t values on the software and export the data in an excel file.

APPENDIX H

DENSITOMETRY PROTOCOL

1. Save western blot images as .tif files.

2. Open each blot in ImageJ software.

3. Draw a rectangular box around lane 1 of the blot and press the #1. This should make a little "1" appear inside the rectangle you drew on the image.

4. Using the keyboard arrows, move the rectangle to the right to now surround lane 2 of the blot and press the #2. This should make a little "2" appear in the box surrounding lane 2.

5. Repeat this process for all lanes, pressing #2 for all until the last lane when you would press #3.

6. After pressing #3, a new window will appear containing a box for each lane with a peak inside. This represents the band in on the blot so they will differ depending on the size and darkness of the band. Hence, no peak will be present if there is no band in that lane.

7. Then using the line tool, draw a line to close the bottom of the peaks at their minimums on either side.

8. Then using the wand tool, highlight the now closed peaks and a third window will pop up with values representing the size and darkness of the bands.

9. Repeat this for the loading control and use the values to make the protein of interest relative to the loading control.

REFERENCES

1 Streeter, D. D., Jr., Spotnitz, H. M., Patel, D. P., Ross, J., Jr. & Sonnenblick, E. H. Fiber Orientation in the Canine Left Ventricle During Diastole and Systole. *Circ. Res.* **24**, 339-347, (1969).

2 Pinto, A. R. *et al.* Revisiting Cardiac Cellular Composition. *Circ. Res.* **118**, 400-409, (2016).

3 Brutsaert, D. L. Cardiac Endothelial-Myocardial Signaling: Its Role in Cardiac Growth, Contractile Performance, and Rhythmicity. *Physiol. Rev.* **83**, 59-115, (2003).

4 Shah, A. M. *et al.* The Cardiac Endothelium: Cardioactive Mediators. *Prog. Cardiovasc. Dis.* **39**, 263-284, (1996).

5 Hulsmans, M. *et al.* Macrophages Facilitate Electrical Conduction in the Heart. *Cell* **169**, 510-522.e520, (2017).

6 Benjamin, E. J. *et al.* Heart Disease and Stroke Statistics—2017 Update: A Report from the American Heart Association. *Circulation,* (2017).

7 Heart Attack: What Is Your Risk? *Am. Fam. Physician* **82**, 275, (2010).

8 Mignone, J. L., Kreutziger, K. L., Paige, S. & Murry, C. E. Cardiogenesis from Human Embryonic Stem Cells: Mechanisms and Applications. *Circ. J.* **74**, 2517-2526, (2010).

9 Buikema, J. W., Van Der Meer, P., Sluijter, J. P. G. & Domian, I. J. Engineering Myocardial Tissue: The Convergence of Stem Cells Biology and Tissue Engineering Technology. *Stem Cells* **31**, 2587-2598, (2013).

10 Tompkins, B. A., Natsumeda, M., Balkan, W. & Hare, J. M. What Is the Future of Cell-Based Therapy for Acute Myocardial Infarction. *Circ. Res.* **120**, 252-255, (2017).

11 Quyyumi, A. A. *et al.* Preserve-Ami: A Randomized, Double-Blind, Placebo-Controlled Clinical Trial of Intracoronary Administration of Autologous Cd34+

Cells in Patients with Left Ventricular Dysfunction Post Stemi. *Circ. Res.* **120**, 324-331, (2017).

12 Quyyumi, A. A. *et al.* Cd34(+) Cell Infusion after St Elevation Myocardial Infarction Is Associated with Improved Perfusion and Is Dose Dependent. *Am. Heart J.* **161**, 98-105, (2011).

13 Frangogiannis, N. G. The Inflammatory Response in Myocardial Injury, Repair and Remodeling. *Nat. Rev. Cardiol.* **11**, 255-265, (2014).

14 Frangogiannis, N. G. Regulation of the Inflammatory Response in Cardiac Repair. *Circ. Res.* **110**, 159-173, (2012).

15 Lee, E. J. & Hitscherich, P. *Cardiac Tissue Engineering*. Vol. 2 (Hoboken, NJ): Wiley (2017).

16 Laflamme, M. A. & Murry, C. E. Heart Regeneration. *Nature* **473**, 326-335, (2011).

17 Murry, C. E., Reinecke, H. & Pabon, L. M. Regeneration Gaps: Observations on Stem Cells and Cardiac Repair. *J. Am. Coll. Cardiol.* **47**, 1777-1785, (2006).

18 Bergmann, O. *et al.* Dynamics of Cell Generation and Turnover in the Human Heart. *Cell* **161**, 1566-1575, (2015).

19 Pope, J. H. *et al.* Missed Diagnoses of Acute Cardiac Ischemia in the Emergency Department. *N. Engl. J. Med.* **342**, 1163-1170, (2000).

20 Suter, R. E. The Risk of Missed Diagnosis of Acute Myocardial Infarction Associated with Emergency Department Volume. *Ann. Emerg. Med.* **50**, 203; author reply 203-204, (2007).

21 Mccarthy, B. D., Beshansky, J. R., D'agostino, R. B. & Selker, H. P. Missed Diagnoses of Acute Myocardial Infarction in the Emergency Department: Results from a Multicenter Study. *Ann. Emerg. Med.* **22**, 579-582, (1993).

22 Eschenhagen, T. *et al.* Cardiomyocyte Regeneration: A Consensus Statement. *Circulation* **136**, 680-686, (2017).

23 Cambria, E. *et al.* Translational Cardiac Stem Cell Therapy: Advancing from First-Generation to Next-Generation Cell Types. *NPJ Regen. Med.* **2**, 17, (2017).

24 Dixit, P. & Katare, R. Challenges in Identifying the Best Source of Stem Cells for Cardiac Regeneration Therapy. *Stem Cell. Res. Ther.* **6**, 1-12, (2015).

25 Ellison, G. M. *et al.* Cardiac Stem and Progenitor Cell Identification: Different Markers for the Same Cell? *Front. Biosci.* **2**, 641-652, (2010).

26 Li, T.-S. *et al.* Direct Comparison of Different Stem Cell Types and Subpopulations Reveals Superior Paracrine Potency and Myocardial Repair Efficacy with Cardiosphere-Derived Cells. *J. Am. Coll. Cardiol.* **59**, 942-953, (2012).

27 Chugh, A. R. *et al.* Administration of Cardiac Stem Cells in Patients with Ischemic Cardiomyopathy: The Scipio Trial: Surgical Aspects and Interim Analysis of Myocardial Function and Viability by Magnetic Resonance. *Circulation* **126**, S54-64, (2012).

28 Bolli, R. *et al.* Cardiac Stem Cells in Patients with Ischaemic Cardiomyopathy (Scipio): Initial Results of a Randomised Phase 1 Trial. *Lancet* **378**, 1847-1857, (2011).

29 Makkar, R. R. *et al.* Intracoronary Cardiosphere-Derived Cells for Heart Regeneration after Myocardial Infarction (Caduceus): A Prospective, Randomised Phase 1 Trial. *Lancet* **379**, 895-904, (2012).

30 Pittenger, M. F. *et al.* Multilineage Potential of Adult Human Mesenchymal Stem Cells. *Science* **284**, 143-147, (1999).

31 De Ugarte, D. A. *et al.* Comparison of Multi-Lineage Cells from Human Adipose Tissue and Bone Marrow. *Cells Tissues Organs* **174**, 101-109, (2003).

32 Song, L. & Tuan, R. S. Transdifferentiation Potential of Human Mesenchymal Stem Cells Derived from Bone Marrow. *FASEB J.* **18**, 980-982, (2004).

33 Jiang, Y. *et al.* Pluripotency of Mesenchymal Stem Cells Derived from Adult Marrow. *Nature* **418**, 41-49, (2002).

34 Toma, C., Pittenger, M. F., Cahill, K. S., Byrne, B. J. & Kessler, P. D. Human Mesenchymal Stem Cells Differentiate to a Cardiomyocyte Phenotype in the Adult Murine Heart. *Circulation* **105**, 93-98, (2002).

35 Barry, F. P., Murphy, J. M., English, K. & Mahon, B. P. Immunogenicity of Adult Mesenchymal Stem Cells: Lessons from the Fetal Allograft. *Stem Cells Dev* **14**, 252-265, (2005).

36 Ankrum, J. A., Ong, J. F. & Karp, J. M. Mesenchymal Stem Cells: Immune Evasive, Not Immune Privileged. *Nat. Biotechnol.* **32**, 252-260, (2014).

37 Martens, T. P. *et al.* Mesenchymal Lineage Precursor Cells Induce Vascular Network Formation in Ischemic Myocardium. *Nat. Clin. Pract. Cardiovasc. Med.* **3 Suppl 1**, S18-22, (2006).

38 Hoffmann, J. *et al.* Angiogenic Effects Despite Limited Cell Survival of Bone Marrow-Derived Mesenchymal Stem Cells under Ischemia. *Thorac. Cardiovasc. Surg.* **58**, 136-142, (2010).

39 Rennert, R. C., Sorkin, M., Garg, R. K. & Gurtner, G. C. Stem Cell Recruitment after Injury: Lessons for Regenerative Medicine. *Regen. Med.* **7**, 833-850, (2012).

40 Tomita, S. *et al.* Autologous Transplantation of Bone Marrow Cells Improves Damaged Heart Function. *Circulation* **100**, II247-256, (1999).

41 Jiang, W. *et al.* Intravenous Transplantation of Mesenchymal Stem Cells Improves Cardiac Performance after Acute Myocardial Ischemia in Female Rats. *Transpl. Int.* **19**, 570-580, (2006).

42 Berry, M. F. *et al.* Mesenchymal Stem Cell Injection after Myocardial Infarction Improves Myocardial Compliance. *Am. J. Physiol. Heart Circ. Physiol.* **290**, H2196-2203, (2006).

43 Quevedo, H. C. *et al.* Allogeneic Mesenchymal Stem Cells Restore Cardiac Function in Chronic Ischemic Cardiomyopathy Via Trilineage Differentiating Capacity. *Proc. Natl. Acad. Sci. U. S. A.* **106**, 14022-14027, (2009).

44 Williams, A. R. *et al.* Intramyocardial Stem Cell Injection in Patients with Ischemic Cardiomyopathy: Functional Recovery and Reverse Remodeling. *Circ. Res.* **108**, 792-796, (2011).

45 Li, Y., Yao, Y., Sheng, Z., Yang, Y. & Ma, G. Dual-Modal Tracking of Transplanted Mesenchymal Stem Cells after Myocardial Infarction. *Int. J. Nanomedicine* **6**, 815-823, (2011).

46 Hare, J. M. *et al.* A Randomized, Double-Blind, Placebo-Controlled, Dose-Escalation Study of Intravenous Adult Human Mesenchymal Stem Cells (Prochymal) after Acute Myocardial Infarction. *J. Am. Coll. Cardiol.* **54**, 2277-2286, (2009).

47 Chen, S. L. *et al.* Effect on Left Ventricular Function of Intracoronary Transplantation of Autologous Bone Marrow Mesenchymal Stem Cell in Patients with Acute Myocardial Infarction. *Am. J. Cardiol.* **94**, 92-95, (2004).

48 Assmus, B. *et al.* Transplantation of Progenitor Cells and Regeneration Enhancement in Acute Myocardial Infarction (Topcare-Ami). *Circulation* **106**, 3009-3017, (2002).

49 Strauer, B. E. *et al.* Repair of Infarcted Myocardium by Autologous Intracoronary Mononuclear Bone Marrow Cell Transplantation in Humans. *Circulation* **106**, 1913-1918, (2002).

50 Gaebel, R. *et al.* Cell Origin of Human Mesenchymal Stem Cells Determines a Different Healing Performance in Cardiac Regeneration. *PLoS One* **6**, e15652, (2011).

51 Alvarez-Dolado, M. *et al.* Fusion of Bone-Marrow-Derived Cells with Purkinje Neurons, Cardiomyocytes and Hepatocytes. *Nature* **425**, 968-973, (2003).

52 Nygren, J. M. *et al.* Bone Marrow-Derived Hematopoietic Cells Generate Cardiomyocytes at a Low Frequency through Cell Fusion, but Not Transdifferentiation. *Nat. Med.* **10**, 494-501, (2004).

53 Kinnaird, T. *et al.* Marrow-Derived Stromal Cells Express Genes Encoding a Broad Spectrum of Arteriogenic Cytokines and Promote in Vitro and in Vivo Arteriogenesis through Paracrine Mechanisms. *Circ. Res.* **94**, 678-685, (2004).

54 Schaefer, A. *et al.* Long-Term Effects of Intracoronary Bone Marrow Cell Transfer on Diastolic Function in Patients after Acute Myocardial Infarction: 5-Year Results from the Randomized-Controlled Boost Trial--an Echocardiographic Study. *Eur. J. Echocardiogr.* **11**, 165-171, (2010).

55 Meyer, G. P. *et al.* Intracoronary Bone Marrow Cell Transfer after Myocardial Infarction: 5-Year Follow-up from the Randomized-Controlled Boost Trial. *Eur. Heart J.* **30**, 2978-2984, (2009).

56 Acimovic, I. *et al.* Human Pluripotent Stem Cell-Derived Cardiomyocytes as Research and Therapeutic Tools. *Biomed. Res. Int.* **2014**, 512831, (2014).

57 Xu, C., Police, S., Rao, N. & Carpenter, M. K. Characterization and Enrichment of Cardiomyocytes Derived from Human Embryonic Stem Cells. *Circ. Res.* **91**, 501-508, (2002).

58 He, J.-Q., Ma, Y., Lee, Y., Thomson, J. A. & Kamp, T. J. Human Embryonic Stem Cells Develop into Multiple Types of Cardiac Myocytes: Action Potential Characterization. *Circ. Res.* **93**, 32-39, (2003).

59 Takahashi, K. *et al.* Induction of Pluripotent Stem Cells from Adult Human Fibroblasts by Defined Factors. *Cell* **131**, 861-872, (2007).

60 Du Pre, B. C., Doevendans, P. A. & Van Laake, L. W. Stem Cells for Cardiac Repair: An Introduction. *J. Geriatr. Cardiol.* **10**, 186-197, (2013).

61 Seki, T. & Fukuda, K. Methods of Induced Pluripotent Stem Cells for Clinical Application. *World J. Stem Cells* **7**, 116-125, (2015).

62 Pawani, H. & Bhartiya, D. Pluripotent Stem Cells for Cardiac Regeneration: Overview of Recent Advances & Emerging Trends. *Indian J. Med. Res.* **137**, 270-282, (2013).

63 Taranger, C. K. *et al.* Induction of Dedifferentiation, Genomewide Transcriptional Programming, and Epigenetic Reprogramming by Extracts of Carcinoma and Embryonic Stem Cells. *Mol. Biol. Cell* **16**, 5719-5735, (2005).

64 Bru, T. *et al.* Rapid Induction of Pluripotency Genes after Exposure of Human Somatic Cells to Mouse Es Cell Extracts. *Exp. Cell Res.* **314**, 2634-2642, (2008).

65 Carey, B. W., Markoulaki, S., Beard, C., Hanna, J. & Jaenisch, R. A Single-Gene Transgenic Mouse Strain for Reprogramming Adult Somatic Cells. *Nat. Methods* **7**, 56-59, (2010).

66 Chen, S., Zhang, Q., Wu, X., Schultz, P. G. & Ding, S. Dedifferentiation of Lineage-Committed Cells by a Small Molecule. *J. Am. Chem. Soc.* **126**, 410-411, (2004).

67 Lin, S. L. *et al.* Mir-302 Reprograms Human Skin Cancer Cells into a Pluripotent Es-Cell-Like State. *RNA* **14**, 2115-2124, (2008).

68 Lee, M. Y. *et al.* High Density Cultures of Embryoid Bodies Enhanced Cardiac Differentiation of Murine Embryonic Stem Cells. *Biochem. Biophys. Res. Commun.* **416**, 51-57, (2011).

69 Ungrin, M. D., Joshi, C., Nica, A., Bauwens, C. & Zandstra, P. W. Reproducible, Ultra High-Throughput Formation of Multicellular Organization from Single Cell Suspension-Derived Human Embryonic Stem Cell Aggregates. *PLoS One* **3**, e1565, (2008).

70 Bauwens, C. L. *et al.* Control of Human Embryonic Stem Cell Colony and Aggregate Size Heterogeneity Influences Differentiation Trajectories. *Stem Cells* **26**, 2300-2310, (2008).

71 Mummery, C. L. *et al.* Differentiation of Human Es and Ips Cells to Cardiomyocytes: A Methods Overview. *Circ. Res.* **111**, 344-358, (2012).

72 Laflamme, M. A. *et al.* Cardiomyocytes Derived from Human Embryonic Stem Cells in Pro-Survival Factors Enhance Function of Infarcted Rat Hearts. *Nat. Biotech.* **25**, 1015-1024, (2007).

73 Zhang, J. *et al.* Extracellular Matrix Promotes Highly Efficient Cardiac Differentiation of Human Pluripotent Stem Cells: The Matrix Sandwich Method. *Circ. Res.* **111**, 1125-1136, (2012).

74 Mummery, C. *et al.* Cardiomyocyte Differentiation of Mouse and Human Embryonic Stem Cells. *J. Anat.* **200**, 233-242, (2002).

75 Narazaki, G. *et al.* Directed and Systematic Differentiation of Cardiovascular Cells from Mouse Induced Pluripotent Stem Cells. *Circulation* **118**, 498-506, (2008).

76 Singla, D. K., Long, X., Glass, C., Singla, R. D. & Yan, B. Induced Pluripotent Stem (Ips) Cells Repair and Regenerate Infarcted Myocardium. *Mol. Pharm.* **8**, 1573-1581, (2011).

77 Lepperhof, V. *et al.* Bioluminescent Imaging of Genetically Selected Induced Pluripotent Stem Cell-Derived Cardiomyocytes after Transplantation into Infarcted Heart of Syngeneic Recipients. *PLoS One* **9**, e107363, (2014).

78 Van Laake, L. W. *et al.* Human Embryonic Stem Cell-Derived Cardiomyocytes Survive and Mature in the Mouse Heart and Transiently Improve Function after Myocardial Infarction. *Stem Cell Res.* **1**, 9-24, (2007).

79 Shiba, Y. *et al.* Hesc-Derived Cardiomyocytes Electrically Couple and Suppress Arrhythmias in Injured Hearts. *Nature* **489**, 322-325, (2012).

80 Dai, W. *et al.* Survival and Maturation of Human Embryonic Stem Cell-Derived Cardiomyocytes in Rat Hearts. *J. Mol. Cell. Cardiol.* **43**, 504-516, (2007).

81 Caspi, O. *et al.* Transplantation of Human Embryonic Stem Cell-Derived Cardiomyocytes Improves Myocardial Performance in Infarcted Rat Hearts. *J. Am. Coll. Cardiol.* **50**, 1884-1893, (2007).

82 Fernandes, S. *et al.* Human Embryonic Stem Cell-Derived Cardiomyocytes Engraft but Do Not Alter Cardiac Remodeling after Chronic Infarction in Rats. *J. Mol. Cell. Cardiol.* **49**, 941-949, (2010).

83 Chong, J. J. H. *et al.* Human Embryonic Stem Cell-Derived Cardiomyocytes Regenerate Non-Human Primate Hearts. *Nature* **510**, 273-277, (2014).

84 Laflamme, M. A. *et al.* Formation of Human Myocardium in the Rat Heart from Human Embryonic Stem Cells. *Am. J. Pathol.* **167**, 663-671, (2005).

85 Yang, X., Pabon, L. & Murry, C. E. Engineering Adolescence: Maturation of Human Pluripotent Stem Cell-Derived Cardiomyocytes. *Circ. Res.* **114**, 511-523, (2014).

86 Haraguchi, Y., Shimizu, T., Yamato, M. & Okano, T. Concise Review: Cell Therapy and Tissue Engineering for Cardiovascular Disease. *Stem Cells Transl Med* **1**, 136-141, (2012).

87 Schmid, P. *et al.* Ventricular Myocardial Architecture as Visualised in Postmortem Swine Hearts Using Magnetic Resonance Diffusion Tensor Imaging. *Eur. J. Cardiothorac. Surg.* **27**, 468-472, (2005).

88 Chung, C. Y., Bien, H. & Entcheva, E. The Role of Cardiac Tissue Alignment in Modulating Electrical Function. *J. Cardiovasc. Electrophysiol.* **18**, 1323-1329, (2007).

89 Slaughter, B. V., Khurshid, S. S., Fisher, O. Z., Khademhosseini, A. & Peppas, N. A. Hydrogels in Regenerative Medicine. *Adv. Mater.* **21**, 3307-3329, (2009).

90 Eschenhagen, T. *et al.* Three-Dimensional Reconstitution of Embryonic Cardiomyocytes in a Collagen Matrix: A New Heart Muscle Model System. *FASEB J.* **11**, 683-694, (1997).

91 Barocas, V. H., Girton, T. S. & Tranquillo, R. T. Engineered Alignment in Media Equivalents: Magnetic Prealignment and Mandrel Compaction. *J. Biomech. Eng.* **120**, 660-666, (1998).

92 Kolodney, M. S. & Wysolmerski, R. B. Isometric Contraction by Fibroblasts and Endothelial Cells in Tissue Culture: A Quantitative Study. *J. Cell Biol.* **117**, 73-82, (1992).

93 Costa, K. D., Lee, E. J. & Holmes, J. W. Creating Alignment and Anisotropy in Engineered Heart Tissue: Role of Boundary Conditions in a Model Three-Dimensional Culture System. *Tissue Eng.* **9**, 567-577, (2003).

94 Zimmermann, W. H. *et al.* Tissue Engineering of a Differentiated Cardiac Muscle Construct. *Circ. Res.* **90**, 223-230, (2002).

95 Lee, E. J., Kim Do, E., Azeloglu, E. U. & Costa, K. D. Engineered Cardiac Organoid Chambers: Toward a Functional Biological Model Ventricle. *Tissue Eng. Part A* **14**, 215-225, (2008).

96 Black, L. D., 3rd, Meyers, J. D., Weinbaum, J. S., Shvelidze, Y. A. & Tranquillo, R. T. Cell-Induced Alignment Augments Twitch Force in Fibrin Gel-Based Engineered Myocardium Via Gap Junction Modification. *Tissue Eng. Part A* **15**, 3099-3108, (2009).

97 Birla, R. K. *et al.* Methodology for the Formation of Functional, Cell-Based Cardiac Pressure Generation Constructs in Vitro. *In Vitro Cell. Dev. Biol. Anim.* **44**, 340-350, (2008).

98 Zhang, D. *et al.* Tissue-Engineered Cardiac Patch for Advanced Functional Maturation of Human Esc-Derived Cardiomyocytes. *Biomaterials* **34**, 5813-5820, (2013).

99 Zimmermann, W. H. *et al.* Engineered Heart Tissue Grafts Improve Systolic and Diastolic Function in Infarcted Rat Hearts. *Nat. Med.* **12**, 452-458, (2006).

100 Zimmermann, W. H. & Eschenhagen, T. Cardiac Tissue Engineering for Replacement Therapy. *Heart Fail. Rev.* **8**, 259-269, (2003).

101 Wendel, J. S., Ye, L., Zhang, P., Tranquillo, R. T. & Zhang, J. J. Functional Consequences of a Tissue-Engineered Myocardial Patch for Cardiac Repair in a Rat Infarct Model. *Tissue Eng. Part A* **20**, 1325-1335, (2014).

102 Young, J. L. & Engler, A. J. Hydrogels with Time-Dependent Material Properties Enhance Cardiomyocyte Differentiation in Vitro. *Biomaterials* **32**, 1002-1009, (2011).

103 Bearzi, C. *et al.* Plgf-Mmp9-Engineered Ips Cells Supported on a Peg-Fibrinogen Hydrogel Scaffold Possess an Enhanced Capacity to Repair Damaged Myocardium. *Cell Death Dis.* **5**, e1053, (2014).

104 Johnson, T. D. & Christman, K. L. Injectable Hydrogel Therapies and Their Delivery Strategies for Treating Myocardial Infarction. *Expert Opin. Drug Deliv.* **10**, 59-72, (2013).

105 Ravichandran, R., Venugopal, J. R., Sundarrajan, S., Mukherjee, S. & Ramakrishna, S. Minimally Invasive Cell-Seeded Biomaterial Systems for Injectable/Epicardial Implantation in Ischemic Heart Disease. *Int. J. Nanomedicine* **7**, 5969-5994, (2012).

106 Fujimoto, K. L. *et al.* Synthesis, Characterization and Therapeutic Efficacy of a Biodegradable, Thermoresponsive Hydrogel Designed for Application in Chronic Infarcted Myocardium. *Biomaterials* **30**, 4357-4368, (2009).

107 Hitscherich, P. *et al.* Injectable Self-Assembling Peptide Hydrogels for Tissue Writing and Embryonic Stem Cell Culture. *J. Biomed. Nanotech.* **14**, 802-807, (2018).

108 Galler, K. M., Aulisa, L., Regan, K. R., D'souza, R. N. & Hartgerink, J. D. Self-Assembling Multidomain Peptide Hydrogels: Designed Susceptibility to Enzymatic Cleavage Allows Enhanced Cell Migration and Spreading. *J. Am. Chem. Soc.* **132**, 3217-3223, (2010).

109 Kumar, V. A. *et al.* Self-Assembling Multidomain Peptides Tailor Biological Responses through Biphasic Release. *Biomaterials* **52**, 71-78, (2015).

110 Kumar, V. A. *et al.* Treatment of Hind Limb Ischemia Using Angiogenic Peptide Nanofibers. *Biomaterials* **98**, 113-119, (2016).

111 Kumar, V. A. *et al.* Highly Angiogenic Peptide Nanofibers. *ACS nano* **9**, 860-868, (2015).

112 Gonnerman, E. A., Kelkhoff, D. O., Mcgregor, L. M. & Harley, B. A. The Promotion of Hl-1 Cardiomyocyte Beating Using Anisotropic Collagen-Gag Scaffolds. *Biomaterials* **33**, 8812-8821, (2012).

113 Kai, D., Prabhakaran, M. P., Jin, G. & Ramakrishna, S. Guided Orientation of Cardiomyocytes on Electrospun Aligned Nanofibers for Cardiac Tissue Engineering. *J. Biomed. Mater. Res. B Appl. Biomater.* **98**, 379-386, (2011).

114 Pok, S. *et al.* Biocompatible Carbon Nanotube-Chitosan Scaffold Matching the Electrical Conductivity of the Heart. *ACS Nano* **8**, 9822-9832, (2014).

115 Nunes, S. S. *et al.* Biowire: A New Platform for Maturation of Human Pluripotent Stem Cell Derived Cardiomyocytes. *Nat. Methods* **10**, 781-787, (2013).

116 Radisic, M. *et al.* Functional Assembly of Engineered Myocardium by Electrical Stimulation of Cardiac Myocytes Cultured on Scaffolds. *Proc. Natl. Acad. Sci. U. S. A.* **101**, 18129-18134, (2004).

117 Weber, N., Lee, Y. S., Shanmugasundaram, S., Jaffe, M. & Arinzeh, T. L. Characterization and in Vitro Cytocompatibility of Piezoelectric Electrospun Scaffolds. *Acta Biomater.* **6**, 3550-3556, (2010).

118 Damaraju, S. M., Wu, S., Jaffe, M. & Arinzeh, T. L. Structural Changes in Pvdf Fibers Due to Electrospinning and Its Effect on Biological Function. *Biomed. Mater.* **8**, 045007, (2013).

119 Lee, Y. S. & Arinzeh, T. L. The Influence of Piezoelectric Scaffolds on Neural Differentiation of Human Neural Stem/Progenitor Cells. *Tissue Eng. Part A* **18**, 2063-2072, (2012).

120 Martins, P. M. *et al.* Effect of Poling State and Morphology of Piezoelectric Poly(Vinylidene Fluoride) Membranes for Skeletal Muscle Tissue Engineering. *RSC Advances* **3**, 17938-17944, (2013).

121 Kotwal, A. & Schmidt, C. E. Electrical Stimulation Alters Protein Adsorption and Nerve Cell Interactions with Electrically Conducting Biomaterials. *Biomaterials* **22**, 1055-1064, (2001).

122 Xu, Y., Takai, M. & Ishihara, K. Protein Adsorption and Cell Adhesion on Cationic, Neutral, and Anionic 2-Methacryloyloxyethyl Phosphorylcholine Copolymer Surfaces. *Biomaterials* **30**, 4930-4938, (2009).

123 Yang, X. L., Gu, J. W. & Zhu, H. S. Preparation of Bioelectret Collagen and Its Influence on Cell Culture in Vitro. *J. Mater. Sci. Mater. Med.* **17**, 767-771, (2006).

124 Hsiao, C. W. *et al.* Electrical Coupling of Isolated Cardiomyocyte Clusters Grown on Aligned Conductive Nanofibrous Meshes for Their Synchronized Beating. *Biomaterials* **34**, 1063-1072, (2013).

125 You, J. O., Rafat, M., Ye, G. J. & Auguste, D. T. Nanoengineering the Heart: Conductive Scaffolds Enhance Connexin 43 Expression. *Nano Lett.* **11**, 3643-3648, (2011).

126 Martins, A. M. *et al.* Electrically Conductive Chitosan/Carbon Scaffolds for Cardiac Tissue Engineering. *Biomacromolecules* **15**, 635-643, (2014).

127 Zhou, J. *et al.* Engineering the Heart: Evaluation of Conductive Nanomaterials for Improving Implant Integration and Cardiac Function. *Sci. Rep.* **4**, (2014).

128 Lee, T. J. *et al.* Graphene Enhances the Cardiomyogenic Differentiation of Human Embryonic Stem Cells. *Biochem. Biophys. Res. Commun.* **452**, 174-180, (2014).

129 Kim, T., Kahng, Y. H., Lee, T., Lee, K. & Kim Do, H. Graphene Films Show Stable Cell Attachment and Biocompatibility with Electrogenic Primary Cardiac Cells. *Mol. Cells* **36**, 577-582, (2013).

130 Park, J. *et al.* Graphene–Regulated Cardiomyogenic Differentiation Process of Mesenchymal Stem Cells by Enhancing the Expression of Extracellular Matrix Proteins and Cell Signaling Molecules. *Adv. Healthcare Mat.* **3**, 176-181, (2014).

131 Sayyar, S. *et al.* Covalently Linked Biocompatible Graphene/Polycaprolactone Composites for Tissue Engineering. *Carbon* **52**, 296-304, (2013).

132 Fan, H. *et al.* Fabrication, Mechanical Properties, and Biocompatibility of Graphene-Reinforced Chitosan Composites. *Biomacromolecules* **11**, 2345-2351, (2010).

133 Shin, S. R. *et al.* Cell-Laden Microengineered and Mechanically Tunable Hybrid Hydrogels of Gelatin and Graphene Oxide. *Adv. Mater.* **25**, 6385-6391, (2013).

134 Wan, C. & Chen, B. Poly(Epsilon-Caprolactone)/Graphene Oxide Biocomposites: Mechanical Properties and Bioactivity. *Biomed. Mater.* **6**, 055010, (2011).

135 Pinto, A. M., Gonçalves, I. C. & Magalhães, F. D. Graphene-Based Materials Biocompatibility: A Review. *Colloids Surf. B. Biointerfaces* **111**, 188-202, (2013).

136 Goenka, S., Sant, V. & Sant, S. Graphene-Based Nanomaterials for Drug Delivery and Tissue Engineering. *J. Control. Release* **173**, 75-88, (2014).

137 Zhang, Y., Nayak, T. R., Hong, H. & Cai, W. Graphene: A Versatile Nanoplatform for Biomedical Applications. *Nanoscale* **4**, 3833-3842, (2012).

138 Marchant, D. J. *et al.* Inflammation in Myocardial Diseases. *Circ. Res.* **110**, 126-144, (2012).

139 Swirski, F. K. & Nahrendorf, M. Leukocyte Behavior in Atherosclerosis, Myocardial Infarction, and Heart Failure. *Science* **339**, 161-166, (2013).

140 Frangogiannis, N. G. Emerging Roles for Macrophages in Cardiac Injury: Cytoprotection, Repair, and Regeneration. *J. Clin. Invest.* **125**, 2927-2930, (2015).

141 Nathan, C. & Ding, A. Nonresolving Inflammation. *Cell* **140**, 871-882, (2010).

142 Troidl, C. *et al.* Classically and Alternatively Activated Macrophages Contribute to Tissue Remodelling after Myocardial Infarction. *J. Cell. Mol. Med.* **13**, 3485-3496, (2009).

143 Heinemann, J. C. *et al.* Cb2 Receptor-Mediated Effects of Pro-Inflammatory Macrophages Influence Survival of Cardiomyocytes. *Life Sci.* **138**, 18-28, (2015).

144 Trial, J., Rossen, R. D., Rubio, J. & Knowlton, A. A. Inflammation and Ischemia: Macrophages Activated by Fibronectin Fragments Enhance the Survival of Injured Cardiac Myocytes. *Exp. Biol. Med.* **229**, 538-545, (2004).

145 Ai, X. *et al.* Microfluidic Coculture Device for Monitoring of Inflammation-Induced Myocardial Injury Dynamics. *Anal. Chem.* **90**, 4485-4494, (2018).

146 Hitscherich, P. *et al.* The Effect of Pvdf-Trfe Scaffolds on Stem Cell Derived Cardiovascular Cells. *Biotechnol. Bioeng.* **113**, 1577-1585, (2016).

147 Robertson, C., Tran, D. D. & George, S. C. Concise Review: Maturation Phases of Human Pluripotent Stem Cell-Derived Cardiomyocytes. *Stem Cells* **31**, 10.1002/stem.1331, (2013).

148 Hitscherich, P. *et al.* Electroactive Graphene Composite Scaffolds for Cardiac Tissue Engineering. *J. Biomed. Mater. Res. A* **106**, 2923-2933, (2018).

149 Go, A. S. *et al.* Heart Disease and Stroke Statistics--2014 Update: A Report from the American Heart Association. *Circulation* **129**, e28-e292, (2014).

150 Zimmermann, W. H. *et al.* Three-Dimensional Engineered Heart Tissue from Neonatal Rat Cardiac Myocytes. *Biotechnol. Bioeng.* **68**, 106-114, (2000).

151 Akins, R. E., Schroedl, N. A., Gonda, S. R. & Hartzell, C. R. Neonatal Rat Heart Cells Cultured in Simulated Microgravity. *In Vitro Cell. Dev. Biol. Anim.* **33**, 337-343, (1997).

152 Freed, L. E. & Vunjak-Novakovic, G. Microgravity Tissue Engineering. *In Vitro Cell. Dev. Biol. Anim.* **33**, 381-385, (1997).

153 Wainwright, J. M. *et al.* Preparation of Cardiac Extracellular Matrix from an Intact Porcine Heart. *Tissue Eng. Part C Methods* **16**, 525-532, (2010).

154 Sarig, U. *et al.* Thick Acellular Heart Extracellular Matrix with Inherent Vasculature: A Potential Platform for Myocardial Tissue Regeneration. *Tissue Eng. Part A* **18**, 2125-2137, (2012).

155 Zhang, J. *et al.* Functional Cardiomyocytes Derived from Human Induced Pluripotent Stem Cells. *Circ. Res.* **104**, e30-e41, (2009).

156 E, L. L. *et al.* Enrichment of Cardiomyocytes Derived from Mouse Embryonic Stem Cells. *J. Heart Lung Transplant.* **25**, 664-674, (2006).

157 Muller, M. *et al.* Selection of Ventricular-Like Cardiomyocytes from Es Cells in Vitro. *FASEB J.* **14**, 2540-2548, (2000).

158 Jain, N. & Lee, E. J. Islet Endothelial Cells Derived from Mouse Embryonic Stem Cells. *Cell Transplant.*, (2015).

159 Lee, Y. S., Collins, G. & Arinzeh, T. L. Neurite Extension of Primary Neurons on Electrospun Piezoelectric Scaffolds. *Acta Biomater.* **7**, 3877-3886, (2011).

160 Zhao, Z. *et al.* Modulation of Intracellular Calcium Waves and Triggered Activities by Mitochondrial Ca Flux in Mouse Cardiomyocytes. *PLoS One* **8**, e80574, (2013).

161 Zhao, Z. *et al.* Revisiting the Ionic Mechanisms of Early Afterdepolarizations in Cardiomyocytes: Predominant by Ca Waves or Ca Currents? *Am. J. Physiol. Heart Circ. Physiol.* **302**, H1636-1644, (2012).

162 Worsdorfer, P. *et al.* Connexin Expression and Functional Analysis of Gap Junctional Communication in Mouse Embryonic Stem Cells. *Stem Cells* **26**, 431-439, (2008).

163 Tandon, N. *et al.* Electrical Stimulation Systems for Cardiac Tissue Engineering. *Nat. Protoc.* **4**, 155-173, (2009).

164 Arshi, A. *et al.* Rigid Microenvironments Promote Cardiac Differentiation of Mouse and Human Embryonic Stem Cells. *Sci. Technol. Adv. Mater.* **14**, (2013).

165 Yang, H.-T. *et al.* The Ryanodine Receptor Modulates the Spontaneous Beating Rate of Cardiomyocytes During Development. *Proc. Natl. Acad. Sci. U. S. A.* **99**, 9225-9230, (2002).

166 Fujiwara, M. *et al.* Induction and Enhancement of Cardiac Cell Differentiation from Mouse and Human Induced Pluripotent Stem Cells with Cyclosporin-A. *PLoS One* **6**, e16734, (2011).

167 Van Kempen, M. J., Fromaget, C., Gros, D., Moorman, A. F. & Lamers, W. H. Spatial Distribution of Connexin43, the Major Cardiac Gap Junction Protein, in the Developing and Adult Rat Heart. *Circ. Res.* **68**, 1638-1651, (1991).

168 Boheler, K. R. *et al.* Differentiation of Pluripotent Embryonic Stem Cells into Cardiomyocytes. *Circ. Res.* **91**, 189-201, (2002).

169 Liu, J., Fu, J. D., Siu, C. W. & Li, R. A. Functional Sarcoplasmic Reticulum for Calcium Handling of Human Embryonic Stem Cell-Derived Cardiomyocytes: Insights for Driven Maturation. *Stem Cells* **25**, 3038-3044, (2007).

170 Marks, A. R. Intracellular Calcium-Release Channels: Regulators of Cell Life and Death. *Am. J. Physiol.* **272**, H597-605, (1997).

171 Hu, P. *et al.* Salbutamol and Chronic Low-Frequency Stimulation of Canine Skeletal Muscle. *J. Physiol.* **496**, 221-227, (1996).

172 Satin, J. *et al.* Calcium Handling in Human Embryonic Stem Cell-Derived Cardiomyocytes. *Stem Cells* **26**, 1961-1972, (2008).

173 Bassani, R. A., Ricardo, R. A. & Bassani, J. W. Estimation of the Fractional Sarcoplasmic Reticulum Ca2+ Release in Intact Cardiomyocytes Using Integrated Ca2+ Fluxes. *Gen. Physiol. Biophys.* **31**, 401-408, (2012).

174 Palchesko, R. N., Lathrop, K. L., Funderburgh, J. L. & Feinberg, A. W. In Vitro Expansion of Corneal Endothelial Cells on Biomimetic Substrates. *Sci. Rep.* **5**, 7955, (2015).

175 Atkins, G. B., Jain, M. K. & Hamik, A. Endothelial Differentiation: Molecular Mechanisms of Specification and Heterogeneity. *Arterioscler. Thromb. Vasc. Biol.* **31**, 1476-1484, (2011).

176 Hofmann, J. J. & Iruela-Arispe, M. L. Notch Signaling in Blood Vessels: Who Is Talking to Whom About What? *Circ. Res.* **100**, 1556-1568, (2007).

177 Im, S. H., Kim, C. Y., Jung, Y., Jang, Y. & Kim, S. H. Biodegradable Vascular Stents with High Tensile and Compressive Strength: A Novel Strategy for Applying Monofilaments Via Solid-State Drawing and Shaped-Annealing Processes. *Biomater. Sci.* **5**, 422-431, (2017).

178 Radisic, M. *et al.* Biomimetic Approach to Cardiac Tissue Engineering: Oxygen Carriers and Channeled Scaffolds. *Tissue Eng.* **12**, 2077-2091, (2006).

179 Neal, R. A. *et al.* Three-Dimensional Elastomeric Scaffolds Designed with Cardiac-Mimetic Structural and Mechanical Features. *Tissue Eng. Part A* **19**, 793-807, (2013).

180 Yeong, W. Y. *et al.* Porous Polycaprolactone Scaffold for Cardiac Tissue Engineering Fabricated by Selective Laser Sintering. *Acta Biomater.* **6**, 2028-2034, (2010).

181 Ku, S. H., Lee, M. & Park, C. B. Carbon-Based Nanomaterials for Tissue Engineering. *Adv. Healthc. Mater.* **2**, 244-260, (2013).

182 Cong, H.-P., Chen, J.-F. & Yu, S.-H. Graphene-Based Macroscopic Assemblies and Architectures: An Emerging Material System. *Chem. Soc. Rev.* **43**, 7295-7325, (2014).

183 Shin, S. R. *et al.* Carbon-Nanotube-Embedded Hydrogel Sheets for Engineering Cardiac Constructs and Bioactuators. *ACS Nano* **7**, 2369-2380, (2013).

184 Chan, V., Raman, R., Cvetkovic, C. & Bashir, R. Enabling Microscale and Nanoscale Approaches for Bioengineered Cardiac Tissue. *ACS Nano* **7**, 1830-1837, (2013).

185 Martinelli, V. *et al.* Improving Cardiac Myocytes Performance by Carbon Nanotubes Platforms. *Front. Physiol.* **4**, 239, (2013).

186 Martinelli, V. *et al.* Carbon Nanotubes Promote Growth and Spontaneous Electrical Activity in Cultured Cardiac Myocytes. *Nano Lett.* **12**, 1831-1838, (2012).

187 Martinelli, V. *et al.* Carbon Nanotubes Instruct Physiological Growth and Functionally Mature Syncytia: Nongenetic Engineering of Cardiac Myocytes. *ACS Nano* **7**, 5746-5756, (2013).

188 Ravichandran, P. *et al.* Induction of Apoptosis in Rat Lung Epithelial Cells by Multiwalled Carbon Nanotubes. *J. Biochem. Mol. Toxicol.* **23**, 333-344, (2009).

189 Ye, S. *et al.* Multi-Walled Carbon Nanotubes Induce Apoptosis in Raw 264.7 Cell-Derived Osteoclasts through Mitochondria-Mediated Death Pathway. *J. Nanosci. Nanotechnol.* **12**, 2101-2112, (2012).

190 Andon, F. T. & Fadeel, B. Programmed Cell Death: Molecular Mechanisms and Implications for Safety Assessment of Nanomaterials. *Acc. Chem. Res.* **46**, 733-742, (2013).

191 Wang, J., Sun, P., Bao, Y., Liu, J. & An, L. Cytotoxicity of Single-Walled Carbon Nanotubes on Pc12 Cells. *Toxicol. In Vitro* **25**, 242-250, (2011).

192 Foldvari, M. & Bagonluri, M. Carbon Nanotubes as Functional Excipients for Nanomedicines: Ii. Drug Delivery and Biocompatibility Issues. *Nanomedicine* **4**, 183-200, (2008).

193 Yamaguchi, A. *et al.* Effects of Sustained Stimulation with Multi-Wall Carbon Nanotubes on Immune and Inflammatory Responses in Mice. *J. Toxicol. Sci.* **37**, 177-189, (2012).

194 Buzea, C., Pacheco, Ii & Robbie, K. Nanomaterials and Nanoparticles: Sources and Toxicity. *Biointerphases* **2**, MR17-71, (2007).

195 Madani, S. Y., Mandel, A. & Seifalian, A. M. A Concise Review of Carbon Nanotube's Toxicology. *Nano Reviews* **4**, 10.3402/nano.v3404i3400.21521, (2013).

196 Zhao, J., Park, H., Han, J. & Lu, J. P. Electronic Properties of Carbon Nanotubes with Covalent Sidewall Functionalization. *J. Phys. Chem. B* **108**, 4227-4230, (2004).

197 Wang, J. *et al.* Graphene Sheet-Induced Global Maturation of Cardiomyocytes Derived from Human Induced Pluripotent Stem Cells. *ACS Appl. Mater. Interfaces* **9**, 25929-25940, (2017).

198 Ahadian, S. *et al.* Graphene Induces Spontaneous Cardiac Differentiation in Embryoid Bodies. *Nanoscale* **8**, 7075-7084, (2016).

199 Murray, E. *et al.* A Bio-Friendly, Green Route to Processable, Biocompatible Graphene/Polymer Composites. *RSC Advances* **5**, 45284-45290, (2015).

200 Aphale, A. N. *et al.* Fabrication and Experimental Analysis of Axially Oriented Nanofibers. *J. Nanosci. Nanotechnol.* **16**, 2668-2676, (2016).

201 Roy, S., Mitra, K., Desai, C., Petrova, R. & Mitra, S. Detonation Nanodiamonds and Carbon Nanotubes as Reinforcements in Epoxy Composites—a Comparative Study. *J. Nanotechnol. Eng. Med.* **4**, 011008-011008, (2013).

202 J.O. Aguilar, J. R. B.-Q., F. Aviles. Influence of Carbon Nanotube Clustering on the Electrical Conductivity of Polymer Composite Films. *eXPRESS Polymer Letters* **4**, 292-299, (2010).

203 Hernandez, D. *et al.* Electrical Stimulation Promotes Cardiac Differentiation of Human Induced Pluripotent Stem Cells. *Stem Cells Int* **2016**, 1718041, (2016).

204 Kashou, A. H. & Kashou, H. E.   (StatPearls Publishing LLC., 2017).

205 Spearman, B. S. *et al.* Conductive Interpenetrating Networks of Polypyrrole and Polycaprolactone Encourage Electrophysiological Development of Cardiac Cells. *Acta Biomater.* **28**, 109-120, (2015).

206 Ishii, O., Shin, M., Sueda, T. & Vacanti, J. P. In Vitro Tissue Engineering of a Cardiac Graft Using a Degradable Scaffold with an Extracellular Matrix–Like Topography. *J. Thorac. Cardiovasc. Surg.* **130**, 1358-1363, (2005).

207 Fearnley, C. J., Roderick, H. L. & Bootman, M. D. Calcium Signaling in Cardiac Myocytes. *Cold Spring Harb. Perspect. Biol.* **3**, a004242, (2011).

208 Barry, W. H. & Bridge, J. H. Intracellular Calcium Homeostasis in Cardiac Myocytes. *Circulation* **87**, 1806-1815, (1993).

209 Sato, D., Despa, S. & Bers, Donald m. Can the Sodium-Calcium Exchanger Initiate or Suppress Calcium Sparks in Cardiac Myocytes? *Biophys. J.* **102**, L31-L33, (2012).

210 Zhang, Y. *et al.* Connexin43 Expression Levels Influence Intercellular Coupling and Cell Proliferation of Native Murine Cardiac Fibroblasts. *Cell Commun. Adhes.* **15**, 289-303, (2008).

211 Baumgartner, S. *et al.* Electrophysiological and Morphological Maturation of Murine Fetal Cardiomyocytes During Electrical Stimulation in Vitro. *J. Cardiovasc. Pharmacol. Ther.* **20**, 104-112, (2015).

212 Dewald, O. *et al.* Ccl2/Monocyte Chemoattractant Protein-1 Regulates Inflammatory Responses Critical to Healing Myocardial Infarcts. *Circ. Res.* **96**, 881-889, (2005).

213 Yan, X. *et al.* Temporal Dynamics of Cardiac Immune Cell Accumulation Following Acute Myocardial Infarction. *J. Mol. Cell. Cardiol.* **62**, 24-35, (2013).

214 Miao, L. *et al.* Hydrogen Sulfide Mitigates Myocardial Infarction Via Promotion of Mitochondrial Biogenesis-Dependent M2 Polarization of Macrophages. *Antioxid. Redox Signal.* **25**, 268-281, (2016).

215 Shiraishi, M. *et al.* Alternatively Activated Macrophages Determine Repair of the Infarcted Adult Murine Heart. *J. Clin. Invest.* **126**, 2151-2166, (2016).

216 Melton, D. W., Mcmanus, L. M., Gelfond, J. a. L. & Shireman, P. K. Temporal Phenotypic Features Distinguish Polarized Macrophages in Vitro. *Autoimmunity* **48**, 161-176, (2015).

217 Nahrendorf, M. *et al.* The Healing Myocardium Sequentially Mobilizes Two Monocyte Subsets with Divergent and Complementary Functions. *J. Exp. Med.* **204**, 3037-3047, (2007).

218 Ma, Y., Mouton, A. J. & Lindsey, M. L. Cardiac Macrophage Biology in the Steady-State Heart, the Aging Heart, and Following Myocardial Infarction. *Trans. Res.* **191**, 15-28, (2018).

219 Heidt, T. *et al.* Differential Contribution of Monocytes to Heart Macrophages in Steady-State and after Myocardial Infarction. *Circ. Res.* **115**, 284-295, (2014).

220 Huynh, M. L., Fadok, V. A. & Henson, P. M. Phosphatidylserine-Dependent Ingestion of Apoptotic Cells Promotes Tgf-Beta1 Secretion and the Resolution of Inflammation. *J. Clin. Invest.* **109**, 41-50, (2002).

221 Huebener, P. *et al.* Cd44 Is Critically Involved in Infarct Healing by Regulating the Inflammatory and Fibrotic Response. *J. Immunol.* **180**, 2625, (2008).

222 Ji, N., Lou, H., Gong, X., Fu, T. & Ni, S. Treatment with 3-Bromo-4,5-Dihydroxybenzaldehyde Improves Cardiac Function by Inhibiting Macrophage Infiltration in Mice. *Korean Circ. J.* **48**, 933-943, (2018).

223 Tokutome, M. *et al.* Ppargamma-Targeting Nanomedicine Promotes Cardiac Healing after Acute Myocardial Infarction by Skewing Monocyte/Macrophage Polarization in Preclinical Animal Models. *Cardiovasc. Res.*, (2018).

224 Frangogiannis, N. G. Matricellular Proteins in Cardiac Adaptation and Disease. *Physiol. Rev.* **92**, 635-688, (2012).

225 Frangogiannis, N. G. *et al.* Critical Role of Endogenous Thrombospondin-1 in Preventing Expansion of Healing Myocardial Infarcts. *Circulation* **111**, 2935-2942, (2005).

226 Misenheimer, T. M. & Mosher, D. F. Calcium Ion Binding to Thrombospondin 1. *J. Biol. Chem.* **270**, 1729-1733, (1995).

227 Calzada, M. J. *et al.* Calcium Indirectly Regulates Immunochemical Reactivity and Functional Activities of the N-Domain of Thrombospondin-1. *Matrix Biol.* **27**, 339-351, (2008).

228 Luo, X. *et al.* Stim1-Dependent Store-Operated Ca(2)(+) Entry Is Required for Pathological Cardiac Hypertrophy. *J. Mol. Cell. Cardiol.* **52**, 136-147, (2012).

229 Youm, J. B. Electrophysiological Properties and Calcium Handling of Embryonic Stem Cell-Derived Cardiomyocytes. *Integr. Med. Res.* **5**, 3-10, (2016).

230 Ambily, A. *et al.* The Role of Plasma Membrane Stim1 and Ca(2+)Entry in Platelet Aggregation. Stim1 Binds to Novel Proteins in Human Platelets. *Cell. Signal.* **26**, 502-511, (2014).

231 Duquette, M. *et al.* Members of the Thrombospondin Gene Family Bind Stromal Interaction Molecule 1 and Regulate Calcium Channel Activity. *Matrix Biol.* **37**, 15-24, (2014).

232 De Haan, J. J., Smeets, M. B., Pasterkamp, G. & Arslan, F. Danger Signals in the Initiation of the Inflammatory Response after Myocardial Infarction. *Mediators Inflamm.* **2013**, 206039, (2013).

233 Murry, C. E., Giachelli, C. M., Schwartz, S. M. & Vracko, R. Macrophages Express Osteopontin During Repair of Myocardial Necrosis. *Am. J. Pathol.* **145**, 1450-1462, (1994).

234 Waller, A. H., Sanchez-Ross, M., Kaluski, E. & Klapholz, M. Osteopontin in Cardiovascular Disease: A Potential Therapeutic Target. *Cardiol. Rev.* **18**, 125-131, (2010).

235 Xie, Z., Singh, M. & Singh, K. Osteopontin Modulates Myocardial Hypertrophy in Response to Chronic Pressure Overload in Mice. *Hypertension* **44**, 826-831, (2004).

236 Stawowy, P. *et al.* Increased Myocardial Expression of Osteopontin in Patients with Advanced Heart Failure. *Eur. J. Heart Fail.* **4**, 139-146, (2002).

237 Graf, K. *et al.* Myocardial Osteopontin Expression Is Associated with Left Ventricular Hypertrophy. *Circulation* **96**, 3063-3071, (1997).

238 Trueblood, N. A. *et al.* Exaggerated Left Ventricular Dilation and Reduced Collagen Deposition after Myocardial Infarction in Mice Lacking Osteopontin. *Circ. Res.* **88**, 1080-1087, (2001).

239 Shirakawa, K. *et al.* Il-10-Stat3-Galectin-3 Axis Is Essential for Osteopontin-Producing Reparative Macrophage Polarization after Myocardial Infarction. *Circulation*, (2018).

240 Lan, F. *et al.* Abnormal Calcium Handling Properties Underlie Familial Hypertrophic Cardiomyopathy Pathology in Patient-Specific Induced Pluripotent Stem Cells. *Cell Stem Cell* **12**, 101-113, (2013).

241 Rosenberg, P. Socking It to Cardiac Hypertrophy: Stim1-Mediated Ca2+ Entry in the Cardiomyocyte. *Circulation* **124**, 766-768, (2011).

242 Hulot, J. S. *et al.* Critical Role for Stromal Interaction Molecule 1 in Cardiac Hypertrophy. *Circulation* **124**, 796-805, (2011).

243 Zheng, C. *et al.* Gastrodin Inhibits Store-Operated Ca(2+) Entry and Alleviates Cardiac Hypertrophy. *Front. Pharmacol.* **8**, 222, (2017).

244 Martinez, F. O. & Gordon, S. The M1 and M2 Paradigm of Macrophage Activation: Time for Reassessment. *F1000Prime Reports* **6**, 13, (2014).

245 Poh, Y. C. *et al.* Generation of Organized Germ Layers from a Single Mouse Embryonic Stem Cell. *Nat. Commun.* **5**, 4000, (2014).

246 Schroeder, I. S., Rolletschek, A., Blyszczuk, P., Kania, G. & Wobus, A. M. Differentiation of Mouse Embryonic Stem Cells to Insulin-Producing Cells. *Nat. Protoc.* **1**, 495-507, (2006).

247 Schmittgen, T. D. & Livak, K. J. Analyzing Real-Time Pcr Data by the Comparative C(T) Method. *Nat. Protoc.* **3**, 1101-1108, (2008).

248 Nakipova, O. V. *et al.* Store-Operated Ca(2+) Entry Supports Contractile Function in Hearts of Hibernators. *PLoS One* **12**, e0177469, (2017).

249 Mckay, R. G. *et al.* Left Ventricular Remodeling after Myocardial Infarction: A Corollary to Infarct Expansion. *Circulation* **74**, 693-702, (1986).

250 Pfeffer, M. A. & Braunwald, E. Ventricular Remodeling after Myocardial Infarction. Experimental Observations and Clinical Implications. *Circulation* **81**, 1161-1172, (1990).

251 Mcwhorter, F. Y., Wang, T., Nguyen, P., Chung, T. & Liu, W. F. Modulation of Macrophage Phenotype by Cell Shape. *Proc. Natl. Acad. Sci. U. S. A.* **110**, 17253-17258, (2013).

252 Mosser, D. M. & Edwards, J. P. Exploring the Full Spectrum of Macrophage Activation. *Nat. Rev. Immunol.* **8**, 958-969, (2008).

253 Chung, J., Choi, M. J., Jeong, S. Y., Oh, J. S. & Kim, H. K. Chemokines Gene Expression of Raw 264.7 Cells by Actinobacillus Actinomycetemcomitans Lipopolysaccharide Using Microarray and Rt-Pcr Analysis. *Mol. Cells* **27**, 257-261, (2009).

254 Kobusiak-Prokopowicz, M. *et al.* Kinetics of Chemokines in Acute Myocardial Infarction. *Kardiol. Pol.* **62**, 301-314; discussion 315-306, (2005).

255 Choi, P. & Reiser, H. Il-4: Role in Disease and Regulation of Production. *Clin. Exp. Immunol.* **113**, 317-319, (1998).

256 Bers, D. M. Cardiac Excitation-Contraction Coupling. *Nature* **415**, 198-205, (2002).

257 Currie, S. & Smith, G. L. Enhanced Phosphorylation of Phospholamban and Downregulation of Sarco/Endoplasmic Reticulum Ca2+ Atpase Type 2 (Serca 2) in Cardiac Sarcoplasmic Reticulum from Rabbits with Heart Failure. *Cardiovasc. Res.* **41**, 135-146, (1999).

258 Fernandes, A. A. *et al.* Serca-2a Is Involved in the Right Ventricular Function Following Myocardial Infarction in Rats. *Life Sci.* **124**, 24-30, (2015).

259 Kojima, A., Kitagawa, H., Omatsu-Kanbe, M., Matsuura, H. & Nosaka, S. Presence of Store-Operated Ca2+ Entry in C57bl/6j Mouse Ventricular Myocytes and Its Suppression by Sevoflurane. *Br. J. Anaesth.* **109**, 352-360, (2012).

260 Wen, H. Z., Z. ; Fefelova, N. ; Xie, Lh. Potential Arrhythmohenic Role of Trpc Channels and Store-Operated Calcium Entry Mechanism in Mouse Ventricular Myocytes. *Front. Physiol.* **(In Press)**, (2018).

261 Subraman, V., Thiyagarajan, M., Malathi, N. & Rajan, S. T. Opn -Revisited. *J. Clin. Diagn. Res.* **9**, ZE10-13, (2015).

262 Komatsubara, I. *et al.* Spatially and Temporally Different Expression of Osteonectin and Osteopontin in the Infarct Zone of Experimentally Induced Myocardial Infarction in Rats. *Cardiovasc. Pathol.* **12**, 186-194, (2003).

263 Bornstein, P. & Sage, E. H. Matricellular Proteins: Extracellular Modulators of Cell Function. *Curr. Opin. Cell Biol.* **14**, 608-616, (2002).

264 Robertson, B. W., Bonsal, L. & Chellaiah, M. A. Regulation of Erk1/2 Activation by Osteopontin in Pc3 Human Prostate Cancer Cells. *Mol. Cancer* **9**, 260-260, (2010).

265 Kahles, F., Findeisen, H. M. & Bruemmer, D. Osteopontin: A Novel Regulator at the Cross Roads of Inflammation, Obesity and Diabetes. *Mol. Metab.* **3**, 384-393, (2014).

266 Dalal, S. *et al.* Osteopontin Stimulates Apoptosis in Adult Cardiac Myocytes Via the Involvement of Cd44 Receptors, Mitochondrial Death Pathway, and Endoplasmic Reticulum Stress. *Am. J. Physiol. Heart Circ. Physiol.* **306**, H1182-1191, (2014).

267 Lopez-Guerrero, A. M., Pascual-Caro, C., Martin-Romero, F. J. & Pozo-Guisado, E. Store-Operated Calcium Entry Is Dispensable for the Activation of Erk1/2 Pathway in Prostate Cancer Cells. *Cell. Signal.* **40**, 44-52, (2017).

268 Pozo-Guisado, E. *et al.* Phosphorylation of Stim1 at Erk1/2 Target Sites Modulates Store-Operated Calcium Entry. *J. Cell Sci.* **123**, 3084-3093, (2010).

269 Suezawa, C. *et al.* Time-Dependent Changes in Plasma Osteopontin Levels in Patients with Anterior-Wall Acute Myocardial Infarction after Successful Reperfusion: Correlation with Left-Ventricular Volume and Function. *J. Lab. Clin. Med.* **145**, 33-40, (2005).

270 Hofmann, U. & Frantz, S. Role of Stromal Cell Derived Factor-1 in Myocardial Healing—Novel Insights from Comparative Studies in the Fetal and Postnatal Myocardium. *Transl. Pediatr.* **7**, 239-241, (2018).

271 Saxena, A. *et al.* Stromal Cell-Derived Factor-1 Alpha Is Cardioprotective after Myocardial Infarction. *Circulation* **117**, 2224-2231, (2008).

272 Jarrah, A. A. *et al.* Sdf-1 Induces Tnf-Mediated Apoptosis in Cardiac Myocytes. *Apoptosis* **23**, 79-91, (2018).

273 Lambert, J. M., Lopez, E. F. & Lindsey, M. L. Macrophage Roles Following Myocardial Infarction. *Int. J. Cardiol.* **130**, 147-158, (2008).

274 Ye, Y. *et al.* Serum Chemokine Ccl17/Thymus Activation and Regulated Chemokine Is Correlated with Coronary Artery Diseases. *Atherosclerosis* **238**, 365-369, (2015).

275 Vandervelde, S. *et al.* Increased Inflammatory Response and Neovascularization in Reperfused Vs. Non-Reperfused Murine Myocardial Infarction. *Cardiovasc. Pathol.* **15**, 83-90, (2006).

276 Lutz, M. *et al.* Osteopontin Predicts Clinical Outcome in Patients after Treatment of Severe Aortic Stenosis with Transcatheter Aortic Valve Implantation (Tavi). *Open Heart* **4**, e000633-e000633, (2017).

277 Rosenberg, M. *et al.* Osteopontin, a New Prognostic Biomarker in Patients with Chronic Heart Failure. *Circ. Heart Fail.* **1**, 43-49, (2008).

278 Unni, E., Kittrell, F. S., Singh, U. & Sinha, R. Osteopontin Is a Potential Target Gene in Mouse Mammary Cancer Chemoprevention by Se-Methylselenocysteine. *Breast Cancer Res.* **6**, R586-592, (2004).

279 Breitkopf, K. *et al.* Thrombospondin 1 Acts as a Strong Promoter of Transforming Growth Factor Beta Effects Via Two Distinct Mechanisms in Hepatic Stellate Cells. *Gut* **54**, 673-681, (2005).

280 Nishii, K. *et al.* Targeted Disruption of the Cardiac Troponin T Gene Causes Sarcomere Disassembly and Defects in Heartbeat within the Early Mouse Embryo. *Dev. Biol.* **322**, 65-73, (2008).

281 Wuytack, F. *et al.* A Sarco/Endoplasmic Reticulum Ca(2+)-Atpase 3-Type Ca2+ Pump Is Expressed in Platelets, in Lymphoid Cells, and in Mast Cells. *J. Biol. Chem.* **269**, 1410-1416, (1994).

282 Pugach, E. K., Richmond, P. A., Azofeifa, J. G., Dowell, R. D. & Leinwand, L. A. Prolonged Cre Expression Driven by the Alpha-Myosin Heavy Chain Promoter Can Be Cardiotoxic. *J. Mol. Cell. Cardiol.* **86**, 54-61, (2015).

283 Oshima, Y. *et al.* Pivotal Role of Bcl-2 Family Proteins in the Regulation of Chondrocyte Apoptosis. *J. Biol. Chem.* **283**, 26499-26508, (2008).

284 Ni, H.-M. *et al.* Caspase Inhibition Prevents Tumor Necrosis Factor-A–Induced Apoptosis and Promotes Necrotic Cell Death in Mouse Hepatocytes In vivo and In vitro. *Am. J. Pathol.* **186**, 2623-2636, (2016).

285 Wang, X., Spandidos, A., Wang, H. & Seed, B. Primerbank: A Pcr Primer Database for Quantitative Gene Expression Analysis, 2012 Update. *Nucleic Acids Res.* **40**, D1144-D1149, (2012).

286 Pereira, L. D. V. *Stem Cells: Promise and Reality*. (Hackensack, NJ): World Scientific Publishing Company (2017).

287 Abdelwahid, E. *et al.* Stem Cell Death and Survival in Heart Regeneration and Repair. *Apoptosis* **21**, 252-268, (2016).

288 Barbash, I. M. *et al.* Systemic Delivery of Bone Marrow–Derived Mesenchymal Stem Cells to the Infarcted Myocardium. *Circulation* **108**, 863, (2003).

289 Dong, H., Paramonov, S. E., Aulisa, L., Bakota, E. L. & Hartgerink, J. D. Self-Assembly of Multidomain Peptides: Balancing Molecular Frustration Controls Conformation and Nanostructure. *J. Am. Chem. Soc.* **129**, 12468-12472, (2007).

290 D. Simms, P. E. C. a. P. C. Trizol: A New Reagent for Optimal Single-Step Isolation of Rna. *Focus* **15**, 99-103, (1993).